STUDY OF ELECTROMAGNETIC COUPLING BETWEEN GRAPHENE AND LOCALIZED SURFACE PLASMON RESONANCE

NIU JING

NATIONAL UNIVERSITY OF SINGAPORE

2013

STUDY OF ELECTROMAGNETIC COUPLING BETWEEN GRAPHENE AND LOCALIZED SURFACE PLASMON RESONANCE

NIU JING

(B. ENG. (HONS.), NATIONAL UNIVERSITY OF SINGAPORE)

A THESIS SUBMITTED

FOR THE DEGREE OF DOCTOR OF PHILOSOPHY

DEPARTMENT OF ELECTRICAL AND COMPUTER ENGINEERING

NATIONAL UNIVERSITY OF SINGAPORE

2013

DECLARATION

I hereby declare that the thesis is my original work and it has been written by me in its entirety. I have duly acknowledged all the sources of information which have been used in the thesis.

This thesis has also not been submitted for any degree in any university previously.

Niu Jing

14 August 2013

Acknowledgements

First I want to thank my supervisor, Professor Hyunsoo Yang. It has been an honor to be his PhD student. I appreciate all the advices, time and ideas he contributed to help me finish my journey as a PhD student. From him I learned the way to realize a need in the research area, analyze it to find out the possible ways to deal with it, carry out necessary actions to start research experiment and analyze the results professionally. The enthusiasm he has for various research areas motivates me throughout my PhD journey. I am thankful for the excellent examples he provides to me as an academic advisor and research scientist.

I would like to appreciate the help and support from all my friends who are working together with me in Professor Yang's group. They have been really kind and helpful to me through the four years PhD life. They are the reliable ones who are always willing to give a hand when I am facing obstacles.

I also want to express my appreciation to the support given by Mr. Jung Yoon Yong Robert and Ms. Musni our helpful lab officers.

Last but not least, I want to thanks God for giving me the chance to further my education as a PhD student and company me throughout the journey. And take care of my health, mind and study throughout this very important period of my life.

Table of Contents

Summary

Localized surface plasmon resonance (LSPR) excited in metal nanoparticles has been utilized in various graphene based optoelectronic applications. However, the electromagnetic coupling between LSPR and graphene has not been studied systematically. In this thesis, the electromagnetic coupling between the two parties is studied by varying the spacer layer thickness between them. The investigation starts with very thin spacer layer. By increasing the spacer layer thickness in a very small range from 0.3 nm to 0.8 nm an obvious blue shift is observed in the resonance wavelength of LSPR. The induced shifting corresponds to a resonance wavelength shift of approximately 12 nm for every nanometer change in the distance between the two parties. The observed phenomenon is regarded as a result caused by the formation of oscillating image dipoles in graphene film. Theoretical analysis based on a dipole approximation has been carried out and agrees well with the experimental results. After that, thicker spacer layers are utilized in the experiment. By increasing the spacer layer from 0 to 15 nm a blue-shift is observed. Based on the results obtained, the coupling strength is examined using the plasmon ruler equation. Further increment of the spacer layer thickness induces a red-shift of the resonance, and the resonance wavelength finally saturates, when the thickness of the spacer layer is more than 20 nm.

In addition, the electromagnetic enhancement characteristics for surface enhanced Raman spectroscopy (SERS) of graphene have been studied. Various excitation lasers with different wavelengths have been used to study the relationship between the laser wavelength and SERS. The thickness of the spacer layer between graphene and nanoparticles is varied to study the relationship between the enhancement factor and electromagnetic coupling strength. Both theoretical and experimental results show that the enhancement factor is modulated because of electromagnetic coupling between graphene and nanoparticles.

Finally a novel structure with graphene nanomesh and metal nanoparticles is proposed. The quality of graphene is monitored carefully before and after the patterning process by Raman spectroscopy. The measurement results show that, gold nanoparticles in the hole of graphene nanomesh structure enhance the light absorption of graphene nanomesh. This makes the structure a promising candidate to construct photodetectors with high on/off ratio, efficiency and wavelength selectivity.

List of figures

List of Abbreviations

AFM: Atomic force microscopy

CVD: Chemical vapor deposition

FWHM: Full width at half maximum

IERS: Interference-enhanced Raman scattering

ITO: Indium tin oxide

LSPR: Localized surface plasmon resonance

SEM: Scanning electron microscopy

SERS: Surface enhanced Raman spectroscopy

SiC: Silicon carbide

STM: Scanning tunneling microscopy

TEM: Transmission electron microscopy

WSSERES: Wavelenth-scaaned surface enhanced Raman excitation spectroscopy

Chapter 1: Introduction

1.1 Graphene

Graphene is a monolayer of carbon atoms with a honeycomb lattice arrangement. It can be regarded as a building block of carbon materials into all other dimensionalities, and it is the first one atom thick two-dimensional crystal investigated by human being. The theoretical study of graphene has been carried out for around sixty years,[1, 2] it was regarded as a material which cannot exist in a natural form. This is mainly due to a common understanding that two-dimensional systems are thermodynamically unstable at finite temperatures,[3] The epitaxial growths of quasi two-dimensional films requires a supporting substrate to stabilize the film which typically introduces significant modifications to the electrical characteristics of the target film.[4] The first experimental proof of the existence of graphene was made very recently in 2004 by Geim and co-workers.[5] The employed method is named mechanical exfoliation, where bulk graphite is repetitively pealed with adhesive tapes until the thinnest flakes are found and transferred to a specially designed substrate. The single atomic carbon layer is attached to the substrate mainly through the Van Der Waals force which reduces the effects induced by substrate up to a certain extent allowing researchers to investigate the intrinsic properties of graphene.[6] Since then, the characteristic of graphene has been investigated intensively. It was found that graphene can have a charge mobility up to 200,000 $cm^2V^{-1}s^{-1}$, a thermal conductivity as high as 5300 W/mK at room temperature, an opacity as low as 2.3% and a Young's modulus of 1 terapascals.[7-12] The unique properties of graphene make it one of the most intensively studied materials around the world.

Until now, mechanical exfoliated graphene provides the best purity, mobility, and optoelectronic properties compared to graphene made by other methods. As the method to produce high quality graphene is so simple and cheap, the progress of graphene research has advanced so quickly. Despite the superior

properties of mechanical exfoliated graphene, there are some major draw backs. For example, the process is random, thus the location and number of layers cannot be premeditated. In addition, it can normally produce small size graphene in the order of a few tens of micrometers.[5] Therefore, mechanical exfoliated graphene is widely used in laboratory for scientific research, but it is not suitable for mass production. The rise of the interest in graphene motivates researchers around the world to investigate more desirable methods for mass production of graphene possible.

I. Mass production of graphene

Due to continuous efforts by researchers around the world, many new synthesizing methods have been recently developed. These new methods aim to synthesize large-area, high quality graphene films with controllable numbers of layer. Among them, growing graphene on metal thin films with chemical vapor deposition (CVD) process is one of the most promising methods. CVD growth has been tried on various kinds of metals, such as Ru, Ir, Ni and Cu.[13-16] Here, CVD graphene grown on top of Ni is used as an example to illustrate the synthesize process. The process starts with the deposition of a thin layer of metal films on top of a substrate, or using a thin metal foil as the initial substrate. The substrate is subsequently heated to 1000 degree Celsius with carefully controlled temperature gradient in the Ar/H_2 environment, followed by introducing methane into the annealing chamber with a proper flow rate of 10 to 20 min. After carburization, the substrate is taken out from the annealing chamber and cooled down to room temperature at a fast rate ($10 \text{ to } 20\ ^{\circ}Cs^{-1}$).[15, 17] The non-equilibrium surface segregation process causes the carbon solubility in Ni to decrease during the fast cooling process, and the segregation of carbon atoms on top of the Ni substrate to form graphene films. Transferring of graphene films to a substrate can be done by chemical etching of Ni to obtain freestanding films in solution, followed by collecting it with an arbitrary substrate,[15] or by using transfer-printing method with PMMA acting as a stamp to allow the adhesion of graphene thin films on it,

followed by transferring to the target substrate. The size of the graphene thin films can reach the centimeter range with a sheet resistance as low as 350 Ω/□.[11]

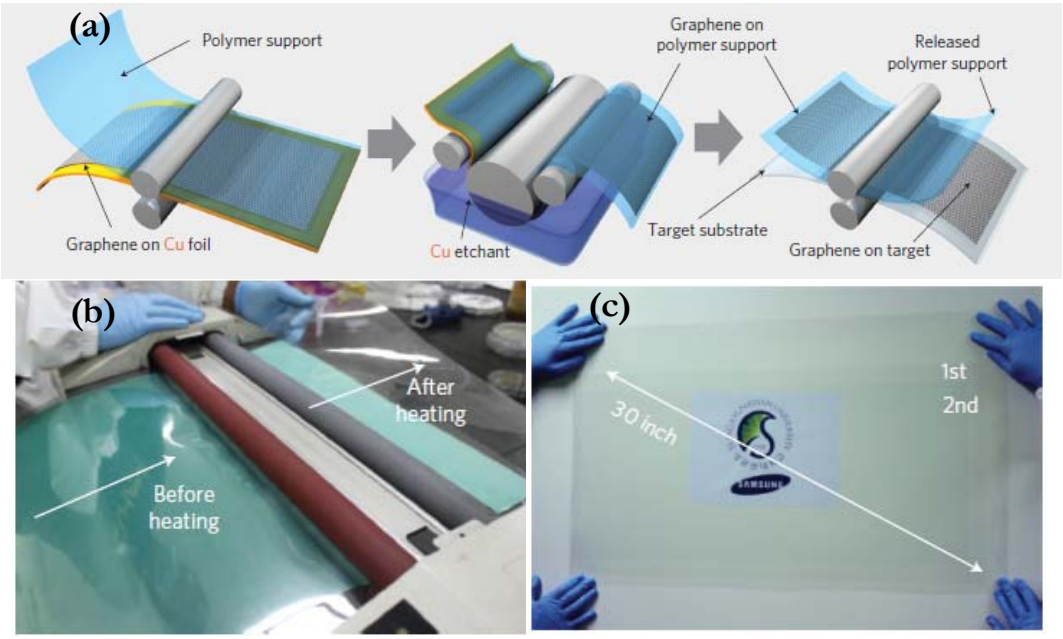

Figure 1. (a) Schematic of the steps of roll-to-roll transfer of graphene from copper foil to targeted substrate. (b) Picture of transferring graphene films from a thermal release tape to a polymer film. (c) A transparent graphene film on a 35-inch polymer sheet.[18]

Bae *et al*. made a big progress in synthesizing large scale graphene using CVD method inside a quartz tube. They have successfully made 30-inch graphene films using a roll-to-roll method on top of a roll of flexible copper film. A special heat treatment is introduced to the foil before the growing process to increase the grain size of copper in order to have a large grain size in graphene. After growth, the copper foil with graphene on top is inserted in-between two rollers together with a thermal release tape. The following copper etching process leaves graphene on the flexible thermal release tape, on which graphene is ready to be transferred to a target substrate by applying mild heat treatment. The transferring process is shown in Figure 1. The graphene films produced show a high electrical and optical quality. By introducing chemical doping to the films, the sheet resistance can be reduced to 30 Ω/□ with transparency as high as 90%. This makes the large-scale transparent electrodes based on graphene becomes highly promising for commercial applications.[18]

In addition to the CVD method, there are some other methods which are capable of growing large scale graphene films. Among them, graphene grown on silicon carbide (SiC) substrates can be considered as the most appropriate candidate for electronics applications because graphene can be prepared on an insulating SiC substrate, which is required for electronic devices. SiC automatically provides graphene film with an insulating substrate. The synthesis process consists of heating up the SiC substrate in ultrahigh vacuum under a high temperature (typically ~ 1400 °C). As desorption of Si happens on the surface, graphene thin films is formed. The number of graphene layers can be controlled by the duration of heating process.[19]

Liquid-phase exfoliation is another high yield production method of graphene. Unlike the above mentioned two methods, large-scale exfoliation is carried out instead of large-scale growth. Graphite is exfoliated in specific solvents to produce defect-free mono and multiple layer graphene.[20, 21] The prerequisite of the solvent is to match its surface energy to that of graphene. It is experimentally shown that both aqueous and non-aqueous solvents can be utilized.[20, 21] The process starts with chemical wet dispersion and continues with ultrasonication in the solvent. A high yield of single layer graphene can be achieved by sonication in water with sodium deoxycholate, and subsequently sedimentation-based ultracentrifugation. Isolation of graphene flakes with controlled thickness can be achieved, when bile salt sodium cholate is utilized together with density gradient ultracentrifugation.[22] Thin graphene conductive films can be synthesized by vacuum filtering.[21]

Chemically derived graphene from graphite oxide is another process with low-cost and massive scalability. The process starts with the oxidization of graphite films following Hummers method to create graphite oxide which is water dispersible. With an addition of mechanical energy, the hydrophilicity of graphite oxide leads to water intercalation between the graphite oxide sheets and separate into individual atomic thin films. By thermal annealing or treatment with chemical reducing agents to deoxidize the graphene oxide films, graphene can be produced.[23, 24] Furthermore, well controlled graphene nanoribbons can be made by surface-

assisted coupling of molecular monomer precursors.[25] Different precursors (e.g. 10.10'-dibromo-9,9'-bianthryl precursor monomers) are utilized to vary the topology of the nanoribbons, thus subsequently the shape of the ribbons. The single crystalline Au or Ag surface is used as a substrate for the growth of graphene nanoribbons. The precursor monometers are deposited on the substrate surface by thermal sublimation. By maintaining the substrate at a specific temperature, dehalogenation and radical addition are induced. The subsequent thermal activation steps form the linear polymer chains. In the second thermal activation, surface-assisted cyclodehydrogenation creates graphene nanoribbons or ribbons with complex shapes depending on the precursors and the temperature applied in the process.[25]

The quality of the film, type of defects, substrate, and so forth are strongly affected by the production method. Thus, the properties of graphene vary for different methods.[26] Various applications are illustrated in Figure 2 depending on the quality and cost due to the different fabrication methods.[27] As shown, graphene is already demonstrating its potential in various fields thanks to the great efforts by researchers and engineers. The next two sub-chapters will discuss the applications of graphene in electronic and photonic fields.

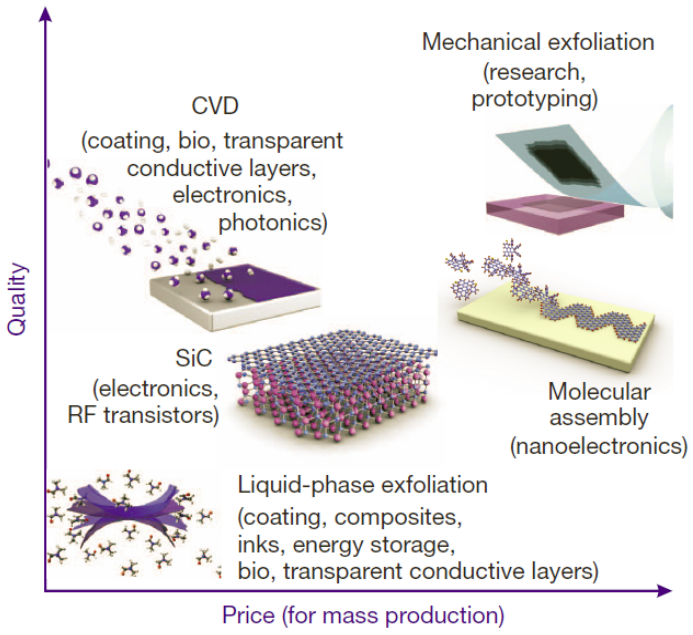

Figure 2. The relationship between cost and quality of the graphene, together with information for application of graphene made by different methods.[27]

II. Graphene electronics

While new synthetic routes to high-quality graphene have been developed, novel device structures utilizing extraordinary properties of graphene are proposed in various schemes. Taking advantage of its high carrier mobility, graphene high-frequency transistors have been intensively studied recently,[28] with a prediction that in less than ten years the requirements for the future electronics will increase the necessary cut-off frequency to 850 GHz and oscillation frequency to 1.2 THz.[26] The requirement is too high to be fulfilled by even III-V materials, and this is the place where graphene come into the picture as a promising replacement.[26]

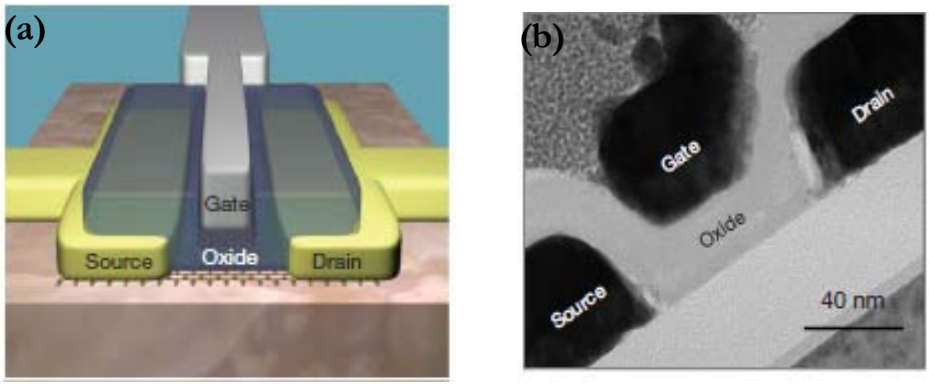

Figure 3. (a) Schematic of the top-gated graphene transistor. (b) Cross-section TEM image of a graphene transistor with gate length of 40 nm.[29]

The first report of graphene transistors working at Gigahertz frequencies was by IBM in 2009.[30] A top-gated transistor with the graphene channel was fabricated using micromechanically exfoliated graphene. The cutoff frequency can reach 26 GHz with a gate length of 150 nm.[30] Soon after that, the same research group from IBM demonstrated a top-gated graphene transistor made of CVD graphene on a diamond-like carbon substrate with a cutoff frequency up to 155 GHz and the gate length of 40 nm. Besides the fast operation speed, another fascinating characteristic of the device is the little temperature dependence of the device performance down to 4.3 K.[29] Figure 3 shows the schematic and TEM image of the device. The device demonstrates the potential of graphene in high frequency transistors, but the cut-off

frequency is still far below the required value. One of the main reasons that limit the cut-off frequency is the degradation of the quality of pristine graphene lattice, which happens during the graphene-dielectric integration process.[31, 32] In addition, the misalignment of source, drain and gate electrodes in graphene device is another reason that limits the performance of graphene high-frequency devices.[33] But a high-speed graphene transistors designed by Lei *et al*. overcomes these two limitations by using a self-aligned nanowire as a top gate. The cut-off frequency can reach as high as 300 GHz,[33] where Co_2Si-Al_2O_3 nanowire is utilized as the top gate. Firstly, Co_2Si nanowires with diameters of ~ 300 nm is synthesized through chemical vapor deposition.[34] Then the Al_2O_3 shell of the nanowire is coated by atomic layer deposition. Mechanically exfoliated graphene flakes are used in the device. The nanowire is transferred on top of graphene flakes through physical dry transfer process.[35] The electrodes are defined by electron-beam lithography. The self-alignment is achieved by deposition of a 10 nm platinum layer cover the whole surface of the device and the nanowire functions as a mask which separates the platinum film into source and drain region. The channel length is decided by the diameter of the nanowire. Figure 4 shows the schematic and the scanning electron microscopy (SEM) image of the transistor.[33] The cut-off frequency can be further increased up to 1THz with a shortened channel of 100 nm.[36]

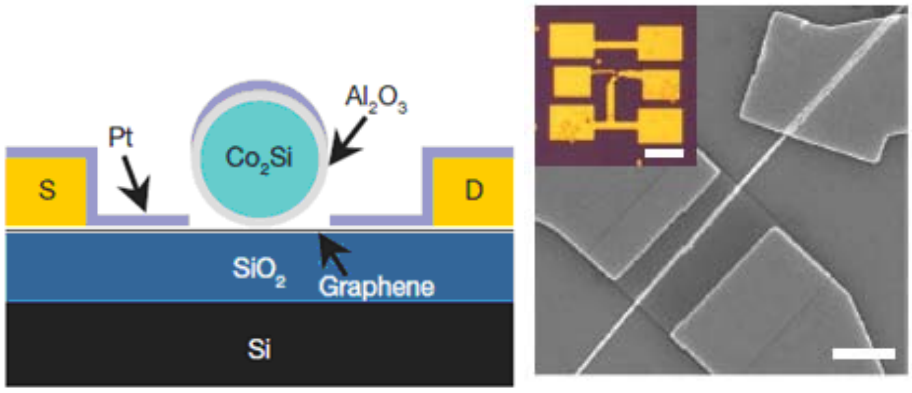

Figure 4. Left: Schematic of graphene transistor with self-aligned nanowire top gate. Right: SEM image of the nanowire top gate transistor. Scale bar is 1 μm. Inset is an optical microscope image of the device. Scale bar is 50 μm.[33]

Although graphene transistors have had a breakthrough progress recently, it still faces other challenges. One of the major challenges is a low on-off switching ratio. This is not a key concern for individual high-frequency transistor and analog electronics, but it is an important parameter for a graphene based integrated circuits.[37-39] The main reason of a low on-off ratio is the lack of a bandgap in graphene. Various approaches have been tried to open a bandgap in graphene, for example, the creation of nanoribbon, chemically modification of graphene, and bilayer control.[25, 40, 41] However, the highest on-off ratio achieved so far is ~ 10^3 and the process introduces defects to graphene.[38, 42] Recently a novel graphene field-effect tunneling transistor has solved this problem by using graphene boron nitride or molybdenum disulfide heterostructures, in which atomically thin boron nitride or molybdenum disulfide functions as a vertical transport barrier. A switching ratio of up to 10,000 is achieved.[26] With the great efforts put in by researchers and engineers around the world, it is envisioned that the future electronic circuits could be totally graphene based, with graphene field-effect transistors and conductive graphene interconnects.[43]

In addition to the channel material for fast transistors, graphene is suggested as a transparent conducting material replacing indium tin oxide (ITO) in touch screen or flexible electronics.[44] Nowadays, electronic products with a large display or touch screen panel have become very popular, for example iPhone, Amazon Kindle, and Samsung LCD. The persistent increase of these kinds of electronic devices is expected to continue for the foreseeable future.[45] To develop a display or touch panel, one of the essential parts is the transparent and conductive electrode. Presently, ITO is the main material used for transparent and conductive electrodes. Due to its scarcity of supply, it is necessary to search for a suitable substitute. Graphene fulfills the entire requirements as a promising candidate to replace ITO as a conductive and flexible electrode. First, the sheet resistance of graphene can reach as small as 30 ohm per square, when it is highly doped. Secondly, the transmittance of a single graphene layer is approximately 97.7% from ultraviolet to near infrared range.[12] Thirdly, the endurance and fracture strain of graphene far exceeds any other candidate in this field.[8, 46]

A fully functional touch-screen panel device which uses graphene as the conductive transparent electrodes has already been developed with a better strain resistance compared with an ITO based device as shown in Figure 5.[18] Another major application of transparent conductive materials is thin film solar cells.[45] Graphene has been already used as transparent electrodes to construct organic and dye-sensitized solar cells.[47, 48] Recently, Li *et al.* showed that graphene can also serve as an active layer to form a Schottky junction with n-doped silicon.[49] The potential of graphene is explored extensively in the optoelectronic field and it is foreseeable that considering the graphene-related research growing at a fast pace in various areas, more graphene based electronic devices will emerge in the future.

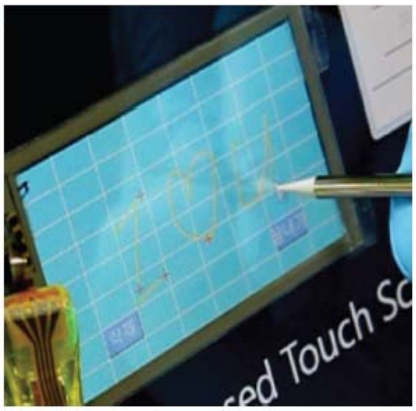

Figure 5. Graphene based touch-screen panel.[18]

III. Graphene photonics

As has been discussed in the previous section, graphene has been intensively studied in the field of electronics due to its extraordinary electronic properties. In addition, it is considered as a very promising material for novel photonic devices because of its unique optical characteristics and graphene has been already utilized in many photonics devices.[50, 51] Despite graphene is only a single atomic layer material, it can absorb ~ 2.3% of incident light which is wavelength-independent from the visible to infrared range.[12, 52]

The strength of interband transition of graphene is among the largest of all materials.[53] The interband optical absorption can reach saturation with a lower

saturation threshold compared with materials normally used as a saturable absorber,[54] which can work over visible to infrared region. Graphene thin films have been utilized as a saturable absorber in a mode-lock fiber laser. It is capable of generating ultrashort soliton pulses of 756 fs.[54]

One of the essential building blocks for on-chip optical interconnects is an optical modulator.[55] Some of the important qualities for an desirable optical modulator are a large operation bandwidth, high modulation speed, and small footprint.[55, 56] However, semiconductor optical modulators are facing many challenges to fulfill the requirements.[57-59] In contrast, graphene is considered as a promising material to develop a modulator with various advantages.[60] First of all, the wavelength-independent optical absorption which covers all telecommunications bandwidths as well as the infrared range enables the broadband operation of the device.[12, 50] Secondly, the high carrier mobility facilitates a high-speed operation. Thirdly, graphene is compatible with CMOS integration processes at wafer scales.[15] The drawback of graphene optical modulators is the limited absorption of single layer graphene. However, a graphene based optical modulator overcomes this problem by integrating graphene with an optical waveguide.[60] The device works under ambient conditions, and the modulation is achieved by tuning the Fermi level of graphene electrically. The operation speed is up to 1.2 GHz and covers a broad operation spectrum range from 1.35 to 1.6 μm. The size of the device is only 25 μm^2.[60] A schematic and an optical microscope image of the device are shown in Figure 6. The graphene film is synthesized through a CVD method and transferred onto a Si wave-guide. A thin Al_2O_3 layer acts as a spacer layer between the waveguide and the graphene film. The Si wave-guide is specially designed, such that the electric field near graphene is maximized.[60] With some modification of the structure, it is suggested that a bandwidth of up to 50 GHz can be achieved by a graphene modulator.[42]

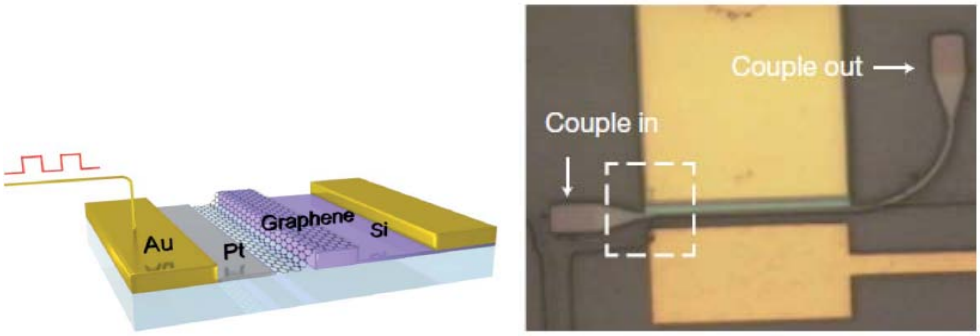

Figure 6. Left: Schematic illustration of the device. Right: Optical image of the modulator.[60]

Another promising graphene photonics device is a graphene photodetector. The wavelength-independent absorption of incident light of graphene at least from 300 nm to 6 μm facilitates to fabricate a photodetector with wide operational wavelengths.[52] The high carrier mobility of graphene allows ultrafast graphene photodetectors.[61] A graphene photodetector with a photo-response of up to 40 GHz has been reported.[61] This photodetector can operate with no source-drain bias, and zero dark current. Different from normal semiconductor photodetectors, the device has a planar structure with graphene as the light absorption material. A SEM image of the device is shown in Figure 7. The electron-hole pairs generated by incident light are separated by built-in internal fields instead of an external applied bias. The build-in field is caused by the charge transfer between graphene and the metal electrodes, which results in a band bending in the graphene channel near the interface of graphene and electrodes.[62] Thus, the gate bias and the location of the incident light beam on the graphene channel are important parameters which determine the magnitude of the photocurrent. The strongest photocurrent will be generated, when light is incident near the interfaces.[62] Despite all the superior quality of this novel device, there is one major drawback. The highest external photoresponsivity is only ~ 0.5 mAW^{-1}.

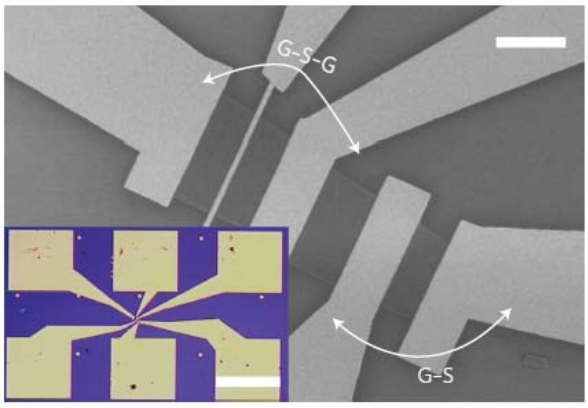

Figure 7. SEM image of the graphene photodetector; inset, optical image of the photodetector. The scale bar in the main panel is 2 μm, in the inset is 80 μm.[61]

The low photoresponsivity is mainly due to the build-in electric field only existing in the region near to the electrode-graphene interface, and majority of the graphene channel is not contributing for photocurrent generation. Another reason is the limited absorption of thin graphene film. To overcome the first obstacle, a device with multiple, interdigitated metal fingers is developed.[52] The schematic of the structure is shown in Figure 8. In order to break the symmetry of the built-in electric field profile in the graphene channel, adjacent metal fingers are made of two different metals. In this way the most of photocurrent generating along the graphene channel will not be canceled out and will be extracted. The highest external photoresponsivity achieved by this device is 6.1 mAW^{-1} and it functions well when used in a 10 $Gbits^{-1}$ optical data link. Compared with the first structure as shown in Figure 7 the bandwidth of this device is not broad. The limitation of the bandwidth is determined by the RC time constant of the device.[52] In the multiple finger structure, the graphene has a larger area compared to the first device leading to an increased capacitance value.

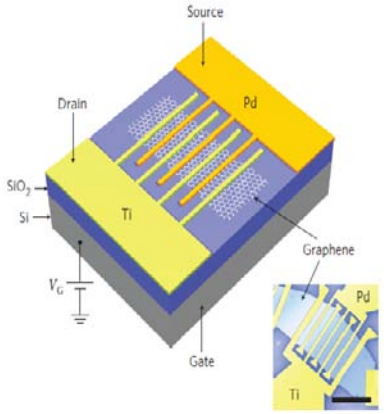

Figure 8. Schematic of the photodetector with multiple metal fingers. Inset: SEM of the device. Scale bar is 5 μm.[52]

In order to increase the absorption of light by the graphene film, a waveguide can be integrated to the graphene film by increasing the interaction length of light with graphene.[42] Another method is to use localized surface plasmonics to increase the local electric field.[63] The optical characteristic of Graphene and metal nanoparticles together as a system is another interesting research topic to study.[64, 65] And it has been shown that with plasmonics nanostructures the efficiency of graphene photodetectors is increased by 20 times.[63] The SEM image of the device is shown in Figure 9. Since, the build-in potential is the highest at the interface between the electrode and graphene channel. The metal nanoparticles are patterned by electron beam lithography near the contact edge to facilitate the largest enhancement. Lasers with different wavelengths are utilized to test the enhancement of photovoltage over the visible spectrum range, and enhancement is observed for all wavelengths. However, the maximum enhancement is achieved at a wavelength close to the resonance wavelength of the localized surface plasmon excited on the metal nanoparticles. By changing the dimensions of the nanoparticles, the resonance can be adjusted to any wavelength in the visible range,[63] in order to achieve wavelength selectivity in graphene photodetors.[66] In addition, with localized surface plasmon excited in metallic nanostructures on top of graphene thin film, surface-enhanced Raman scattering enables a significant increase of Raman intensity from graphene.[67, 68] More details of the wavelength selectivity and the surface-enhanced Raman spectroscopy will be

discussed in this thesis. Moreover, it is obvious that localized surface plasmon plays an important role in many graphene research areas. A general introduction of localized surface plasmon will be given in the next part of this chapter.

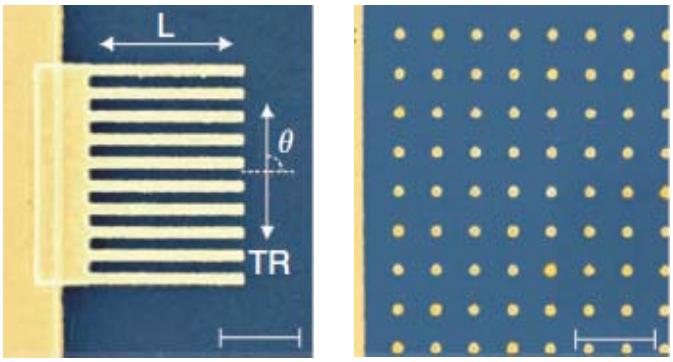

Figure 9. Left: SEM image of contacts with plasmonic nanostructures (in false colors). Right: Enlarged image of nanoparticles. Scale bar is 1 μm. [63]

1.2 Localized surface plasmon resonance

LSPR is regarded as charge density oscillations confined to metallic nanostructures induced by incident light with a resonance wavelength. The schematic diagram in Figure 10 gives an illustration of LSPR in spherical metal nanoparticles.[69] By exciting LSPR by light, the local electromagnetic fields of the nanostructures will be largely enhanced, together with strong light scatterings and intense absorption bands. Long before the term, localized surface plasmon was invented, people already used metal nanoparticles to beautify glass with different colors. The Lycurgus cup was created by the Romans in 400 A.D. Because of the excitation of LSPR in the metal nanoparticles which is embedded inside the glass, the cup reveals different colors depends on whether light is passing through it or shining behind it.

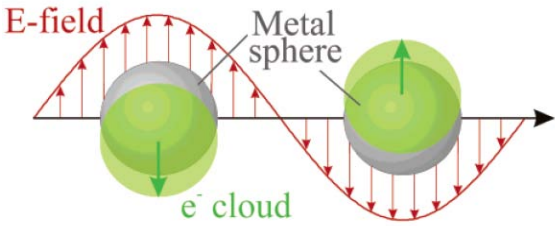

Figure 10. Schematic illustrates the plasmon oscillation for sphere nanoparticles.[70]

The scientific research of LSPR started as early as 1800s, when Faraday started the investigations of colloidal gold.[71] The first rationalization of LSPR was done by Gustav Mie in 1908 and it still remains popular at present.[72] The Mie theory is considered as a relatively simple solution to Maxwell's equations relevant to particles. In the calculations there are some assumptions: firstly, the particle and the environment are described by bulk optical dielectric functions, and secondly, both of the parties are homogeneous.[69, 73] For the case that the size of nanoparticle is not significantly smaller than the wavelength of incident light, higher-order multipole modes need to be considered, and the full Mie equation should be used. However, when the size of the nanoparticles is much smaller than the wavelength of exciting light, only dipole absorption is considered, and the Mie theory gives a simplified formula for the extinction cross-section as below:[73]

$$\sigma_{\text{ext}} = \frac{9V\epsilon_{\text{m}}^{3/2}}{c} \cdot \frac{\omega\epsilon_2(\omega)}{[\epsilon_1(\omega) + 2\epsilon_{\text{m}}]^2 + \epsilon_2(\omega 2)^2}$$

in which σ_{ext} is the extinction cross section, V is the volume of the spherical particle, c is the speed of light, ω is the angular frequency of the incident light, ϵ_m is the dielectric constant of the surrounding medium, and $\epsilon_1(\omega)$ and $\epsilon_2(\omega)$ are the real and imaginary part of the dielectric function of the nanoparticles. The height and bandwidth of the absorption peak can be well estimated by $\epsilon_2(\omega)$.[73] The formula shows that if $\epsilon_2(\omega)$ is small or not wavelength dependent, the excitation of LSPR happens when $\epsilon_1(\omega) \approx -2\epsilon_m$. Thus the frequency when LSPR is excited (or the resonance frequency) is a function of the dielectric function of the

nanoparticles and the environment. Although the formula is independent of the nanoparticle's size, the lack of size dependence of the formula can be accommodated by assuming the dielectric function of the nanostructures is size dependent.[74, 75] Indeed both experimental and theoretical results proved that the resonance frequency is very sensitive to change of the refractive index of the metal, the surrounding environment, and the size and the shape of the nanoparticles. A group of researchers have studied the effect introduced by the change of the refractive index of the surrounding media. Silver nanoparticles with the same size and shape are made and the extinction spectrum is measured to study the change of the LSPR in different solvents.[76] The used solvents are pyridine, cyclohexane, methylene chloride, acetone and nitrogen, with a refractive index of 1.51, 1.43, 1.42, 1.36, and 1 respectively. It is observed that as the refractive index of solvent decreases, the resonance wavelength progresses towards a shorter wavelength as shown in Figure 11. The relationship between the refractive index of the surrounding media and the resonance wavelength is linear.[76]

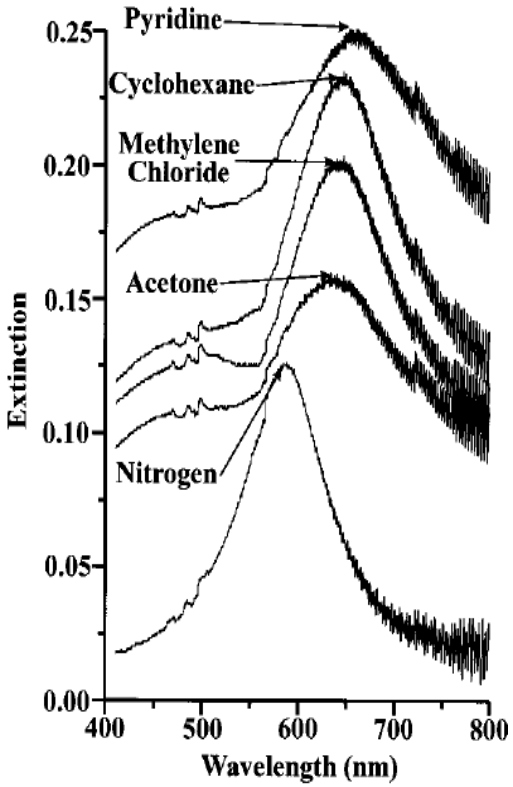

Figure 11. Extinction spectra of silver nanoparticles in various solvents.[76]

The tuning of LSPR wavelength through adjusting the size of nanoparticles has been studied by different groups both theoretically and experimentally. One of the theoretical studies was carried out based on the entrenched Mie theory together with a discrete dipole approximation method.[77] It is found that the relationship between the resonance wavelength and the size of the nanoparticles is linear. The resonance wavelength shifts to a longer range, when the size increases.[77] The data is plotted in Figure 12.

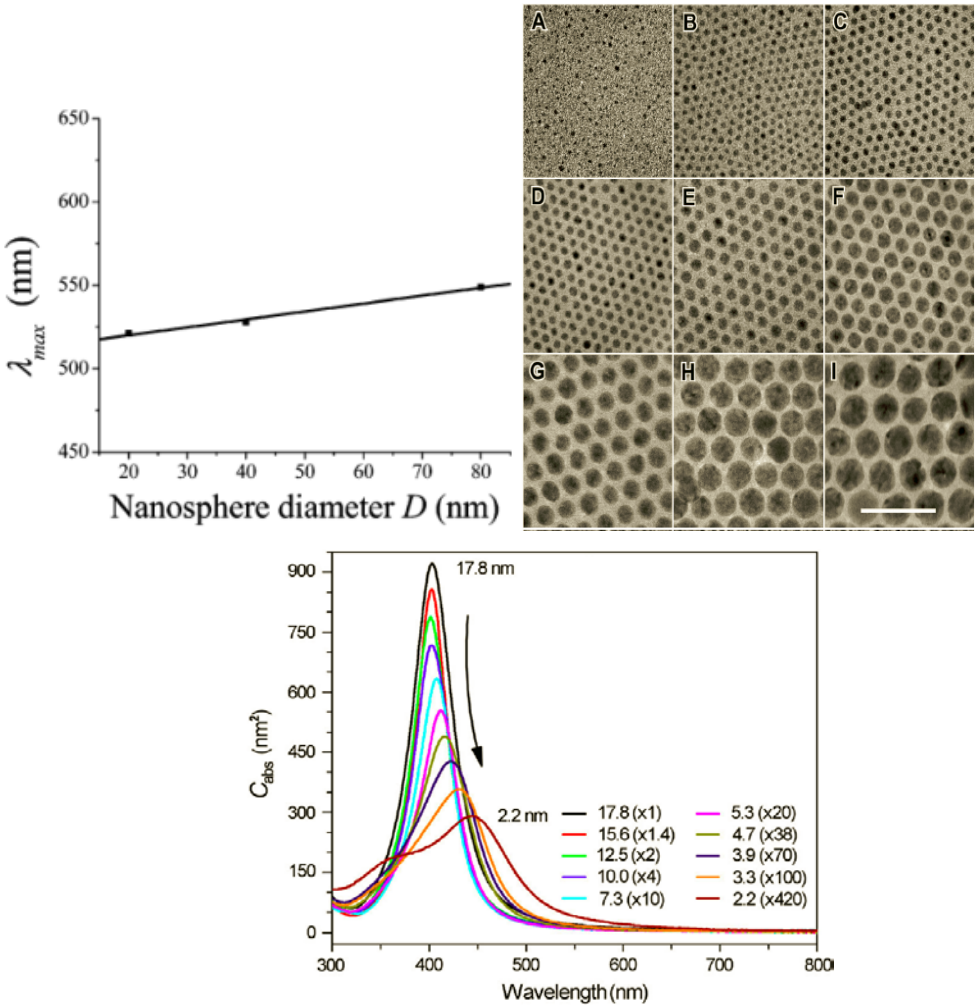

Figure 12.Top left: theoretical calculation of the variation of surface plasmon resonance wavelength with the size of gold nanoparticles.[77] Top right: TEM image of silver nanoparticles with various diameters. The length of the scale bar is 50 nm. Bottom: the absorption cross section vs. the wavelength for silver nanoparticles with different sizes. To have a clear display of the spectra, each spectrum was multiplied by an arbitrary factor listed in the parentheses.[78]

Researches about the effect of the shape have been also carried out. As it is difficult to separately study the effect of size and shape of nanoparticles experimentally, some researchers introduced the concept of aspect ratio.[76] The nanoparticles are created by using a single layer of nanospheres as the mask for silver deposition. A schematic of the nanosphere mask and an AFM image of the deposited silver nanoparticles are shown in Figure 13. By varying the size of the nanosphere and the deposited thickness, the aspect ratio can be adjusted. In addition, annealing in vacuum at 300 degree results in an increase of the height of the particle and makes it more elliptical. The extinction spectrum of silver nanoparticles with different aspect ratios is measured and shown in Figure 14.[76] Nanospheres with different diameters are used as the mask to create silver nanoparticles with various lateral dimensions. The aspect ratio is given by *a/b*. For samples with same *a* value, they are created using nanospheres with same diameter, and *b* represents the height of nanoparticles which can be changed by varying the thickness of the silver deposited. Oblate nanoparticles have a large aspect ratio, and spherical nanoparticles have an aspect ratio as one.[76] In order to find out the relationship between the resonance wavelength and aspect ratio, a comparison needs to be made for different cases. For samples F, G and H *a* is the same, the only variable is the value of *b*. It can be seen that as *b* decreases or the aspect ratio increases, the resonance wavelength shifts to the longer range. For the samples of D, E and H *b* is approximately the same, but *a* is changed. The same result for the relationship between aspect ratio and it is found that the wavelength becomes longer when the aspect ratio increases. Lastly, samples F and C are the results for the same sample after and before went through annealing process, a blue-shift is induced to the resonance wavelength by the annealing process. And all the result agrees well on the relationship between aspect ratio and resonance wavelength.[76]

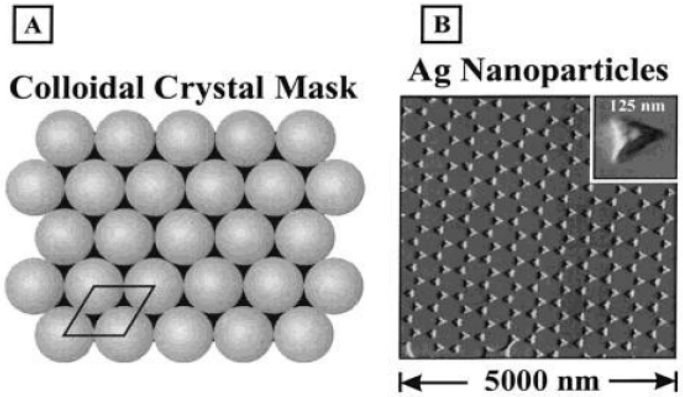

Figure 13. (A) The schematic of the nanospheres used as mask for silver deposition.(B) AFM image of nanoparticles on the substrate after removing of nanosphere mask.[76]

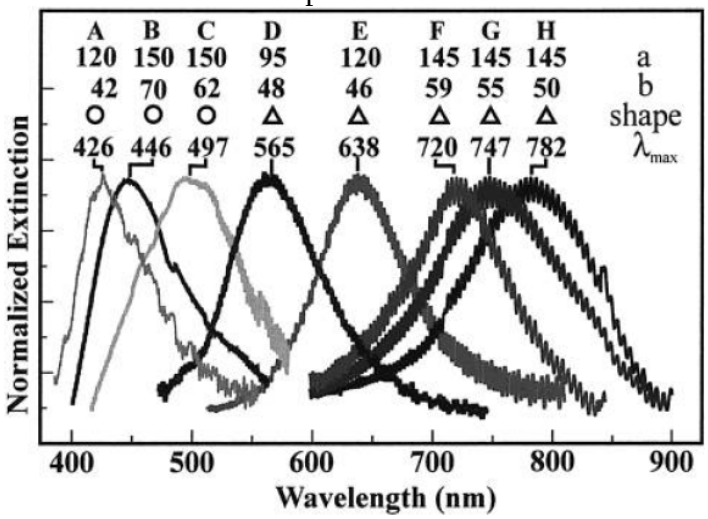

Figure 14. The normalized extinction spectra of silver nanoparticles with different aspect ratio.[76]

Because the many effects introduced by LSPR only happen near the resonance wavelength including the enhanced electromagnetic field of the nanoparticles and the intense absorption bands, managing the position of the resonance wavelength of LSPR in the spectrum is vital for achieving advances in many applications for example, sensing, imaging, solar energy, and medicine,[77, 79-82] which is also valid for all applications where LSPR is employed to aid the performance of graphene devices.

1.3 Objectives and scope of this thesis

As has been mentioned before, LSPR excited in metal nanoparticles has been already used to support the operation of a variety of graphene applications,[63, 66, 67] in which metal nanoparticles are deposited on top or in the vicinity of graphene. For example, the selectivity of graphene photodetector is achieved through varying the size of gold nanoparticles deposited on top of the graphene film.[63] However, the effects of the presence of graphene to LSPR have not been studied before. It is very likely that graphene will influence the characteristics of LSPR, since the graphene film is a very conductive layer and the electromagnetic field surrounding nanoparticles is strong. Thus, to inclusively study the optical characteristics of the graphene and metal nanoparticle system, the interaction between graphene and LSPR through the coupling of electromagnetic field should be considered. It is important to evaluate the interaction of the system in order to gauge the performance of the applications. In addition, it may provide another method to control the optical characteristics of the system, if the coupling strength between the two parties can be adjusted systematically. Therefore, in this thesis the research of the electromagnetic coupling between graphene and LSPR is carried out. The experimental results and discussion are included in the following chapters.

The experimental procedures are discussed first to facilitate a better understanding of the research to be carried out. To begin with an experiment of graphene, it is essential to verify the number of layer of the graphene film. Multiple techniques are used to identify the number of layer, followed by the investigation of the quality of the film. A thin layer of insulator is inserted between graphene and the metal nanoparticles. Metal nanoparticles are created by depositing a very thin layer of metal film. The size of the nanoparticles is examined through analyzing the SEM images taken. When the nanoparticle array or patterned graphene film with a well-defined shape and period is needed, electron beam lithography is utilized. The optical characteristics of the system are investigated to facilitate the study of the effect introduced to the enhancement of

the graphene Raman signal from graphene. The details of the above mentioned processes are included in chapter 2.

In order to control the coupling strength between graphene and LSPR, the distance between them is varied by adjusting the thickness of the insulator layer inserted in-between. The examination starts with very thin spacer layers and the results show that the surface plasmon resonance wavelength can be tuned by varying the thickness of the spacer layer. By increasing the thickness of the spacer layer, the resonance wavelength is shifted to a smaller value. The tunability that can be achieved is better than when a thin conductive metal film is used in the place of graphene. The research has carried out further to study the shifting of the surface plasmon resonance wavelength, when the thickness of the spacer layer increases more. The results demonstrate a blue-shift of 29 nm first and a further increment induces a red-shift of 17 nm in the resonance wavelength. The shift finally saturates, when the thickness of the spacer layer increases more than 20 nm. The shift is due to the change of the electromagnetic field coupling strength between the localized surface plasmon excited in the metal nanoparticles and the graphene film. Theoretical calculations based on dipole approximation are carried out, and the results agree well with the experimental data. The electromagnetic coupling strength is also examined by the plasmon ruler equation. The details can be found in chapters 3 and 4 of this thesis. Since the electromagnetic coupling between graphene and metal nanoparticles changes the optical characteristics of LSPR, it will introduce modulations to the optical systems in which these two parties are used. The electromagnetic enhancement characteristics for SERS of graphene have been also studied. Different excitation lasers are utilized to study the relationship between the laser wavelength and SERS. Both experimental results and theoretical calculation show that the extinction spectrum of metal nanoparticles is modulated by the presence of graphene. The experimental results of the relationship between the wavelength of the excitation lasers and the enhancement factor fit well with the calculated results. An exponential relationship is observed between the enhancement factor and the thickness of the spacer. The details can be found in chapter 5 of this thesis. In addition, the optical

characteristics of patterned graphene nanomesh with metal nanoparticles have also been studied. Finally electron beam lithography is chosen to pattern graphene nanomeshes with various sizes and periods. The reflection spectrum shows that the absorption is enhanced with nanoparticles filling the holes of the patterned nanomesh structure. The details are in chapter 6. In chapter 7, the thesis is concluded with a summary of all the accomplishments and the proposed future works.

Chapter 2: General experimental techniques

2.1 Introduction

To start experiment with graphene, the first step is making good quality graphene films or flakes. For the experiments in this thesis, both CVD and SiC graphene are utilized. CVD graphene is used to study the shifting of LSPR induced by electromagnetic coupling between graphene and gold nanoparticles. A 1 cm × 1 cm single layer CVD graphene film is grown on a copper film and transferred to a transparent borosilicate glass substrate. A transparent substrate is used to enable the transmission measurement. Borosilicate glass (BOROFLOAT® 33 glass) is chosen because of its good transmission over a wide light spectrum and ability to withstand high temperature treatment. The SiC graphene samples are epitaxial graphene thin films grown on a Si-terminated 6H-SiC (0001) surface. Descriptions for the synthesis processes can be found in the first chapter.

It is also essential to verify the quality of graphene films and the number of layers before any further experimental process. Different methods can be utilized for the verification process. Atomic force microscopy (AFM), transmission electron microscopy (TEM), scanning tunneling microscopy (STM) and Raman spectroscopy are some of the methods that can be used to check the morphology, number of layers and quality of graphene. For the graphene films used in the experiments here, both scanning tunneling microscopy and Raman spectroscopy are used to find the layer number and verify the quality of graphene films. Both electron beam and thermal evaporators are used to deposit a thin insulator film and metal nanoparticles. For patterning of graphene film and metal nanoparticles, different methods are tested, such as interference lithography, nanoimprinting, and electron beam lithography. Among those, electron beam lithography is selected because it is capable of varying the size and period of the nanomesh structure as demanded. LSPR is characterized by a UV-visible spectrophotometer. For samples

with very small sizes normally in μm range, a microspectrometer is used for the evaluation. Description of all the techniques mentioned above will be discussed in this chapter and more detailed description of the techniques being utilized in the experiments discussed in this thesis will be included.

2.2 Graphene thickness and quality verification

Graphene is a fascinating material with a combination of interesting properties.[43] Not only single layer graphene but also multi-layer graphene has been studied. Recent theoretical and experimental results showed that although multi-layer graphene shared some physical properties with single layer graphene they also demonstrate unique physical properties of themselves.[83] For example, because of the lack of a bandgap in single layer graphene, it is not possible to completely switch off a single layer graphene transistor.[84] However experiments with bilayer graphene show that a tunable bandgap can be developed and controlled with an applied gate bias.[85] For the case of trilayer graphene, it is regarded as a semimetal whose band overlay between the conduction and valence bands can be adjusted with gate bias.[86] Thus, to facilitate a precise scientific experiment of graphene, it is always necessary to verify the thickness or number of layers of graphene. For exfoliated graphene flakes transferred to a Si wafer, the Si substrate is capped with a SiO_2 layer with a specific thickness normally ~300 nm. This is to facilitate a large contrast ratio between graphene and the substrate so that even single layer graphene is visible under an optical microscope.[5] For different thicknesses of graphene the contrast spectrum is different. Figure 15(a) shows optical microscopy images of exfoliated graphene flakes with different number of layers which are published in literature.[87] Figure 15(b) shows graphene flakes made in house by the author with a single layer flake surrounded by multilayer graphene flakes, from which the contrast difference between them is clearly demonstrated. This provides a simple and efficient way to obtain a rough estimation of the thickness of graphene flakes. It is also possible to identify the number of layers using contrast imaging. In Figure

15, the contrast images were taken by scanning white light illumination across the graphene sample.[87] Another technique, such as AFM, STM or Raman spectroscopy can be used together with the optical contrast method to determine the layer number of graphene flakes. Note that the contrast method is only applicable for exfoliated flakes on the special designed Si/SiO_2 substrates. For other types of graphene such as, CVD graphene and SiC graphene which are supported by other substrates, the contrast method is not effective.

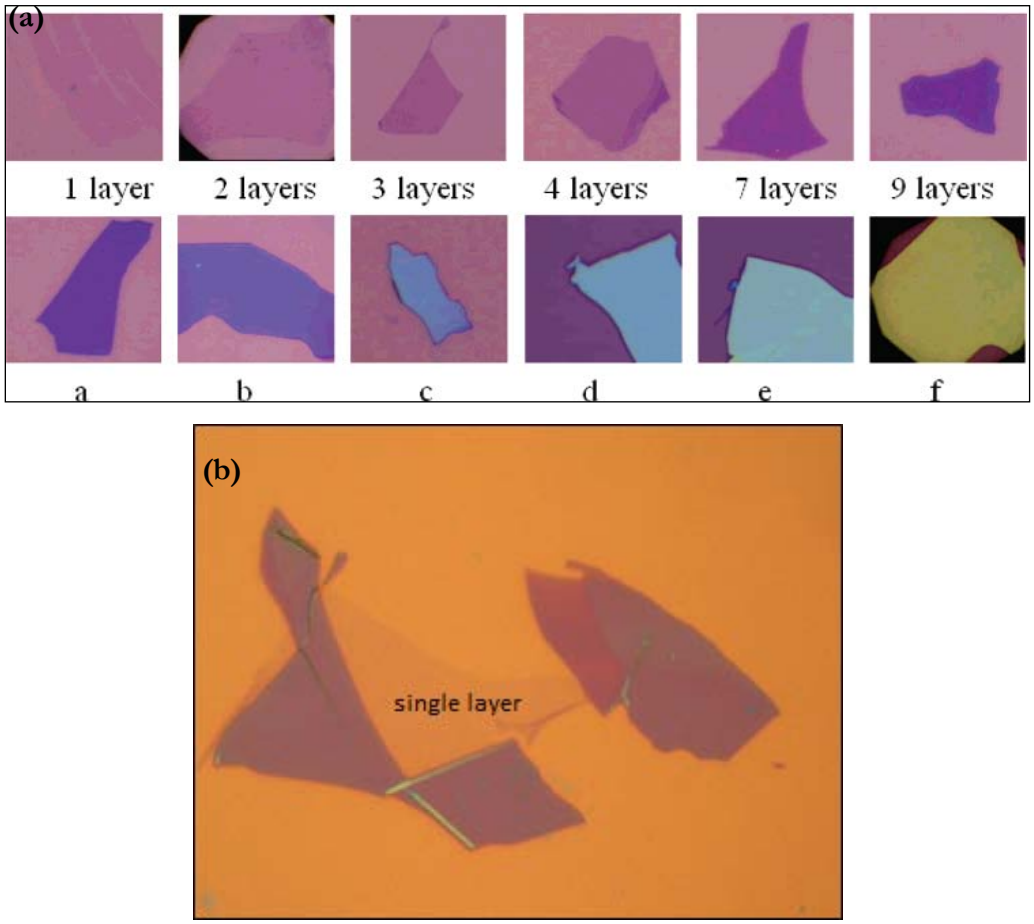

Figure 15. (a) Optical image of graphene flakes with different thickness. A to f are flakes with thickness more than 10 layers and thickness increases from sample a to f.[87] (b) Optical image of single layer flake surrounded by thicker layer graphene flakes.

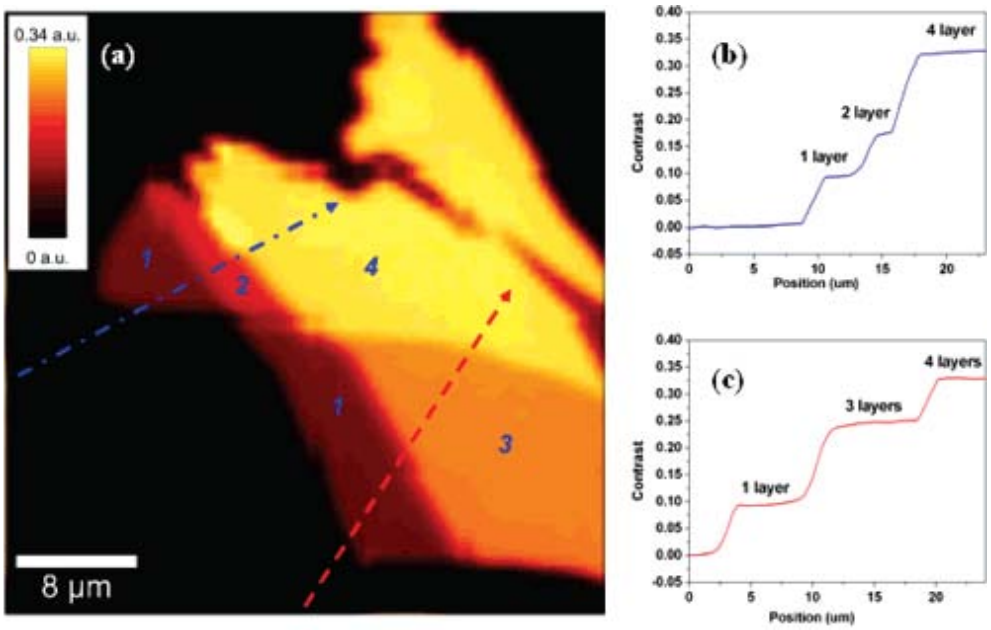

Figure 16.(a) contrast image of graphene flakes with different numbers of layers. (b,c) The contrast value of the graphene flake following the dash line. [87]

Among various techniques that can be used to measure the number of layers of gaphene, AFM in a tapping mode is the first one that has been utilized. The estimated average thickness of single layer graphene is 0.35 nm which is consistent with the interlayer spacing of bulk graphite.[5] However, the measurement results of graphene thickness vary from 0.35 to 1 nm.[88-90] The variation may be attributed to the presence of adsorbed oxygen or change in the interaction between the tip and sample for different set-up and environment.[88, 91] In scanning probe techniques some measurement error is often involved. Therefore, based on the experience of the author it is more reliable to confirm the results by another technique.

Besides AFM, STM is another scanning probe technique that can be used to verify the thickness of graphene and it is utilized in the experiments carried out with SiC graphene as discussed in this thesis. The atomic resolution of STM makes it appropriate for the identification of the number of graphene layer.[92, 93] The tip of STM is atomically sharp and can be brought very close to the sample surface. Typically the distance is only a few nanometer between the tip and sample.[94] A bias voltage will be applied across the sample and the tip. Due to the small gap between the tip and sample, electrons can tunnel through the potential barrier of the gap with

the applied bias. The gap distance and the tunneling current have an exponential relationship, which makes STM a technique competent to measure topography with an atomic resolution. In addition, STM is capable to image atomic and electronic structures of the sample surface.[94] To measure the topography of the sample, STM can work under two modes. One is a constant current mode in which the feedback loop will be used to monitor the tunneling current between the sample and tip. For increasing tunneling currents, the tip will be retracted, while for decreasing tunneling currents, it will be lower. The motion of the tip will be used to map the topography of the sample. The second mode is a constant height mode, in which the distance between the tip and sample is fixed. The change of the tunneling current will be used to deduce the STM image of the sample.

In order to characterize graphene with STM, the bias voltage should be kept at a relevantly low value (less than 0.4 V). For high bias voltages, instead of graphene, the underlayer substrate will contribute to the image.[94, 95] The verification of the number of graphene layer can be done by the examination of the atomically resolved STM image. It is shown that for single layer SiC graphene, the STM image shows hexagon protrusions, whereas for multilayer grahpene, it shows triangular array of protrusions,[93, 95] as shown in Figure 17.[96]

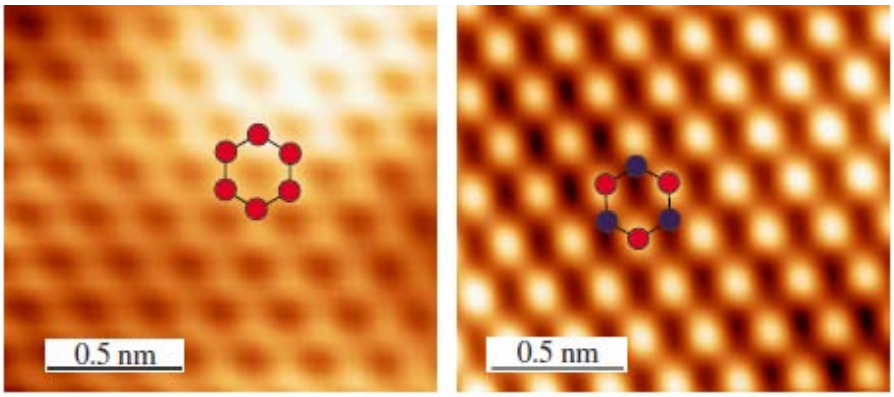

Figure 17. Atomically resolved STM image of single layer (left) and triple layer SiC graphene.[96]

In addition, the interface induced roughness decreases exponentially with increasing the graphene layer thickness. Thus, the thickness of graphene can be

confirmed through examining the interface induced roughness.[96] Figure 18 shows STM images taken on SiC samples with the number of graphene layer varying from 0 to 3. Figure 18(a) shows when no graphene is grown on SiC substrate. It can be seen that as the thickness of graphene increases, the interface induced corrugation reduces and the atomic corrugation of graphene lattice becomes clearer. The plot of interface induced roughness against the layer thickness of graphene is in Figure 19.[96] As discussed above, STM is an effective way to determine the layer number of graphene.

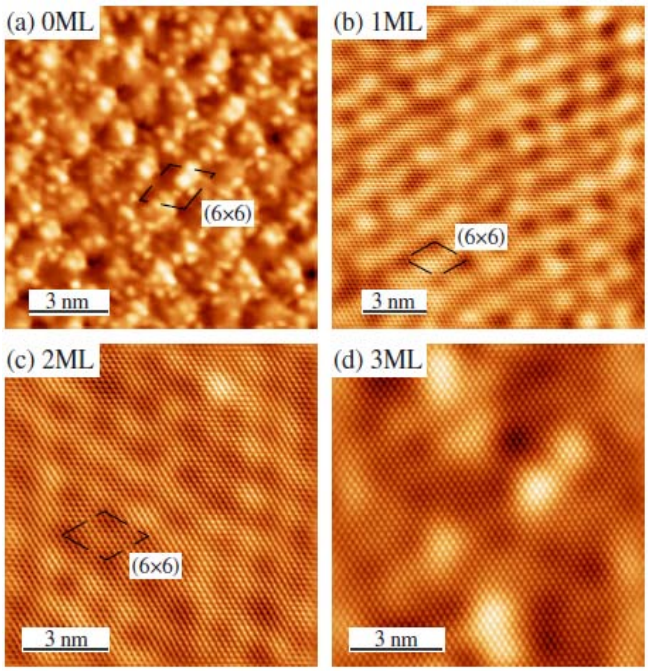

Figure 18. STM images of SiC graphene with thickness vary from 0 to 3 monolayer.[96]

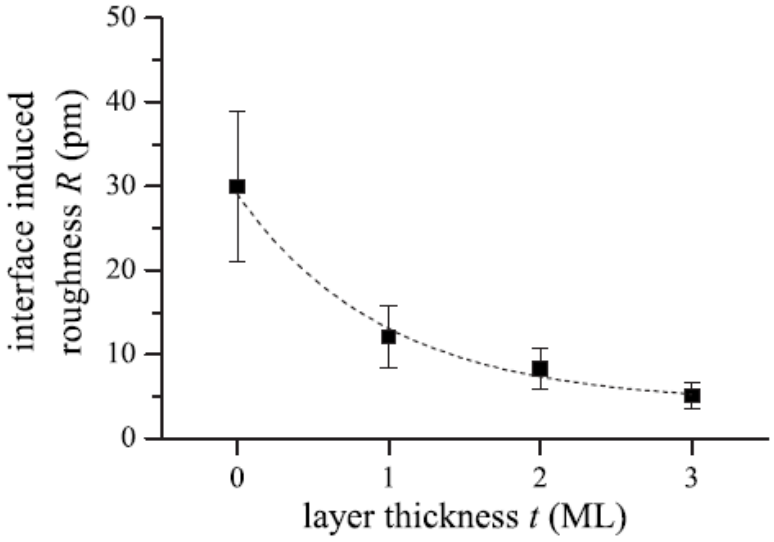

Figure 19. Plot of interface induced roughness versus number of layers of graphene.[96]

Among all the techniques that can be used to analyze the thickness of graphene films, Raman spectroscopy is an non-destructive one which has a high throughput and provides accurate results.[97] It has been extensively utilized in all the experiments of this thesis to confirm the number of layers of graphene. Raman spectroscopy is a spectroscopic technique used to study vibrational, rotational, and other low-frequency modes in a system based on inelastic scattering of monochromatic light.[98] The Raman effect is caused by the deformations of molecular under electric fields, and the deformation is determined both by the electric field and the molecular polarizability. The incident light beam is an oscillating electromagnetic wave which interacts with the sample and causes the formation of dipole which deforms the molecules. The periodical deformation causes molecules to vibrate under a certain vibration mode. Thus, one part of the energy of incident light will be absorbed and the reemitted light will have a frequency shift compared to the incident light.[99] The shift provides information about vibration, rotation and other low frequency transitions in molecules.

Raman spectroscopy is a very useful tool to characterize the structural characteristics and properties of graphene. It is an non-destructive and high throughput method to determine the number of layers in graphene thin films.[100] It

is also capable of monitoring the doping, defects, thermal conductivity and strain of graphene.[101-104] The Raman spectrum of graphene has some common features. The *G* and *2D* peaks should be always present for high quality graphene films; they are located around 1580 and 2715 cm^{-1} in the spectrum, respectively. For films with defect, a *D* peak at around 1350 cm^{-1} appears. The *G* peak corresponds to the E_{2g} phonon at the Brillouin-zone center. The *2D* peak is the second order of the *D* peak, which originates from a momentum conserved process, and thus it will still be present in a film without defects. For measurements under different conditions, for example with different laser wavelengths, the position of the peak will have a slight shift. With different carbon layer numbers, the *G* peak position will also shift and the *2D* peak will have difference in both the shape and position.[89] Figure 20(a) shows the Raman spectra of exfoliated graphene flakes with different carbon layer numbers on top of the standard Si/SiO_2 substrate made and measured in house by the author. One of the hallmarks to distinguish single layer from multilayer exfoliated graphene is the line width and shape of the *2D* peak.[100] Both the position and shape of *G* and *2D* peaks are examined carefully in our experiments to confirm the layer number of CVD and SiC graphene samples. For a single layer graphene film, the *2D* peak will have a narrow line width of ~ 30 cm^{-1} with a single Lorentzian profile fit.[100] However, for CVD graphene transferred on arbitrary substrate, an electronic coupling between graphene layers may not be present, therefore the *2D* peak may appear to be the same for single layer and few layer graphene films.[17] Thus in our experiment, besides examining the Raman spectrum, we also measured the transmission spectrum of the sample to verify the number of layer. The experimental results showed that an additional layer of graphene film will introduce an increment in absorption of ~ 2.3% for both exfoliated and CVD graphene.[12, 18] The Raman spectra for graphene supported by different substrates are also different. For SiC graphene, the substrate introduces additional peaks in the interested spectrum range. Similar to exfoliated and CVD graphene, single layer epitaxial graphene has some unique characteristics in its Raman spectroscopy data that distinguish it from that of multilayer graphene. The *2D* peak of single layer graphene is wider which is ~ 60

cm^{-1} compared to that of exfoliated graphene. However, it is narrower than that of double layer graphene which is ~ 95 cm^{-1}.[105] Thus, the width of *2D* peak is examined first in this work followed by analyzing the position of both the *G* and *2D* peaks, since an increment of the layer number will cause a shifting of them to lower frequencies.[105] As mentioned before, STM is used together with Raman spectroscopy to verify number of layer of SiC graphene. Raman spectra of different thicknesses of graphene on SiC substrates are shown in Figure 20(b).[105]

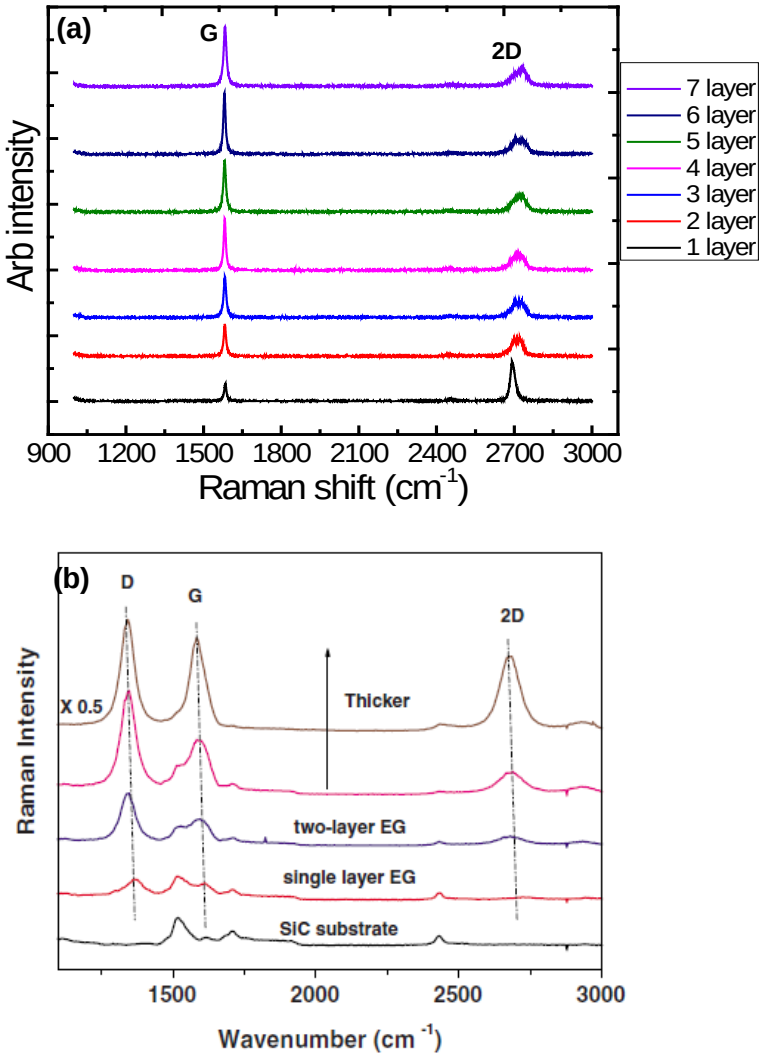

Figure 20. Raman spectra of graphene with different layer numbers on Si/SiO_2 (a) and SiC (b) substrate, excited by 488 nm (a) and 532 nm (b) lasers, respectively.[89, 105]

2.3 Thin film and metal nanoparticle deposition

There are different techniques available to deposit thin films of metal or insulator on top of a substrate. The techniques that are used in this thesis are thermal evaporation and electron beam evaporation. The deposition process needs to be executed with great care, because it may cause the formation of defects in the graphene film.[106] Based on the experience of the author, an evaporator with a larger distance between the sample and source is often preferred to reduce the defects in the graphene film. In addition, the deposition of metals with higher melting points will induce higher defects level in graphene.

Thermal evaporation as stated in the name, heats up the material until it is vaporized and subsequently condenses to a thin metal film on the substrate surface placed above the source material.[107] A simple schematic of the thermal evaporator is shown in Figure 21.[107] The process is carried out in vacuum under a low pressure, so that the vaporized particles travel directly from the source to the substrate surface. Among various ways to heat up the source material, in the experiments of this thesis, resistance heating is utilized in which a current passes through a metal plate on which the source material is hold. Thermal evaporation is also used to fill the holes of graphene nanomesh patterned by electron beam lithography to form particles with a diameter of ~ 100 nm.

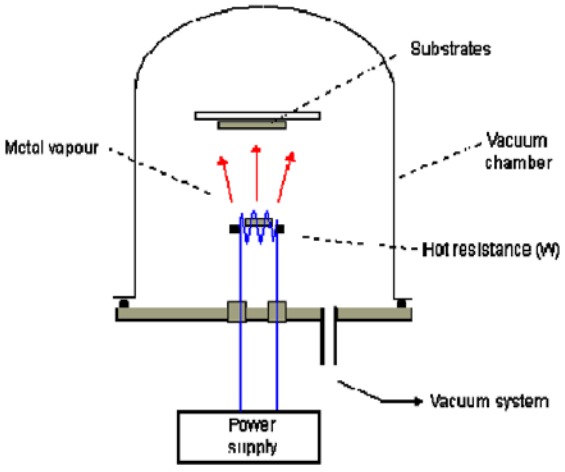

Figure 21. Schematic illustration of a thermal evaporator[107]

The similarity between thermal and electron beam evaporation is that they both heat up the source material until it vaporizes. A schematic of the electron beam evaporation is shown in Figure 22.[107] However, in electron beam evaporation, electron beam are directed to bombard the source material to vaporize it. The electron beams are generated from an electron gun and directed to the substrate by applying a very high potential difference between the filament and the substrate. Magnetic field is used to curve the trajectory of electron beam towards the position of the sample substrate. In the experiments of this thesis, a thin Al film is deposited by electron beam evaporation. The thickness of the film was kept under 3 nm and it was naturally oxidized under ambient conditions to form an Al_2O_3 thin film. The thickness of the Al thin film is monitored by quartz crystals in the evaporator and later confirmed by an ellipsometer.

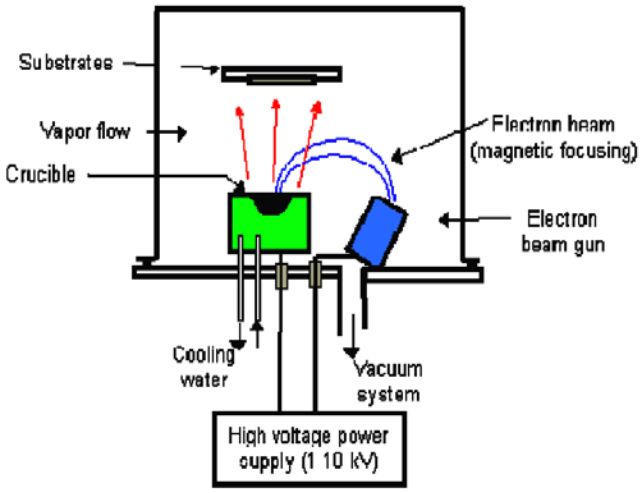

Figure 22. Schematic illustration of an electron beam evaporator[107]

In addition to the deposition of thin metal films, evaporators also play an important role in creating metal nanoparticles on the graphene surface. The formation of metal nanoparticles on top of graphene film by annealing evaporated thin metal films has been done by different research groups.[108-110] Their results show that the formation of gold nanoparticles on graphene films with different layer numbers can even help to identify the number of layers of graphene. It is also shown the potential of graphene to be utilized in synthesis of clean and densely packed nanoparticles without aggregating, which could be valuable in various

applications such as optics, nanofluidics, information storage, and electronics applications.[110] As has been mentioned before, metal nanoparticles are made in the vicinity of graphene film in order to study the electromagnetic coupling between graphene and metal nanoparticles. The formation of metal nanoparticles through the process of depositing metal thin film followed by annealing has been studied. Figure 23 shows SEM images of nanoparticles formed on single and double layer graphene. The author found that increasing layer number of graphene, longer annealing time, and thicker metal film result in a larger particle size. Metal nanoparticles can also be formed without the annealing process. The formation of nanoparticles will be possible, when the surface of sample is hydrophobic to the metal deposited and the thickness of the deposition is very thin.[111] For the experiments in this thesis, the formation of gold nanoparticles is done by either deposition of very thin gold on top of single layer graphene only or both deposition and annealing processes. The size and distribution of the nanoparticles are examined by scanning electron microscopy.

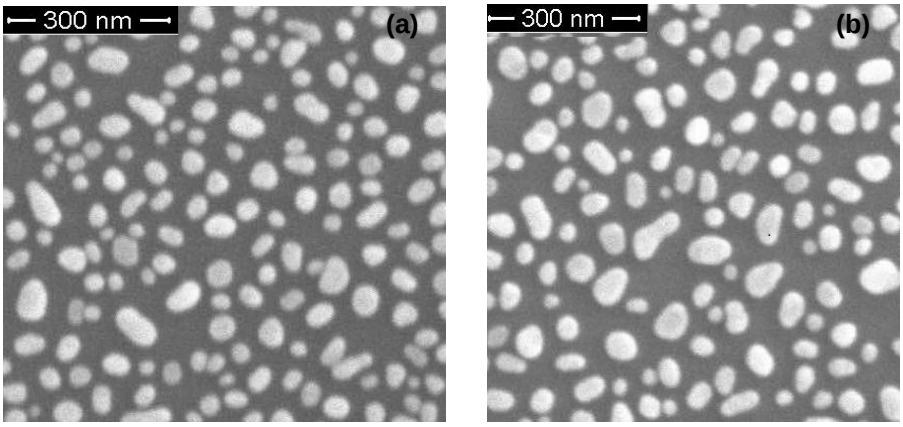

Figure 23. SEM of silver nanoparticles formed on single (a) and double (b) layer exfoliated graphene flakes.

2.4 Patterning method

Patterning of graphene films into nanostructures has been of great interest for researchers. because an energy gap is expected to be formed through the quantum confinement effect of graphene in a two dimensional or zero dimensional structure.[112, 113] Thus far, a variety of graphene nanostructures have been successfully made, such as, nanoribbons, quantum dots or nanomeshes.[114-117] And various techniques have been utilized to pattern graphene, for example, lithographic, chemical and sonochemical methods.[90, 113, 114, 118] Among the techniques that have been used, electron beam lithography is one that has been utilized very often. For the experiments of this thesis, graphene nanomesh has been patterned by electron beam lithography, as it is capable of patterning graphene nanostructure with various shapes, sizes and periods. Different groups have made graphene nanoribbons with electron beam lithography and their results show that by controlling the width of the nanoribbon, the bandgap can be engineered.[90, 113] The relationship between the ribbon width and the bandgap is inversely proportional. [71,92] The electronic transport property of graphene nanoribbons has been prevously studied through the field effect transistor structure. Figure 24 shows a set of devices each with multiple ribbons of different widths.[113] The energy bandgap of the nanoribbons are measured under a low temperature. The relationship between the energy bandgap and the width of ribbon is plotted in Figure 24. [113]

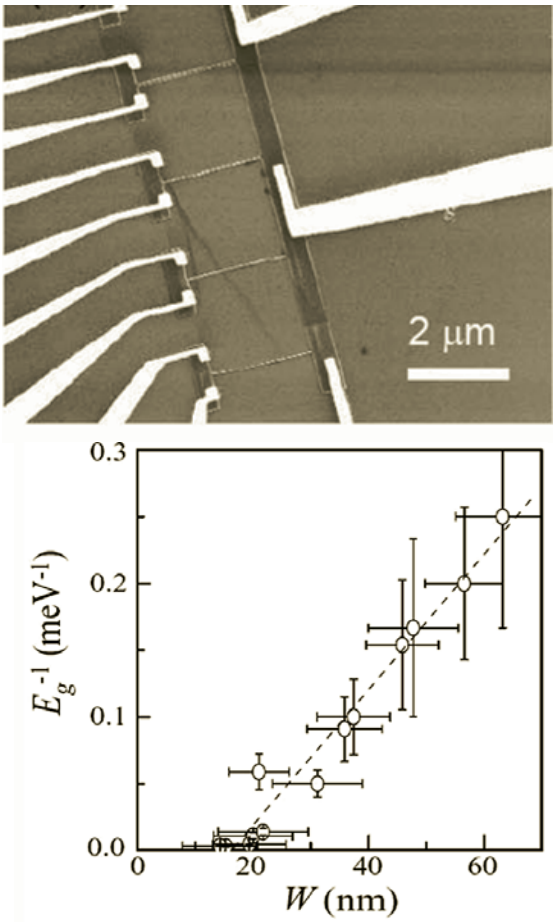

Figure 24. Top: SEM image of graphene nanoribbon device with many parallel ribbons and each device with varying width. Bottom: The plot of inverse energy gap vs. ribbon width.[113]

Although electron beam lithography offers an flexibility to pattern graphene, the process could introduce defects to graphene.[106] The electron beam can knock off graphene atoms, inducing reaction with the substrate or depositing amorphous carbon atoms, to cause defects in graphene films. [106] It is found that bilayer graphene is more stable compared with monolayer graphene under electron beam radiation. The defect level is also a function of dose introduced during the electron lithography process. A higher dose will introduce more disorder into the film. The quality of graphene is examined by Raman spectroscopy in which the presents of *D* peak indicates the formation of disorder in graphene film. The intensity of *D* peak will increase proportional to the level of disorder. Figure 25 shows a comparison between single layer graphene and bilayer graphene after exposing to electron

radiation for the same dose. The relationship between dosage and the induced disorder is also illustrated in Figure 26.[106] In the graphene nanomesh created in the experiments of this thesis, the PMMA/MMA double layer resist is used for the patterning. Arrays of periodic holes are patterned and developed, followed by oxygen plasma etching to remove graphene in the hole area thus creating nanomeshes. Since graphene in the hole area under direct radiation of electron beam will be removed, the disorder created by the direct electron beam radiation is not critical for this experiment. However, the electron beam radiation will still be able to cause defects to the graphene that is surrounding the hole area. Thus, the effective width of a graphene ribbon is narrower than the width observed under a microscope.[119] Therefore, the calibration of the dose and the acceleration voltage has been carried out carefully in the experiments in order to obtain the desired nanomesh structure. The dimensions of the nanomesh and nanoparticles are examined by AFM. The results of the above mentioned processes are discussed in chapter 5.

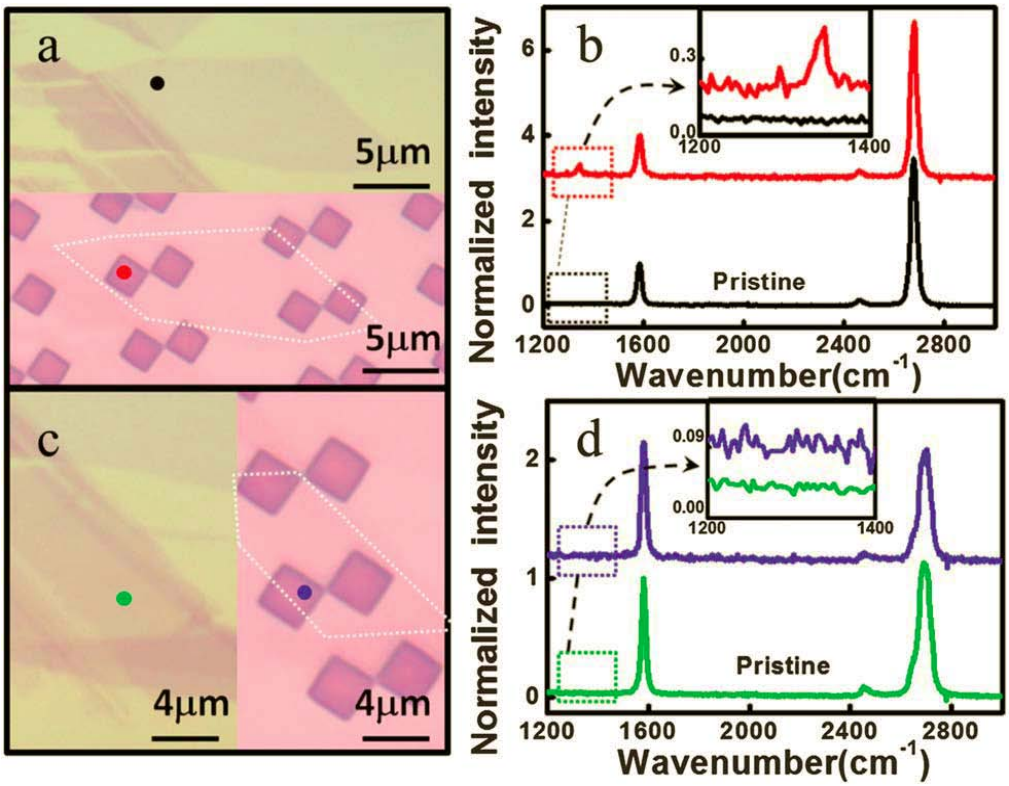

Figure 25. (a) (c) Optical images of single layer (bilayer) graphene before and after electron beam radiation. The lower (right) image shows graphene with resist after

development. The dosage applied is 0.004 nC μm^{-2}(b) (d)Raman spectra of single layer (bilayer) graphene before and after electron beam radiation.

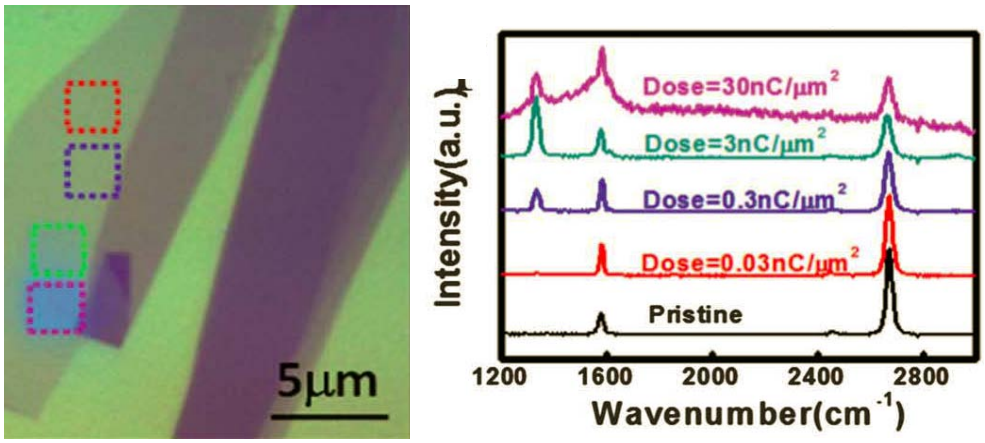

Figure 26. Left: Optical image of single layer graphene after electron beam radiation. The area in different squares are exposed with different dosage. Right: The Raman spectra corresponding to the squares corresponding to the same color codes.[106]

In addition to electron beam lithography, nanoimprinting lithography is another technique that is competent to make graphene nanostructures with a very small dimension. Graphene nanoribbons with a sub-20 nm width and nanomeshes with a sub-10 nm width were made by nanoimprinting.[120, 121] The procedures of the nanoimprinting include five steps. First of all, a polymeric resist for imprinting is spin coated on a graphene film. Secondly, the template with the inverse image of the desired structure is used to press onto the sample with the aid of elevated temperature. After that, the template is removed from the structure leaving the desired pattern on the resist. Subsequently, etching of graphene by oxygen plasma is carried out to remove the unwanted graphene area. Lastly, the resist is removed.[121] An illustration of the procedures of making graphene nanomeshes with nanoimprinting is shown in Figure 27. It is found that the on/off ratio of field effect transistor made of a graphene nanomesh is enhanced with reducing of the average ribbon width in the nanomesh structure. An opening of a bandgap in nanomesh is confirmed experimentally. The SEM image of the mesh structure is shown in Figure 28.[121] Nanoimprinting provides a quick turn-around time to produce multiple samples with the same dimensions compared to electron beam

lithography.[120] Therefore, nanoimprinting was utilized in our work to make nanostructures. As a new imprinting template needs to be made for any variation of the dimension of the nanostructure, nanoimprinting is more expensive and time consuming for this purpose.

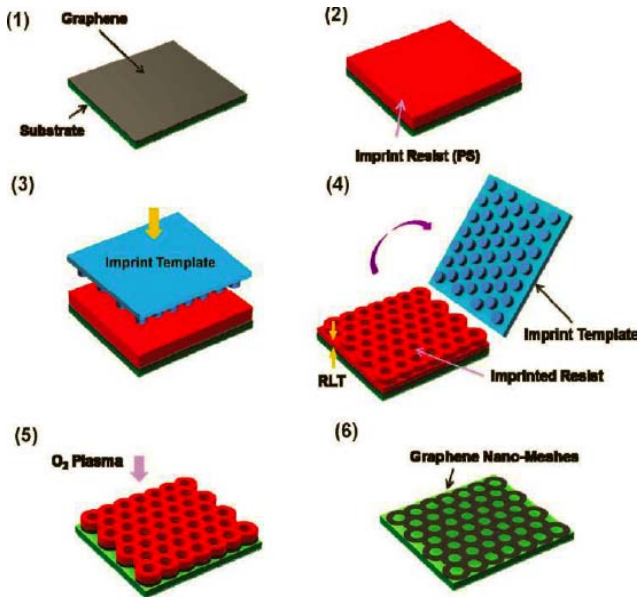

Figure 27. Procedures of nanoimprinting for making graphene nanomesh.[121]

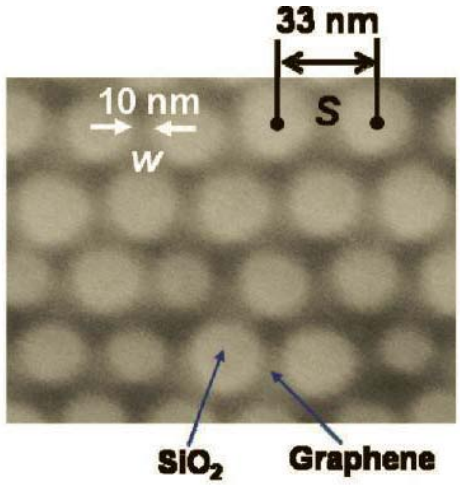

Figure 28. SEM image of graphene nanomesh made by nanoimprinting.[121]

In addition, laser interference lithography is an non-destructive nanopatterning technique especially suitable for large area periodic structures.[122] It is a comparably simply approach in which two coherent laser beams illuminate the photoresist simultaneously to form standing waves and create period structures. The

size of the structure can be adjusted by changing the angle of incident of the laser beams.[122] For this work nanomeshes were also made by interference lithography on CVD graphene. However, after the deposition of metal films and the lift-off process, graphene is also removed. Thus, electron beam lithography is finally chosen to generate nanopatterns for the experiments in this thesis.

In summary, for this work after making of CVD and SiC graphene films, the quality and the layer number were examined by Raman spectroscopy and STM. Only graphene films with fine quality were utilized in the experiments. For the deposition of thin films, electron beam and thermal evaporators are used. The thickness of the film is monitored by the quartz crystal in the evaporation machine and confirmed by an ellipsometer after the deposition process. The nanoparticles are made by the deposition of a very thin metal film on top of graphene. SEM images are taken to monitor the size and distribution of the nanoparticles. An image analyzing software is used to analyze the SEM image. The transmission spectra are taken by a UV-visible spectrometer for the lager patterned area or by a micro-spectrophotometer for a patterned area in the μm range. Raman spectra of the sample are taken after every step of the process to monitor the quality of graphene, and the change of Raman intensity to study the effect introduced by LSPR. Different approaches are tested to pattern graphene, and finally electron beam lithography is chosen to make graphene nanostructures with various sizes.

Chapter 3: Graphene induced tunability of surface plasmon resonance with very thin spacer layers

3.1 Introduction

As has been mentioned before, graphene is considered to be a promising candidate to replace ITO as transparent conductive electrodes in optoelectronics applications. Advances in large scale graphene synthesis methods enable the development of a graphene based touch-screen panel.[123, 124] LSPR phenomenon has been extensively studied recently due to the unique features and it also offers an interesting route to graphene based optoelectronic applications. LSPR in conventional systems is a result of collective electron oscillations excited by light in metal nanoparticles. It induces a strong confinement and enhancement of electric fields near the vicinity of metal nanoparticles.[125] The generation of LSPR stimulates various effects, such as surface enhanced Raman spectroscopy, plasmon enhanced fluorescence, and surface plasmon enhanced absorption in solar cells.[126-129] The plasmon resonance wavelength is a crucial parameter in all of these applications; therefore its tunability to a desired wavelength is greatly beneficial. This can be achieved by controlling size, shape, material of the nanoparticles, and the dielectric constant of the surrounding media.[130] Another effective way of realizing the tunability of LSPR is by the introduction of a metal film in the vicinity of metal nanoparticles. In addition, some other features exhibited by the interaction between a conducting film and metal nanoparticles make it an attractive candidate for nanophotonic applications. For example, the particle-film system functions as an effective optical antenna, capable of localizing the visible radiation to subwavelength dimensions in order to control the interaction between light and matter at the nanoscale.[131] Previously both theoretical and experimental studies proved the tunability of the LSPR

wavelength by changing the distance between metal nanoparticles and a metal film due to the change in the coupling strength of the electromagnetic field surrounding the particles and the metal film.[129, 132] In this experiment, we studied the tunability of the resonance wavelength of LSPR by varying the distance between graphene and Au nanoparticles in a very small length scale. It is estimated that every nanometer of change in the distance between graphene and the nanoparticles corresponds to a resonance wavelength shift of ~12 nm. The nanoparticle-graphene separation changes the coupling strength of the electromagnetic field of the excited plasmon in the nanoparticles and the antiparallel image dipoles in graphene.

3.2 Summary of experiments

A 1 cm × 1 cm single layer graphene thin film, grown by CVD on a copper film is transferred to a transparent borosilicate glass substrate. A Raman spectrum of graphene on a bare borosilicate glass substrate is shown in Figure 29(a). The *G* and *2D* peaks confirm the presence of graphene without detectable D peak suggesting the absence of microscopic disorder in graphene. The transmission spectra of a borosilicate glass substrate without and with graphene are shown in the inset of Figure 29(a). With a graphene layer on top of the glass substrate, the transmittance reduces by ~ 2%, which is comparable with the previously reported opacity of single layer graphene.[12] A layer of Al with a thickness less than 2 nm is deposited on top of the sample by an electron beam evaporator, followed by natural oxidation under ambient conditions. Al_2O_3 films of four different thicknesses are prepared in different areas of the same graphene sample. The thickness of Al_2O_3 is estimated to be 0.3, 0.7, 0.9, and 1.8 nm, respectively, by an ellipsometry technique. On top of the Al_2O_3 layer, 1.5 nm of Au film is deposited and the scanning SEM image shows the formation of Au nanoparticles as shown in the upper inset of Figure 29(b). The Au metal nanoparticles are spheres with a diameter of ~ 10 nm. Figure 29(b) illustrates the structure of the sample. The variation of the Al_2O_3 thickness shows no noticeable

difference in the average size of Au nanoparticles. LSPR is characterized by a UV-visible spectrophotometer in the transmission mode. An unpolarized light beam incident perpendicular to the sample surface is used as the LSPR excitation source.

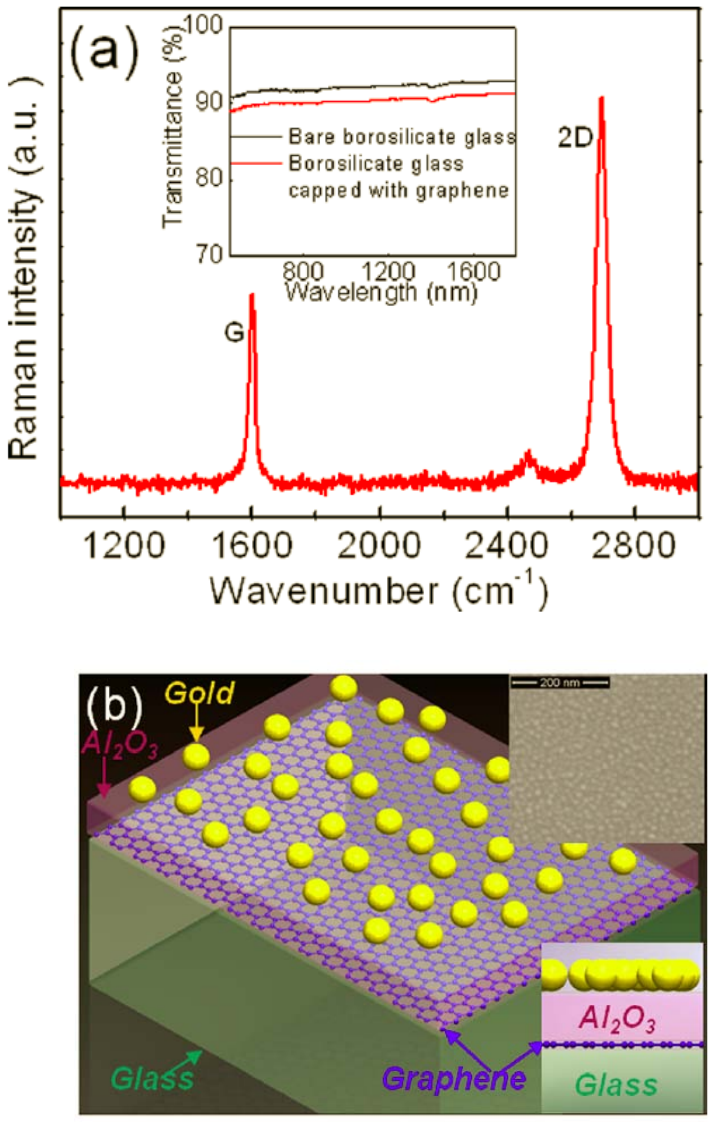

Figure 29. (a) A Raman spectrum of single layer CVD graphene using an excitation wavelength of 532 nm. The inset of (a) shows the transmisstion data of a borosilicate glass substrate without and with graphene. (b) An illustration of the sample structure. The upper inset in (b) is a SEM image of Au nanoparticles formed on top of Al_2O_3. The lower inset in (b) is the cross section view of the device structure.

3.3 Shifting of surface plasmon resonance with very thin Al_2O_3

The transmittance of the bare glass substrate with various thicknesses of Al_2O_3 remains at a constant value in the range of the measurement (400-1800 nm) as shown in Figure 30. A similar result is seen for graphene samples with various thicknesses of Al_2O_3 shown in Figure 31. After the deposition of Au nanoparticles on top of the Al_2O_3 layer, the transmission spectra are taken for both bare glass samples and graphene samples. An obvious difference in transmittance is observed between samples without and with a graphene film as shown in Figure 32 and 33, respectively. In Figure 32 the LSPR resonance dip of the bare glass substrate shows no noticeable difference despite the variation of the Al_2O_3 spacer layer thickness. The resonance wavelength is 569 nm, and the full width at half maximum (FWHM) of the dip is 128 nm. In contrast, for graphene samples in Figure 33, a blue shift of the resonance wavelength is observed with increasing the thickness of the Al_2O_3 spacer layer. By varying the spacer layer thickness from 0.3 to 1.8 nm, the resonance wavelength is shifted from 583 to 566 nm. This corresponds to a resonance wavelength shift of ~ 12 nm for every nanometer change in the distance between graphene and nanoparticles, which is a two fold increase in the tunability in comparison to that introduced by the silver nanoparticles and gold thin film system.[129] In addition, the FWHM of the dips decreases as the thickness of Al_2O_3 layer increases. Figure 34 illustrates the tunability of LSPR wavelength achieved by varying the thickness of the spacer layer between graphene and Au particles. Since the thickness of Al is very small and the deposition is performed at room temperature, Al_2O_3 may not be a continuous film. However, it is clear that the shift in the resonance wavelength and our conclusions are not affected because of the flatness of the system, supported by the results in Figure 30 to 33.

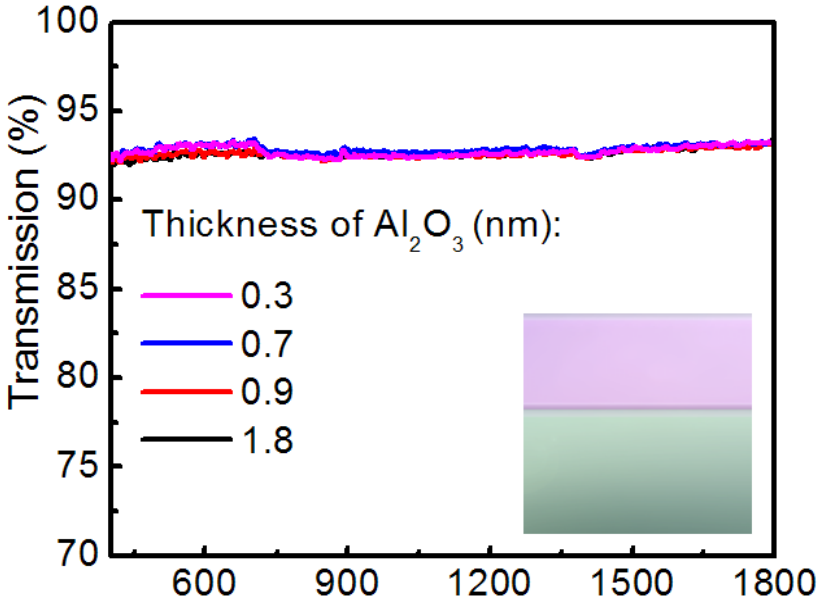

Figure 30. Transmission spectra of a glass substrate capped with different thicknesses of Al_2O_3. Inset: cross section view of the device structure. Purple color: Al_2O_3 layer. Green color: glass substrate.

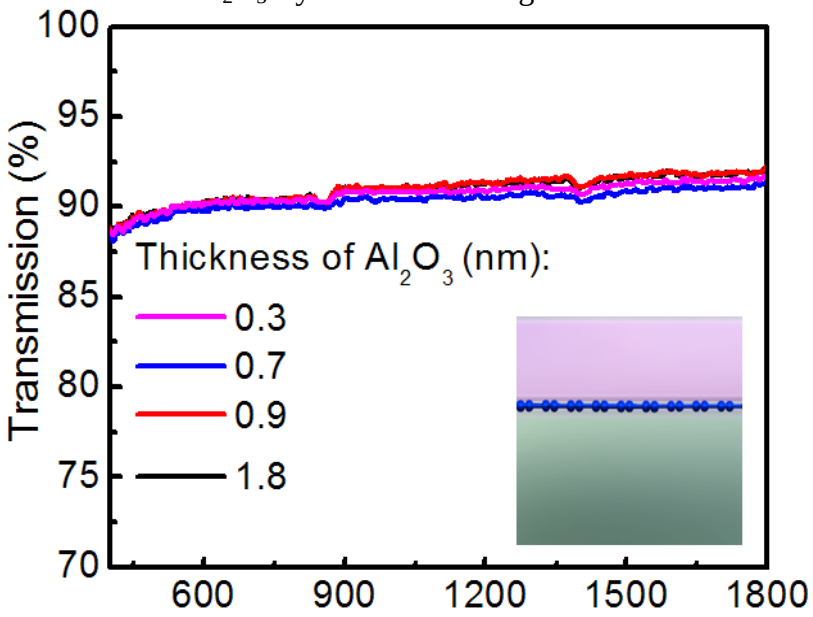

Figure 31. Transmission spectra from samples of glass/graphene/Al_2O_3. Inset: cross section view of the device structure. Purple color: Al_2O_3 layer. Green color: glass substrate.

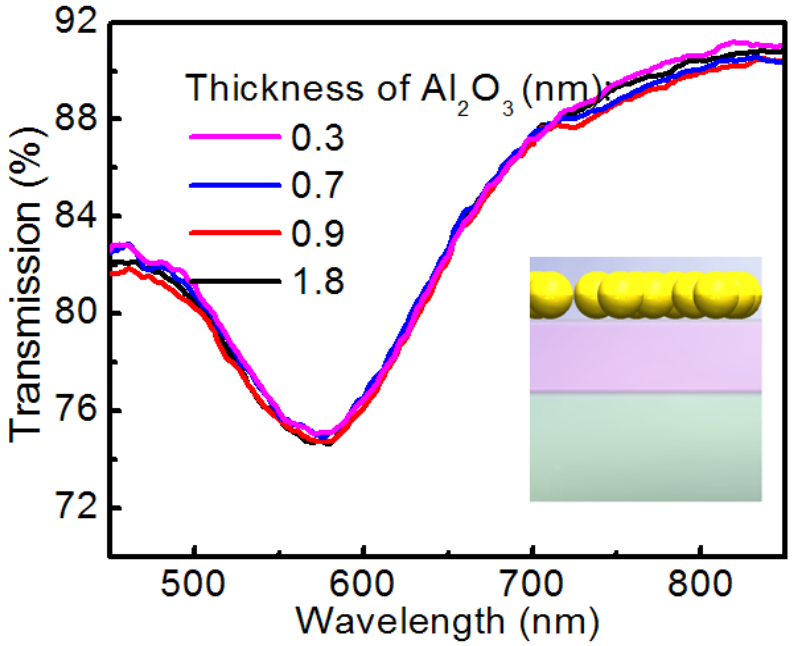

Figure 32. Transmission spectra from samples of glass/Al_2O_3/particles. Inset: cross section view of the device structure. Purple color: Al_2O_3 layer. Green color: glass substrate.

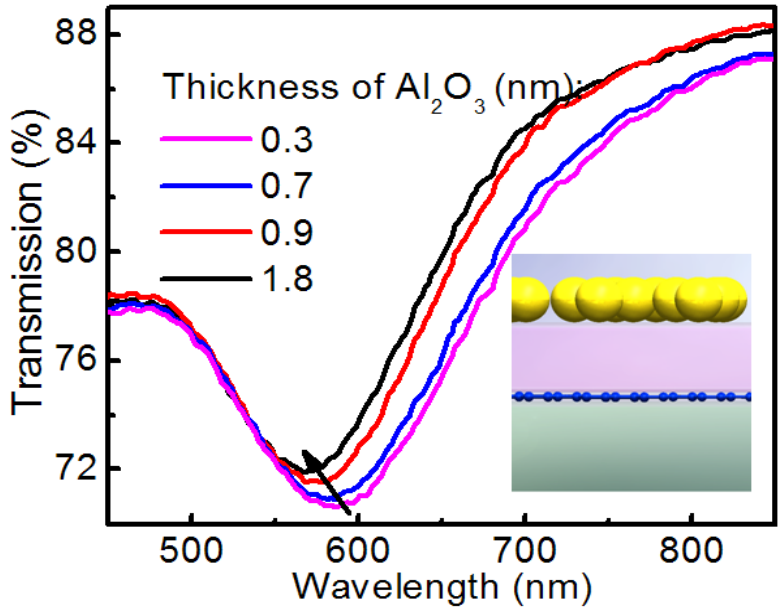

Figure 33. Transmission spectra from samples of glass/graphene/Al_2O_3/particles with various thicknesses of Al_2O_3. Inset: cross section view of the device structure. The arrow shows a shift in the resonance wavelength. Purple color: Al_2O_3 layer. Green color: glass substrate.

In order to evaluate the quality of graphene film after the deposition of metals on top of graphene, Raman measurements with a 488 nm excitation laser for different thicknesses of the spacer layer are carried out as shown in Figure 35.

Although a *D* peak is present in the spectra, there is no noticeable difference for different thicknesses of the spacer layer. Since the level of defect for different thicknesses of Al_2O_3 is similar, the defects are not the origin of the shifting of the LSPR wavelength. In addition, the graphene film is in the early phase of amorphization, according to the model by Ferrari and Robertson.[133] The in-plane correlation length (L_a) is estimated to be ~ 8.7 nm which is well above the limit of conductivity lost of graphene sheet. [134, 135] Therefore, the presence of defects does not affect the functionality of graphene as a conductive film below Au nanoparticles.

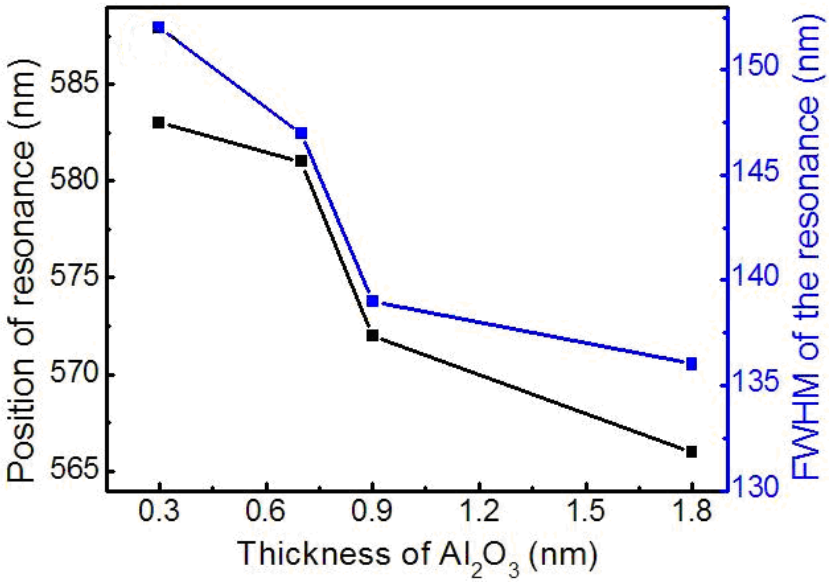

Figure 34. Dependence of the resonance wavelength and FWHM on the thickness of Al_2O_3.

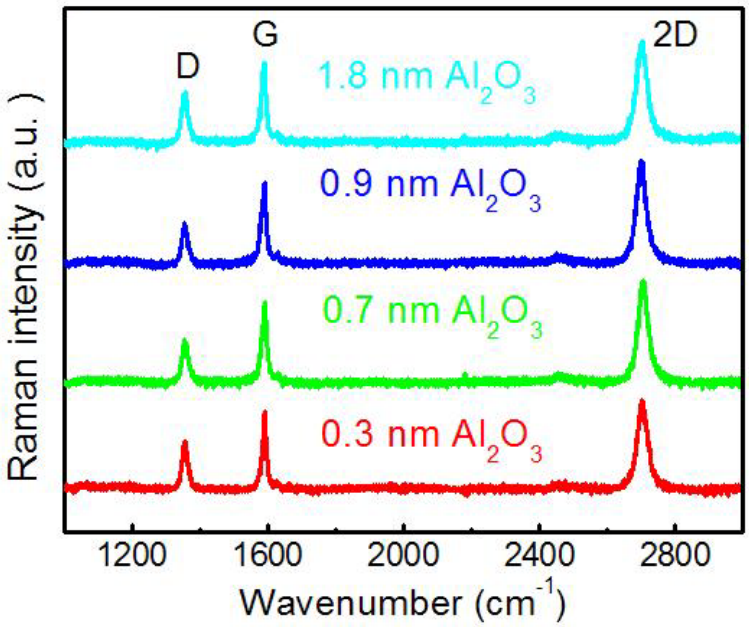

Figure 35. Raman spectra of graphene samples after the deposition of Al_2O_3 and Au nanoparticles.

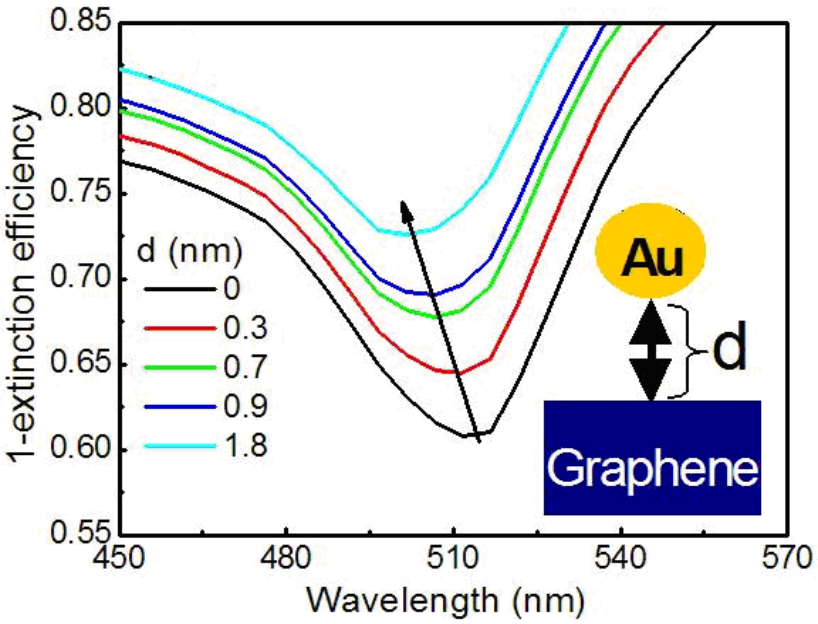

Figure 36. Calculation results of the surface plasmon resonance wavelength excited by vertical electric fields. Inset: the schematic configuration of the structure used for calculation.

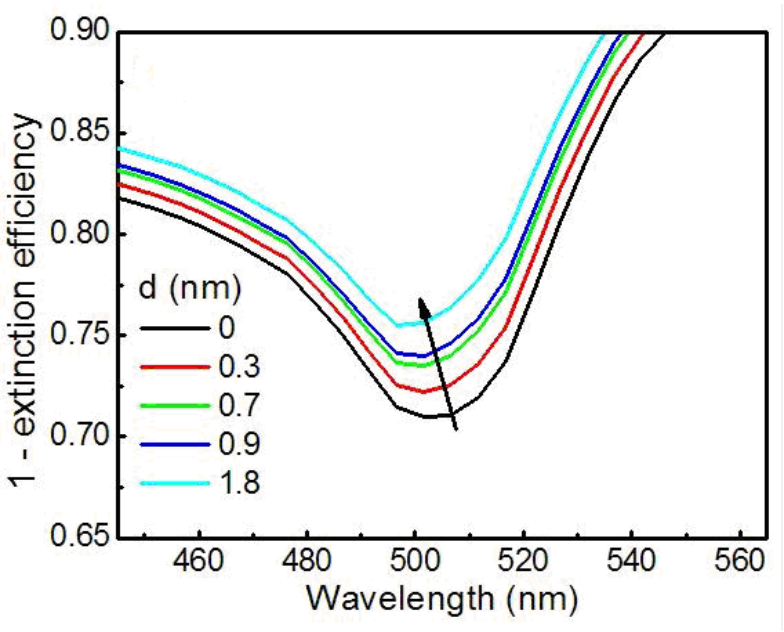

Figure 37. Calculation results based on lateral electric fields. The arrow shows a shift in the resonance wavelength.

3.4 Theoretical analysis

The wavelength shift in LSPR is caused by the coupling between the localized electromagnetic field surrounding the metal nanoparticles and the conducting film.[132] Since the incident unpolarized light beam is perpendicular to the sample surface, the electric field has no vertical component with respect to the sample surface, which means only lateral electron oscillations in the metal nanoparticles can be induced. When the distance between metal nanoparticles and the conducting film is small, an antiparallel image dipole will be formed in the conducting film. The presence of an antiparallel image dipole reduces the internal field in the nanoparticles, which results in a red shift of the resonance wavelength and the interaction between the dipoles decreases as the spacer layer thickness increases.[129] As a result, the resonance wavelength shows a blue shift with increasing the spacer layer. Therefore, our result infers the formation of laterally oscillating image dipoles in graphene. As proposed theoretically, the laterally oscillating image dipoles introduce less resonance shift as compared to the

vertically oscillating image dipoles.[132] To induce the vertically oscillating image dipoles, an electrical field with a component perpendicular to the sample surface must be present. For this purpose, the sample is titled for various angles (30°, 45°, and 60°) in our experimental setup and the transmission spectra are measured. But no additional resonance dip is observed and there is no observable change in the resonance wavelength compared to the case of zero tilting, suggesting that no vertical oscillating dipole is present in our sample.

Theoretical calculation based on dipole approximation has been carried out to compare with the experimental results. A schematic illustration of the structure for calculations is shown in the inset of Figure 36. A gold nanosphere is floating in air above a graphene substrate. The thickness of the substrate is assumed to be semi-infinite. The dielectric constant of graphene is based on an assumption that the optical response of every graphene layer is given by optical sheet conductivity.[136] The dielectric constant of gold is taken from literature.[137] A gold nanosphere is represented by a single dipole. Considering the formation of an antiparallel dipole in the substrate, the polarizability of the gold sphere is given by

$$\alpha = 4\pi a^3 \left(\frac{\varepsilon_1 - \varepsilon_2}{\varepsilon_1 + 2\varepsilon_2} \right) \left[1 - \beta \left(\frac{a}{2d} \right)^3 \left(\frac{\varepsilon_1 - \varepsilon_2}{\varepsilon_1 + 2\varepsilon_2} \right) \left(\frac{\varepsilon_3 - \varepsilon_2}{\varepsilon_3 + \varepsilon_2} \right) \right]^{-1} \quad (1)$$

in which α is the polarizability of the gold sphere, a is the radius of the sphere (5 nm), β is taken as 2 for the vertical electric field or 1 for the lateral electric field, and d is the distance from the edge of the gold sphere to the substrate surface.[132] ε_1, ε_2 and ε_3 are the dielectric constants of gold, surrounding media, and the substrate, respectively. The above equation is derived from the polarizability tensor equation for a small particle as stated below, accounting for the effect of coupling of the dipole to itself through an image dipole in the substrate.[138, 139]

$$\hat{\alpha} = \alpha_0 \left(\hat{I} - k^2 \frac{\alpha_0}{\varepsilon_0} \cdot \hat{G}\left(r_p, r_p \right) \right)^{-1} \quad (2)$$

where α_0 is the polarizability of a spherical particle, $\hat{I}$ is the unit dyadic tensor, *k* is the wave vector of incident light, ε_0 is vacuum permittivity, $\hat{G}^s\left(r,r'\right)$ is the dyadic Green's function that related to the substrate effect, and r_p is the position of the particle in the reference system. α_0 is given by

$$\alpha_0 = \varepsilon_0\varepsilon_2 V 3\frac{\varepsilon_1-\varepsilon_2}{\varepsilon_1+2\varepsilon_2} \tag{3}$$

in which *V* is the volume of the spherical particle. Lastly, with the electrostatic approximation of the Green's function $\hat{G}^s\left(r,r'\right)$, the equation of the polarization tensor becomes[140-142]

$$\hat{\alpha} = \alpha_0\left(\frac{1}{1+\xi\eta}\hat{x}\hat{x}+\frac{1}{1+\xi\eta}\hat{y}\hat{y}+\frac{1}{1+2\xi\eta}\hat{z}\hat{z}\right) \tag{4}$$

in which ξ is a introduced material parameter with $\xi=\left[\left(\varepsilon_2-\varepsilon_3\right)\left(\varepsilon_1-\varepsilon_2\right)\right]/\left[\left(\varepsilon_2+\varepsilon_3\right)\left(\varepsilon_1+2\varepsilon_2\right)\right]$, and η a geometrical parameter with $\eta=\left[a/\left(2d\right)\right]^3$. By substituting these two parameters inside the equation and introducing β to distinguish the vertical and horizontal electric field, equation (1) is obtained. The absorption efficiency Q_{abs} and the scattering efficiency Q_{sca} are given by $Q_{abs}=[k/\pi a^2]\mathrm{Im}\left(\alpha\right)$ and $Q_{sca}=[k^4/6\pi^2a^2]\left|\alpha\right|^2$, respectively.[132] The summation of these two gives the extinction efficiency, Q_{ext}. The calculated result of 1-Q_{ext}, which is proportional to the transmission value, versus wavelength for the vertical electric field is shown in Figure 36 and that of the lateral electric field is shown in Figure 37. Despite of only a single sphere in the calculation, the result is in good agreement with the experimental result, showing a blue shift of the resonance dip as the distance between a sphere and the substrate increases. A small difference in the surface plasmon resonance position between the calculation and experiment could be due to the assumptions in calculation such as a semi-infinite substrate and the structure difference between calculation and experiments.

Simulations using the Finite Difference Time Domain (FDTD) method were carried out as well. A 3D model was constructed based on the structure of the sample. The diameter of the particles was set as 10 nm with a center to center distance of 20 nm between them. The spacer layer is Al_2O_3. Similar to the experimental and theoretical calculation results, a blue-shift is observed when the thickness of the spacer layer increases, as shown in Figure 38.

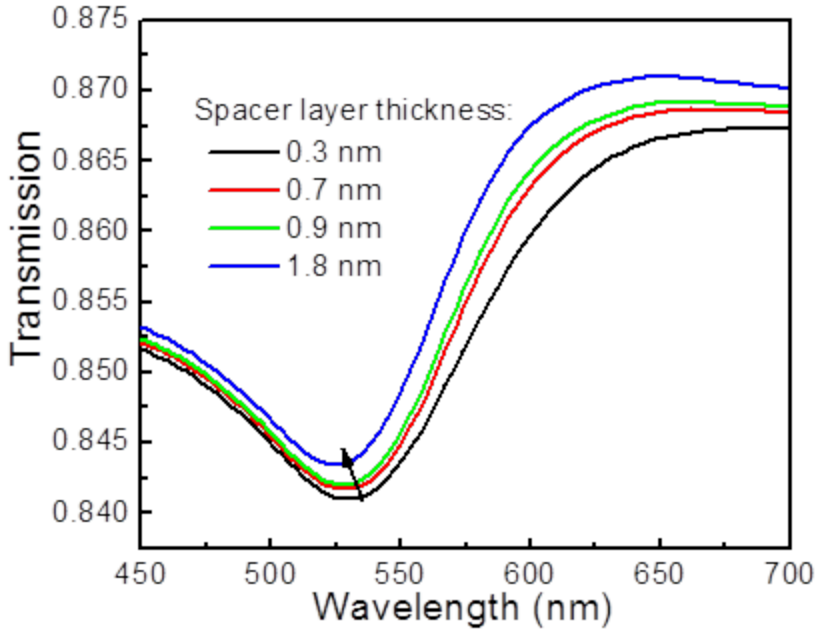

Figure 38. FDTD simulation results. The arrow shows a shift in the resonance wavelength.

3.5 Conclusion

The wavelength of localized surface plasmon resonance depends on the thickness of the Al_2O_3 spacer layer between graphene and Au nanoparticles. The tunability of the surface plasmon resonance wavelength is demonstrated by varying the thickness of spacer layer. By varying the spacer layer thickness from 0.3 to 1.8nm, a blue shift is observed in the resonance wavelength, which shifted from 583 to 566 nm. The observed phenomenon is attributed to the formation of oscillating image dipoles in graphene and the calculation result based on dipole approximation shows good agreement qualitatively with the experimental data. This is the first experimental demonstration of LSPR resonance tuning in the nanoparticle-graphene structure.

Chapter 4: Study of the electromagnetic coupling between graphene and Au nanoparticles with thicker spacer layers

4.1 Introduction

In the work discussed in the previous chapter, the results demonstrate the tunability of the LSPR resonance wavelength by adjusting the electromagnetic coupling between graphene and gold nanoparticles with very thin spacer layers (< 2 nm). In this chapter, we have investigated the coupling of the electromagnetic field between surface plasmon excited in gold nanoparticles and the anti-parallel image dipoles formed in graphene over thicker spacer layers (up to 35 nm). This is to observe the trend of the shifting until the electromagnetic field coupling is too small to cause any effect, and to acquire more insight for the phenomenon. As the spacer thickness increases from 0 to 15 nm, a blue-shift of the surface plasmon resonance from 599 to 570 nm is observed. This is similar as the phenomenon described by previous chapter and can be explained by the reduction of the coupling strength of the electromagnetic field of the excited plasmon in the nanoparticles and the anti-parallel image dipoles in graphene. The experimental results fit well with the plasmon ruler equation reported previously for the near-field electromagnetic field coupling.[143] The decay length is estimated to be 0.36. However, a further increment of the separation to 20 nm shifts the resonance wavelength back to a longer wavelength of 586 nm and the resonance wavelength saturates regardless of any further increment of the separation up to 35 nm. These findings facilitate a better understanding of the electromagnetic coupling and provide an opportunity of wavelength selection in the graphene/spacer/nanoparticle system which could be utilized in multicolor selective optoelectronic devices.

4.2 Experimental results

Single layer graphene grown by CVD on copper films is utilized in the experiment. The CVD graphene thin films are transferred to transparent borosilicate glass substrates for the transmission measurements. Before any experimental steps, it is essential to check the quality of the graphene film. The quality of the graphene on borosilicate glass substrates is examined by Raman spectroscopy. As shown in Figure 39, the absence of the *D* peak and a sharp *2D* peak illustrates high-quality single layer graphene [100]. The transmission data in Figure 40 without and with graphene show a difference of ~ 2.3%, which matches well with the opacity of single layer graphene [12]. A layer of Al thin film less than 3 nm is deposited on top of the graphene samples by electron beam evaporation, followed by natural oxidation under ambient conditions. In order to ensure that the Al thin film is fully oxidized into Al_2O_3, the above steps are repeated for a thicker Al_2O_3 film. The thickness of the film is monitored through quartz crystals during the deposition, and estimated by an ellipsometer after the oxidation process. Subsequently, a 1.5 nm Au film is deposited to form Au nanoparticles. The structure of the sample is illustrated in Figure 41. The size of the nanoparticles is examined by SEM as shown in Figure 42, and there is no observable difference in nanoparticles for various thicknesses of Al_2O_3. An image processing software, ImageJ is utilized to analyze the size of the nanoparticles. The average diameter of the spherical nanoparticles is ~ 10 nm with a standard deviation of 2.4 nm. The variation of the LSPR wavelength in Au nanoparticles is carried out through transmission measurements in an UV-visible spectrophotometer. An unpolarized light source is used to excite LSPR on Au nanoparticles and the incident light illuminates the sample perpendicularly. The excitation of LSPR on Au nanoparticles causes extinction of the transmitted light. Therefore, a dip is observed in the transmission spectrum at the resonance wavelength.

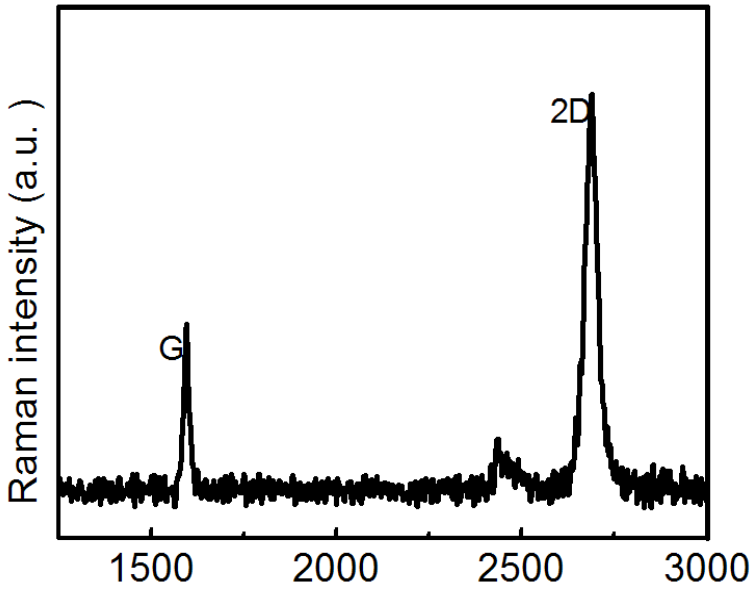

Figure 39. Raman spectrum of single layer CVD graphene with a 488 nm laser.

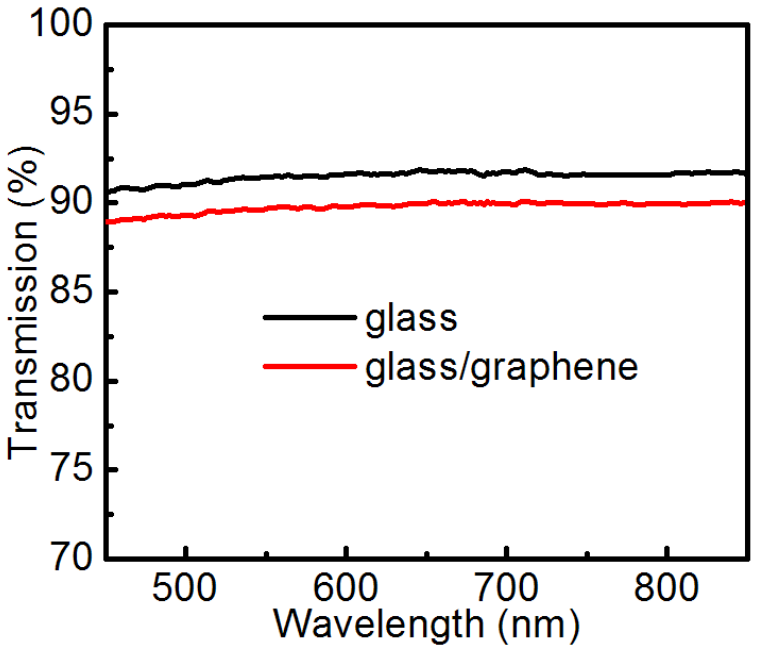

Figure 40. Transmission data of a borosilicate glass substrate without and with graphene.

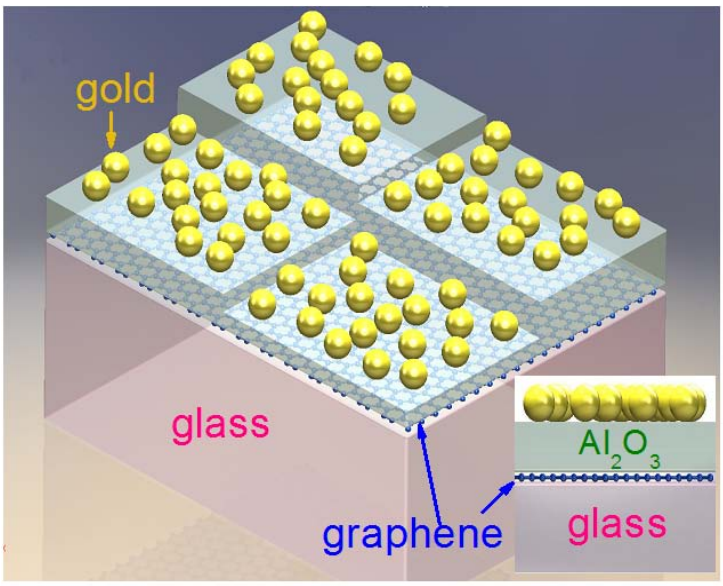

Figure 41. Illustration of the sample structure (inset: cross section view of the device structure).

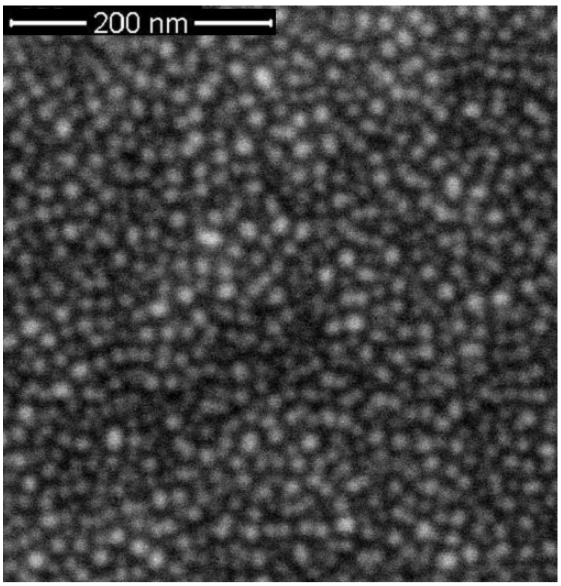

Figure 42. SEM image of Au nanoparticles formed on top of an Al_2O_3 spacer layer.

Seven different Al_2O_3 films from 5 to 35 nm are deposited on bare glass substrates and graphene samples. The samples without graphene function as control samples. All samples have been processed together to minimize any experimental error due to fabrication condition changes. The transmission spectra of the samples have been measured right after the oxidation process. As shown in Figure 43, the transmission spectra remain flat through the measurement range for glass samples capped with different thicknesses of Al_2O_3. The transmission difference is less than 3% between samples capped with various thicknesses of the Al_2O_3 film. A similar result is observed for graphene samples as shown in Figure 44 with slightly smaller transmission values due to graphene. After the formation of Au nanoparticles on the samples, the transmission spectra are measured again. Figure 45 shows the transmission spectra of samples without graphene. The presence of transmission dips and its position agrees well with the resonance wavelength of Au nanoparticles, indicating the excitation of LSPR.[144] A large red-shift of the resonance is observed, when a 5 nm Al_2O_3 layer is introduced between the glass substrate and the Au particles compared to the case when there is no Al_2O_3 in the structure. A further increment of the thickness of the Al_2O_3 layer from 5 to 35 nm induces a small red-shift (~ 9 nm) of the LSPR. The transmission spectra of graphene samples with various Al_2O_3 thicknesses are shown in Figure 46. Unlike the samples without graphene, a blue-shift of 29 nm is observed, when the thickness of the spacer layer increases from 0 to 15 nm. A further increment of the thickness to 20 nm causes a red-shift of the resonance wavelength and no further shifting is observed regardless of the increment of the spacer layer thickness.[140, 142]

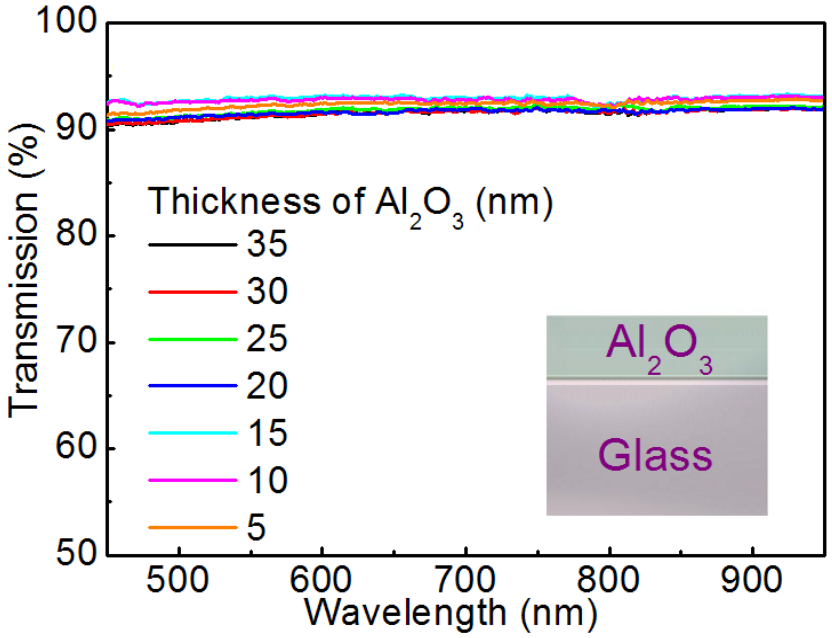

Figure 43. Transmission spectra of glass substrates capped with different thicknesses of Al_2O_3. Inset: shows a cross section view of the structure.

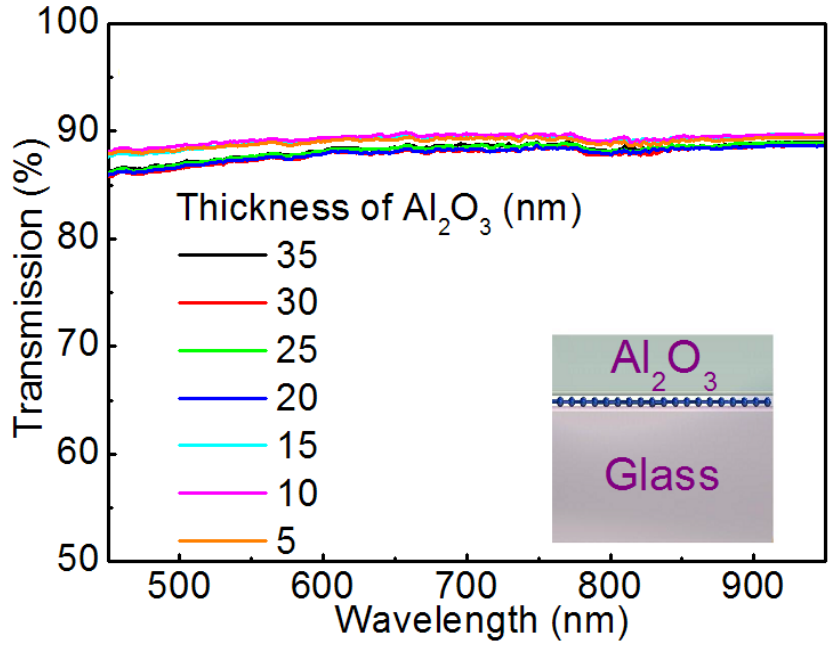

Figure 44. Transmission spectra from a structure of glass/graphene/Al_2O_3. Inset: shows a cross section view of the structure.

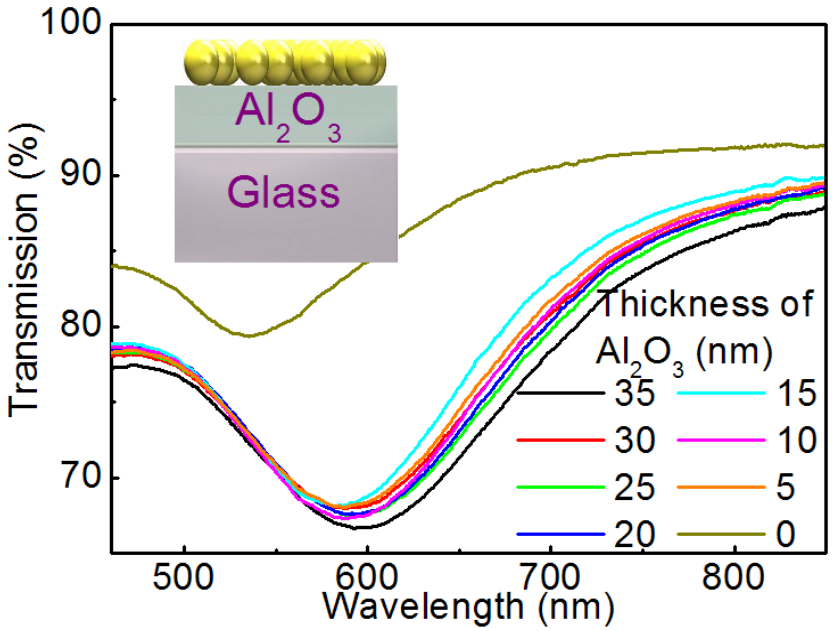

Figure 45. Transmission spectra from a structure of glass/Al_2O_3/particles. Inset: shows a cross section view of the structure.

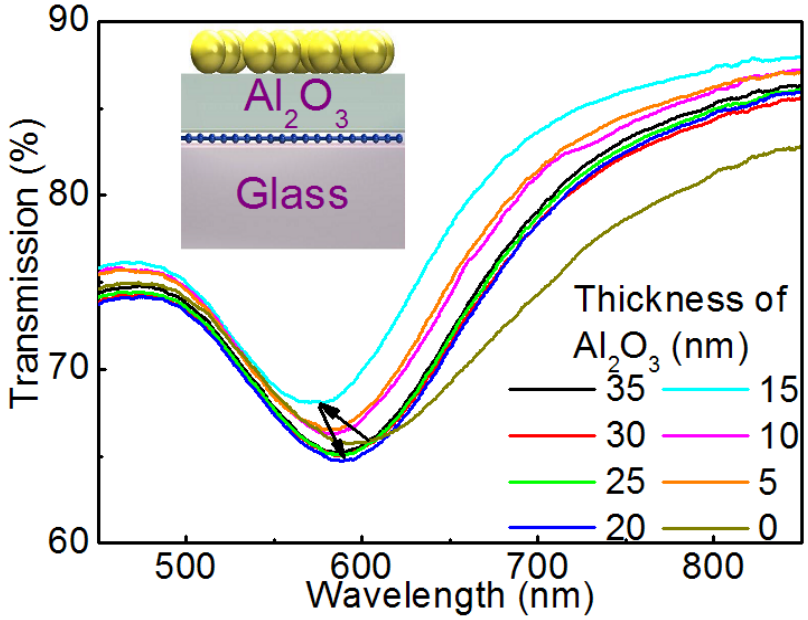

Figure 46. Transmission spectra from a structure of glass/graphene/Al_2O_3/particles with various thicknesses of Al_2O_3. Inset: shows a cross section view of the structure.

4.3 Theoretical analysis

Figure 47 shows the result of the theoretical calculation of the transmission value (1 − extinction efficiency) as a function of the separation between a gold nanosphere and a graphene substrate. The theoretical calculation is carried out based on dipole approximation, which is a common model to study the effect of a conductive film to the LSPR of metal nanoparticles.[145] The structure utilized in the calculation is shown in the inset of Figure 47, in which a gold nanosphere is placed above a graphene substrate with a separation of *d*. The dielectric constant of graphene is calculated by assuming that the optical response of a single graphene layer is given by the optical sheet conductivity, and the dielectric constant of gold is from the literatures.[137, 146] The calculated resonance wavelength as a function of the spacer layer thickness is shown in Figure 48 as a blue line. A blue-shift of the resonance wavelength is clear for thinner insulating layers (0 to 10 nm), however, the resonance wavelength saturates when the thickness increases beyond 10 nm. This model correctly explains the observed blue-shift, but does not describe the subsequent red-shift nor does the model predict the correct resonance wavelength. Such deficiencies are presumably due to the assumptions of the model. For example, only one nanosphere is included in the calculation instead of many nanospheres. It has been observed that when nanoparticles are in close proximity, the coupling of the surface plasmon modes of nanoparticles causes a red-shift of the resonance wavelength.[147-150] Simulations using the FDTD method have also been carried out. Similar to the theoretical calculation results, a blue-shift was observed as the thickness of spacer layer increases.

The experimental and calculation results of the resonance wavelength as a function of the spacer layer thickness are summarized in Figure 48. A different trend in the shifting of LSPR without and with graphene is obvious. For samples without graphene, a red shift of the LSPR can be explained by an increment of the relative permittivity of the physical environment, since the relative permittivity of Al_2O_3 is higher than that of glass and air.[130, 151] For samples with graphene, a

blue-shift can be accounted for by the coupling of the electromagnetic field between the particles and the conducting film.[129, 145] When LSPR is excited in the nanoparticles, an anti-parallel image dipole of the resonance is induced in the metal film. A stronger electromagnetic coupling between the nanoparticles and the metal film causes a longer resonance wavelength. As the separation increases from 0 to 15 nm, the coupling strength reduces resulting in a blue-shift in the resonance wavelength. A fit of our experimental data for spacer layer thickness from 0 to 15 nm by using an exponential equation is shown in Figure 49. The plasmon ruler equation is given by $\Delta\lambda / \lambda_0 = a \times \exp(-x/\tau) + y_0$, where a, τ (decay length), and y_0 are the fitting parameters. λ_0 is the shortest resonance wavelength, $\Delta\lambda$ equals to the change in wavelength compared to λ_0, x is given by the spacer layer thickness (d) over the diameter of nanoparticles (R) [143, 152]. The equation is initially proposed for the particle-particle system to study the plasmon coupling in nanoparticles pairs, and has been also used for particle-substrate system, since the image dipole in the substrate/metal film can be regarded as the actual charge in the other particle.[152] The fitting of our experimental data shows a decay length of 0.36, which agrees well with the decay length (0.3) of the particle-substrate system reported previously.[152]

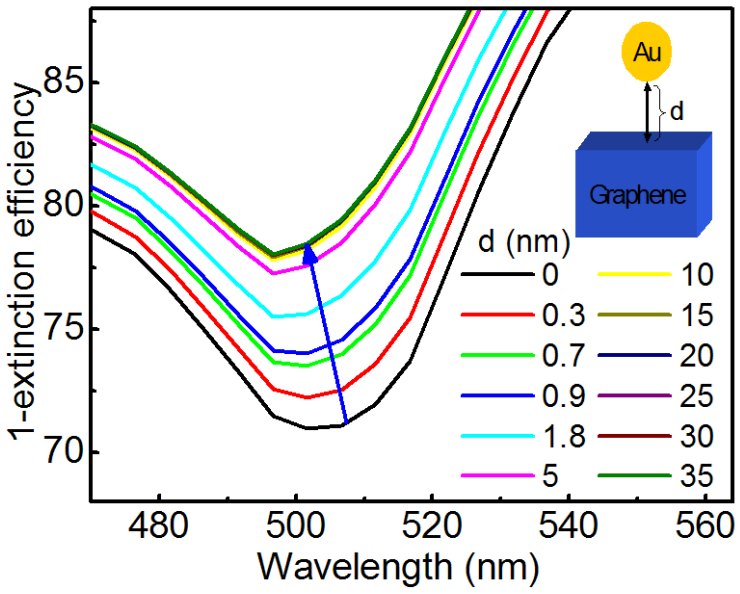

Figure 47. Calculation results of the LSPR wavelength excited by parallel electric fields (inset: structure used for calculation).

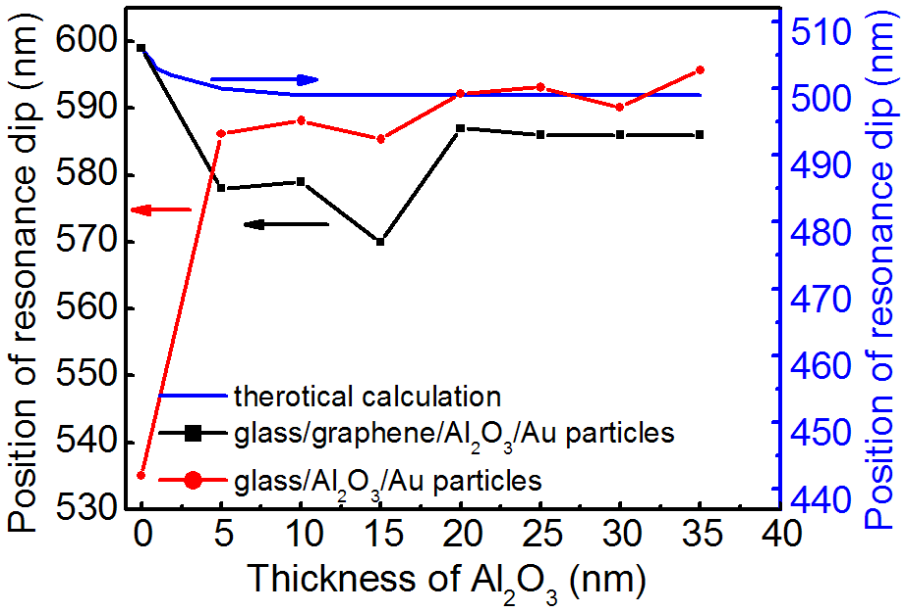

Figure 48. Dependence of the resonance wavelength on the spacer layer thickness for samples without and with graphene.

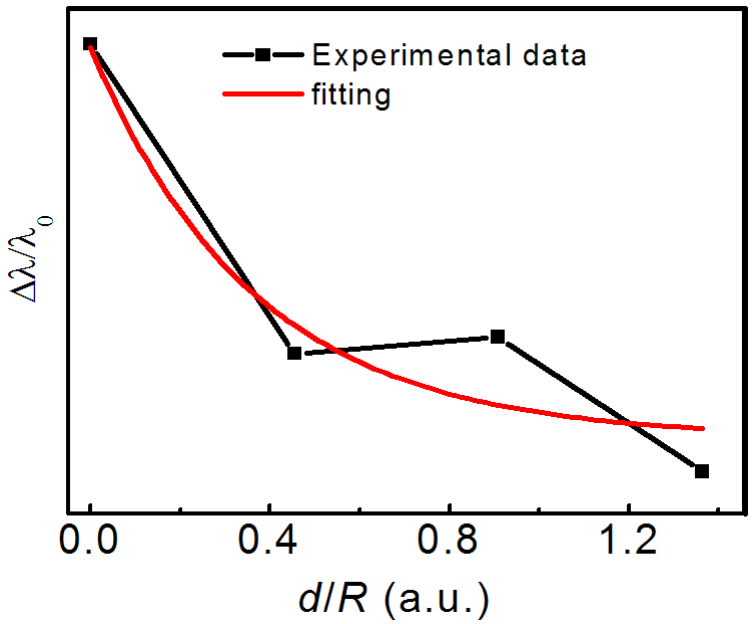

Figure 49. Fitting of experimental data with the plasmon ruler equation.

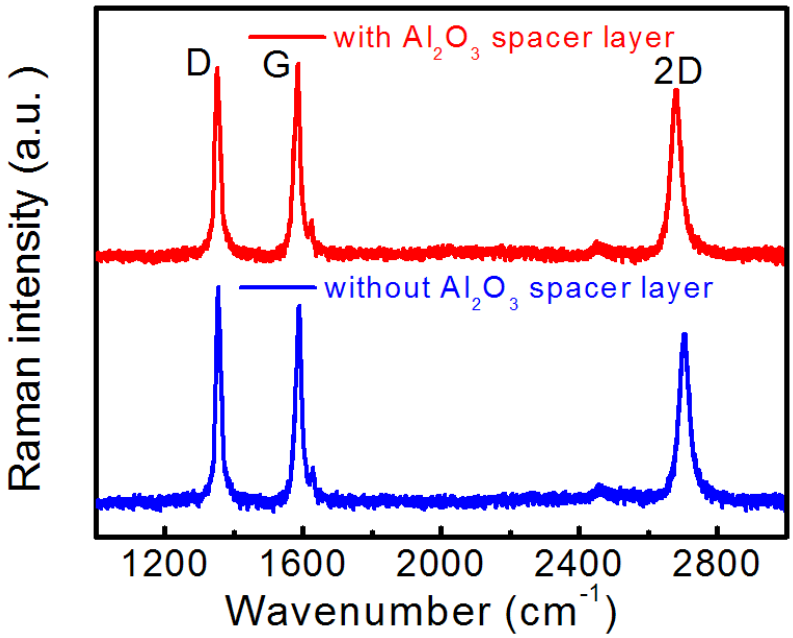

Figure 50. Raman spectra of samples after deposition processes.

A further increment of the distance between nanoparticles and graphene above 15 nm induces a red-shift and then a saturation of the resonance wavelength. The result is different from the previous studies of the two particles system and particle-substrate system, in which only blue-shift is observed with increasing of the spacer layer thickness.[143, 152] However, a similar effect has been reported for a silver nanoparticle and gold thin film system.[153] The blue-shift can be explained by the weakening of the coupling strength of the electromagnetic field as the distance between the particles and graphene increases. The reason of a red-shifting phenomenon could be very complicated, since for an intermediate spacer layer thickness, both the polarizability of the spacer layer and the charge response in the graphene film affect the LSPR of the metal nanoparticles [153]. In our theoretical model, the polarizability of the spacer layer is not considered. For large values of *d*, the resonance wavelength is expected to saturate to the value of the system without graphene. As shown in Figure 48, the resonance wavelength without and with graphene converges to a similar value for very thick spacer layers.

Raman spectra of the graphene samples after the deposition processes are measured as shown in Figure 48 to evaluate the quality of graphene. For graphene capped with different thicknesses of Al_2O_3, the spectra do not show any noticeable difference [64]. For a direct deposition of Au on top of graphene, a slightly smaller *G* to *D* peak ratio is observed as shown in Figure 50. This is reasonable since the evaporation of Au is performed at a higher temperature compared to the case of Al. Although a *D* peak is present in the spectra, the *G* and *2D* peaks are well preserved, demonstrating that the structural integrity of the graphene film is retained. The in-plane correlation length is ~ 4.3 nm and ~ 4.1 nm for graphene capped with and without a spacer layer, respectively [154]. The in-plane correlation length is much larger than the conductivity lost limit of graphene [135, 155]. Therefore, graphene can still function well as a conductive layer.

4.4. Conclusion

By adjusting the thickness of the insulating spacer layer between Au nanoparticles and a single layer graphene thin film, the wavelength of LSPR can be altered. As the separation between Au nanoparticles and graphene increases from 0 to 15 nm, the resonance wavelength has a blue-shift of ~ 29 nm. A further increment of the distance between these two parties causes a red-shift of the resonance, and the shifting saturates when the distance is more than 20 nm. This is the first time that the saturation of the shifting of LSPR wavelength induced by variation of the spacer layer thickness in the metal nanoparticle-graphene film system is achieved. In addition, the unexpected red-shift is also an interesting phenomenon which needs further investigation. Our study facilitates a comprehensive experimental study of the coupling of electromagnetic field of LSPR excited in Au nanoparticles and graphene, Furthermore, our results suggests a straightforward and effective way of achieving multicolor selection of graphene optoelectronic devices.

Chapter 5: Surface enhanced Raman spectroscopy of SiC graphene

5.1 Introduction

Raman spectroscopy is a common and non-destructive tool to characterize the structural characteristics of graphene. The number of layers of graphene can be easily distinguished by the evolution of the shape of the 2*D* peak, and the shifting of the peak position of both the 2*D* and *G* peaks.[89] It is also capable of monitoring the doping, defects, thermal conductivity, and strain of graphene.[104, 156-158] However, the Raman signal of graphene is not strong enough for some fine structural characteristics, such as vacancies, edge structures, and crumpling.[159] This is mainly due to the fact that for Raman scattering, the majority of the incident light undergoes Rayleigh scattering which does not contribute to the Raman signal, and the greater part of the incident light is transmitted through graphene without contributing to the scattered radiation.[159] Therefore, researchers are continuously working on new methods to improve the strength of Raman signal.

The substrate commonly used for mechanical exfoliated graphene is a Si substrate capped with a layer of SiO_2 with a specific thickness, which is designed for easier observation of exfoliated graphene under an optical microscopy. It is found that this special substrate structure not only enhances the optical contrast between graphene and the background, but also provides an enhancement of the Raman signal through interference-enhanced Raman scattering (IERS).[67] Hence, exfoliated graphene with the special Si/SiO_2 substrate always has a stronger Raman signal compared with epitaxial graphene on a SiC substrate. Epitaxial graphene on a SiC substrate is a promising candidate for electronic applications, since it provides a semiconducting substrate by default and comprises a uniform layer compared to CVD graphene.[43] In addition to IERS, SERS is another method that boosts the strength of the Raman signal.[160, 161] Thus far, most of the research studies about SERS of graphene have been carried out on exfoliated graphene,

whereas no results have been published for epitaxial graphene on a SiC substrate. For SERS, metal nanoparticles are often included in the system to induce the primary mechanisms of the enhancement which is the localized electromagnetic field surrounding the nanoparticles caused by LSPR.[162] Two main mechanisms of SERS are chemical enhancement, which requires a direct contact between graphene and nanoparticles, and electromagnetic enhancement.[163-165]

In this experiment, a layer of Al_2O_3 with various thicknesses is inserted between graphene and Au nanoparticles to study the electromagnetic enhancement of SERS solely by eliminating the possibility of chemical enhancement of SERS caused by charge transfer. In addition, through variation of the thickness of Al_2O_3 the effect of the spacer layer on SERS can be studied. The experimental result of the enhancement factor as a function of the excitation laser wavelength agrees well with the theoretical calculation of the extinction spectrum of LSPR, providing a selection guide to laser wavelengths in order to obtain the maximum SERS of graphene. Furthermore, an exponential relationship between the thickness of the Al_2O_3 insulating layer and the electromagnetic enhancement factor is observed.

5.2 Summary of experiments

The graphene used in our experiment is single layer graphene thin films grown on a Si-terminated 6H-SiC (0001) surface. The film thickness is confirmed by STM followed by Raman spectroscopy.[163, 166, 167] Metal nanoparticles are formed by evaporating a thin Au film (5 nm), followed by annealing in 500 °C under an N_2 environment for 20 min. The fabrication processes are shown in Figure 51(a). The SEM images of metal nanoparticles formed on top of the sample with different Al_2O_3 thicknesses show no noticeable change in the average size of diameter (~15 nm). The inset of Figure 51(b) shows one of the SEM images of nanoparticles formed on top of the sample after annealing.

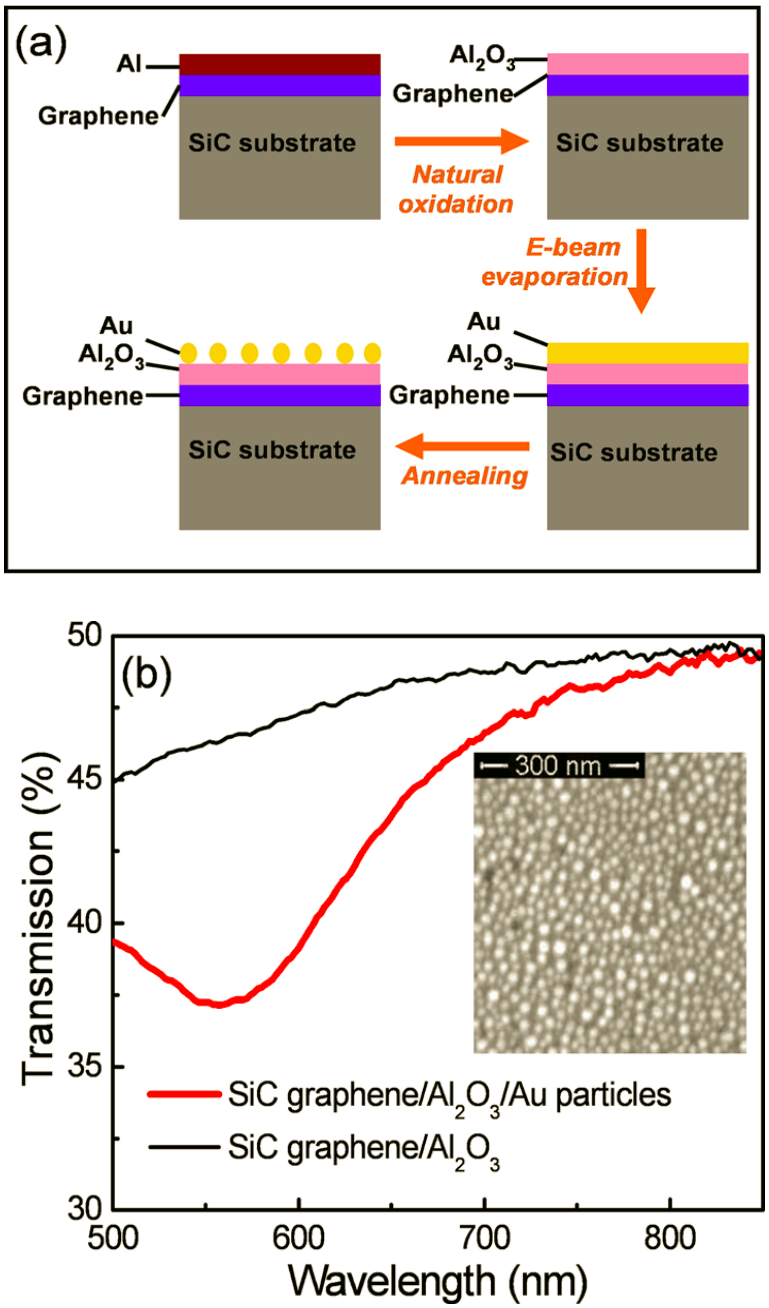

Figure 51. (a) Schematic illustration of sample fabrication process. (b) The transmission spectra of the area without and with Au nanoparticles on the same sample (inset: SEM image of Au nanoparticles formed on top of Al_2O_3).

The transmission spectrum shown in Figure 51(b) is obtained to verify the excitation of LSPR in the structure. The transmission spectra without and with Au nanoparticles show apparent differences. The transmission data with Au

nanoparticles shows an additional valley compared with that without nanoparticles. The minimum transmission appears at ~560 nm which matches well with the LSPR wavelength of gold nanoparticles.[168]

5.3 SERS with different lasers

Raman spectra of the same sample are taken with four excitation lasers with different wavelengths (325, 488, 532, and 785 nm) on the area without and with nanoparticles, as shown in Figure 52(a) and 52(b), respectively. The thickness of Al_2O_3 is 3 nm. The enhancement factor is calculated through two steps. First, the intensity of the *G* peak (~1580 cm^{-1}) for each spectrum is normalized with the SiC substrate peak at ~ 1519 cm^{-1}. The SiC substrate peak is comparable for samples deposited without and with nanoparticles under the same experimental conditions on the same sample; therefore this step allows us to get a more reliable comparison result. Then for each wavelength, the enhancement factor is computed by using the intensity of the *G* peak obtained with Au particles divided by that without particles. It is observed that the enhancement factor of *G* peak is always greater than 1, when the sample is capped with Au particles. Figure 52(c) shows the enhancement factors of four different excitation lasers, indicating the maximum enhancement with a 532 nm laser. Previously, detailed wavelength-scanned surface-enhanced Raman excitation spectroscopy (WS-SERES) and plasmon-sampled surface-enhanced Raman excitation spectroscopy demonstrated that the maximum SERS enhancement occurs when the excitation wavelength of the laser is slightly blue-shifted from the resonance wavelength of LSPR.[169-171] Considering the above observation and that 532 nm is the nearest laser wavelength to the surface plasmon resonance wavelength (560 nm) of Au particles, strong electromagnetic fields surrounding the Au particles induce more electromagnetic enhancement to the Raman intensity. However, an unexpectedly low enhancement factor is obtained, when the 488 nm laser is utilized. As 488 nm is rather close to the LSPR wavelength, its enhancement should be higher than the one obtained with either the 325 or 785 nm laser.

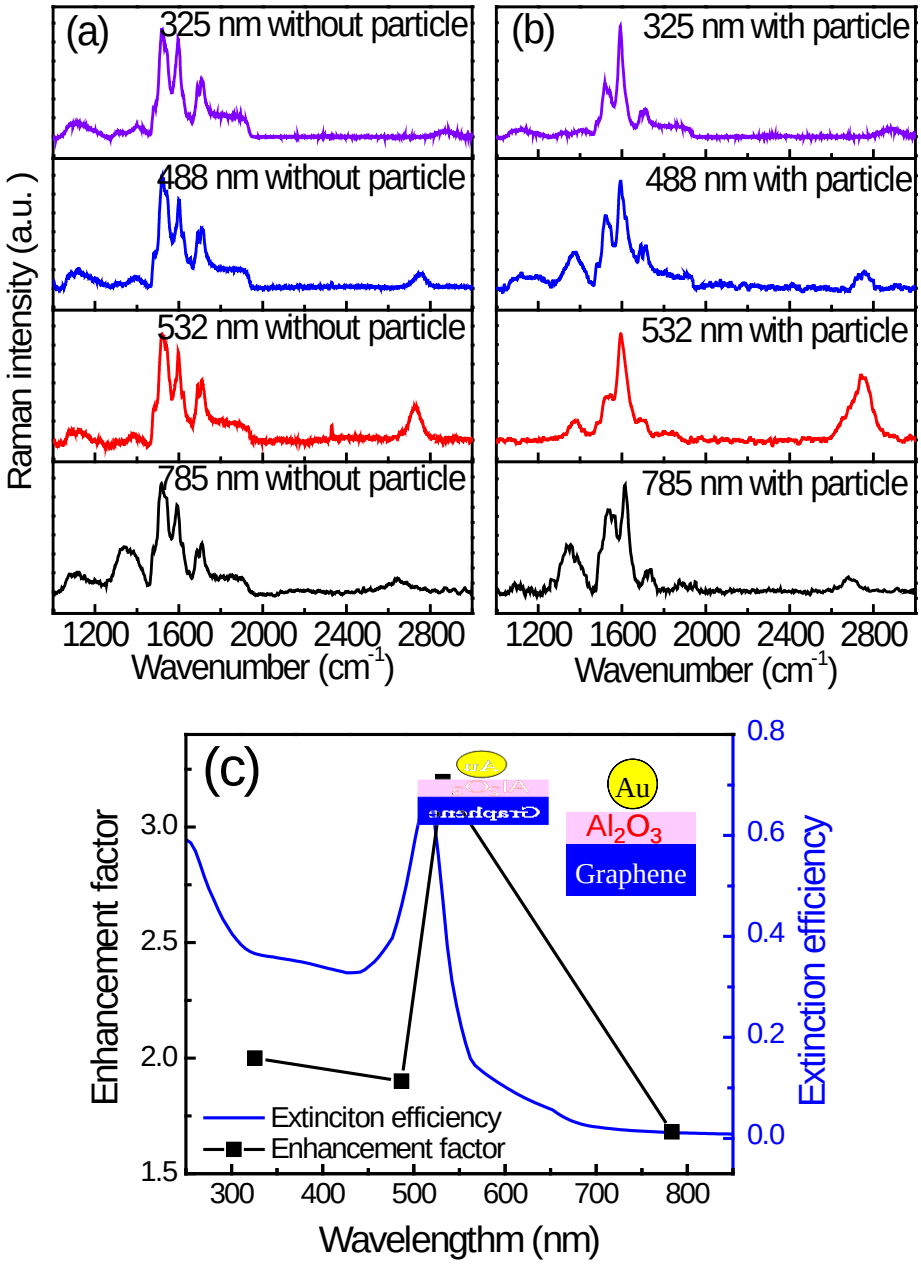

Figure 52. Raman spectra obtained on the same sample with different exitation laser wavelengths (325, 488, 532, and 785 nm) without (a), and with (b) nanoparticles. The thickness of Al_2O_3 is 3 nm. (c) Enhancement factor of the G peak and the calculated extinction efficiency of Au nanoparticles vs. wavelength of excitation lasers (inset: schemtic illustration of the structure used for therotical calculation).

5.4 SERS with different Al_2O_3 thicknesses

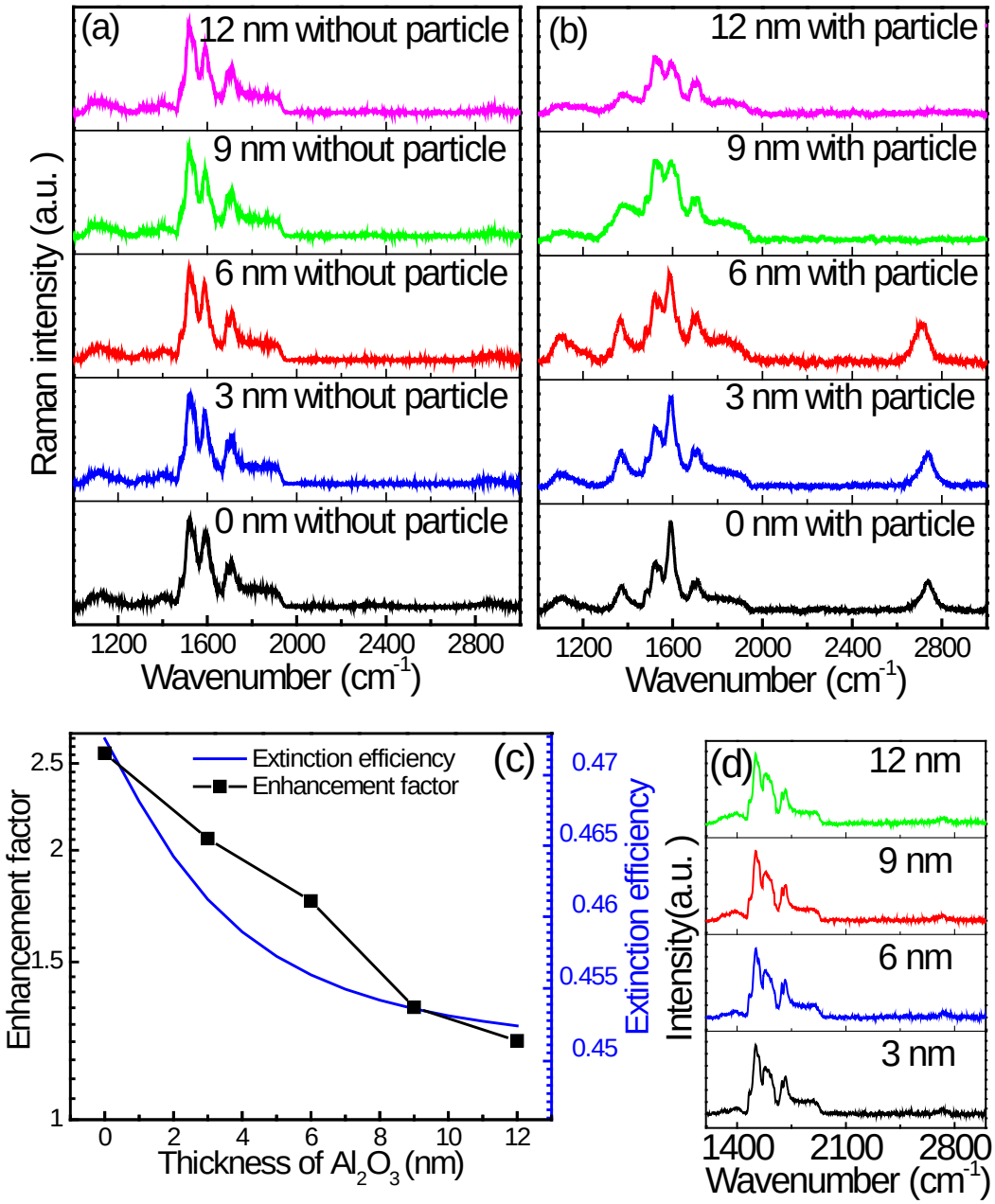

Figure 53. Raman spectra of SiC graphene capped with different thicknesses of Al2O3 from samples without (a), and with (b) nanoparticles. (c) The relationship between the enhancement factor and the thickness of the Al2O3 spacer layer. The calculated extinction efficiency is shown as well. The excitation wavelength of the laser is 488 nm. The y-axis in (c) is on a logarithmic scale. (d) Raman spectra of SiC graphene samples with different thicknesses of Al_2O_3 after removing Au nanoparticles with aqua regia.

The relationship between the enhancement factor and the distance between Au nanoparticles and graphene has also been investigated. For different Al_2O_3 thicknesses, the Raman data before and after the formation of Au nanoparticles have been measured. The excitation wavelength of the laser is 488 nm. Without Au nanoparticles in the structure, the intensity of the *G* peak does not change with various Al_2O_3 thicknesses as shown in Figure 53(a). After forming Au nanoparticles, the enhancement factor of the *G* peak decreases with an increase in the Al_2O_3 thickness, as indicated in Figure 53(b). The enhancement factor falls off exponentially with an increase in the insulator thickness, as shown in Figure 53(c). An enhancement factor of 1.2 is still present when the thickness of Al_2O_3 increases to 12 nm

5.5 Theoretical analysis

It is known through WS-SERES that the line shape of SERS should be similar to that of the LSPR extinction spectra.[169, 172] In order to understand the above observation, theoretical calculations of the extinction efficiency based on dipole approximation have been carried out. The details of the calculation have been discussed in chapter 3. In the calculation, Au nanoparticle with diameter of 15 nm is embedded in a mixture of Al_2O_3 (30%) and air (70%) above graphene. The extinction efficiency is plotted in Figure 52(c). It is clear that the calculation result fits qualitatively well with the experimental data. This shows that the presence of graphene can change the extinction spectrum of Au nanoparticles substantially, which leads to a nonmonotonic change in the enhancement factor of SERS with different excitation wavelength lasers. The enhancement factor can be improved by optimizing the size and interspaces of the nanoparticles.

The extinction efficiency is calculated with various Al_2O_3 thicknesses based on Eq. (1) in chapter 3 as shown in Figure 53(c), and it shows a decreasing trend similar to the experimental data. The observed data can be better accounted

for by the exponential decay of electromagnetic fields of LSPR away from its excitation source (Au nanoparticles) because of the evanescent nature of the LSPR.[173] One recent report also showed an exponential decrease of the photoluminescence enhancement ratio as the thickness of the SiO_2 spacer between graphene and the ZnO layer increases.[129]

In order to ensure that there is no diffusion of Au nanoparticles through the Al_2O_3 spacer layer and get in contact with graphene layer which will allow charge transfer between Au nanoparticles and graphene, Au nanoparticles are etched away using aqua regia. Raman spectra of the samples are taken again as shown in the spectra of Figure 53 (d), the enhancement of *G* peak is absent after Au nanoparticles are etched away. This confirms that the presence of the spacer layer eliminates the possibility of any chemical enhancement of SERS caused by charge transfer. In addition, the change in the thickness of an insulator layer also affects the scattering of light and the modulation of the surface plasmon resonance wavelength,[149] since graphene could change the enhancement factor of the Raman intensity. This result can be applied to the research field where graphene is utilized as a substrate to obtain more strong Raman signals in the characterization of low concentration molecules. Experimental results show that graphene can be considered as a substrate for various molecules to obtain better Raman spectroscopy.[174, 175] Recently Au thin films on graphene have been also used to facilitate enhanced Raman signals of molecules.[176] Our proposed structure with an insulating layer will be particularly useful for certain experiments in which a direct contact between a conducting layer and molecules is not preferred.

5.6 Conclusion

We have studied the SERS induced by metal nanoparticles on SiC epitaxial graphene. By inserting a layer of Al_2O_3 insulator between graphene and nanoparticles, the chemical enhancement of Raman spectroscopy caused by charge transfer is ruled out. The enhancement of Raman scattering is due to the near-field plasmonic effects induced by Au nanoparticles. Excitation lasers with

different wavelengths have been utilized to study the relationship between the laser wavelength and SERS. Theoretical calculations show that the extinction spectrum of Au nanoparticles is modulated by graphene. The experimental results of the relationship between the excitation laser wavelength and the enhancement factor match well with the calculated results. An exponential relationship is observed between the enhancement factor and the thickness of the Al_2O_3 spacer layer.

Chapter 6: Patterned graphene with metal nanoparticles

6.1 Introduction

In previous chapters we have discussed a system with a graphene thin film and metal nanoparticles.[63, 66] So far the utilized graphene film is a continuous one, and patterned graphene nanostructures have not been utilized together with metal nanoparticles. Consequently, experimental results about the optical characteristics of the patterned graphene and metal nanoparticles system have not been studied. In this chapter we propose a novel system in which graphene nanomesh is patterned and isolated gold cylinders fill the vacant (hole) of the nanomesh, as shown in Figure 54. As shown in the schematic, graphene nanomeshes fill the space between gold nanoparticles. When LSPR is excited in metal nanoparticles, the largest electric field will be present in-between two neighboring nanoparticles thus giving rise to the largest enhancement of light absorption.[177] Therefore, the proposed structure is an effective way to enhance the absorption of graphene nanomesh. Different nanopatterning methods such as nanoimprinting and laser interference lithography are evaluated and electron beam lithography is finally chosen to pattern graphene nanomesh. Raman spectroscopy with a laser wavelength of 532 nm is utilized to monitor the quality of graphene before and after the patterning process. The reflection spectra of the samples are obtained using a micro-spectrophotometer. The results demonstrate an enhancement of the absorption of incident light for the proposed graphene nanomesh and gold nanoparticles system. This result is valuable as it demonstrates the potential of constructing a graphene nanomesh photodetector with a high absorption efficiency which is granted by the enhancement of LSPR. In addition, it may provide a high on/off ratio due to very narrow ribbon width, which can induce bandgap for the graphene nanomesh structure. Besides that, wavelength selectivity can be achieved by adjusting the resonance wavelength of LSPR.

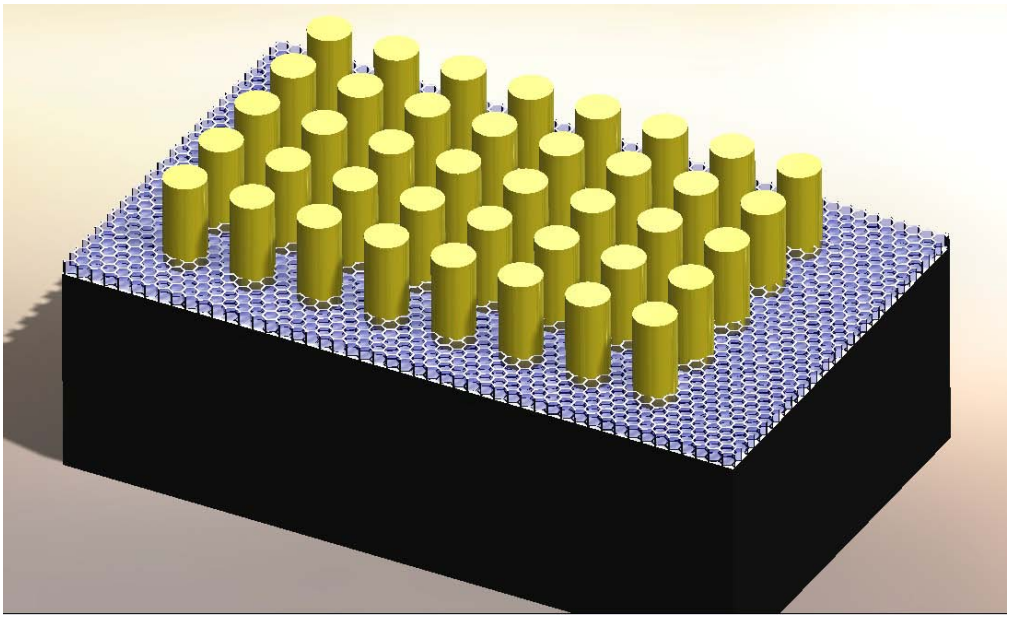

Figure 54. Schematic of graphene nanomesh with metal nanoparticles.

6.2 Fabrication of nanomeshes

In this experiment CVD graphene is transferred on top of silicon substrate (1cm × 1cm) capped with a 300 nm thick SiO_2 Layer. In order to construct a system with graphene nanostructures a proper nanopatterning technique must be utilized. Many nanopatterning techniques have been already used to pattern graphene. An introduction of those that have been investigated in this experiment is included in chapter 2 of this thesis. Nanoimprinting is considered as a high throughput technique for nanopatterning and has been used to make graphene nanomesh.[121] The capability of varying the size and period of the nanostructure using a single imprint stamp is evaluated in this experiment by changing the viscosity of the imprint resist. This is important, since the parameters of the nanostructure need to be changed to vary the resonance wavelength of LSPR. The results show that only a small variation can be introduced to the nanostructure. Thus, nanoimprinting is concluded as not a suitable method for this project. The SEM image of nanoribbons patterned by nanoimprinting is shown in Figure 55.

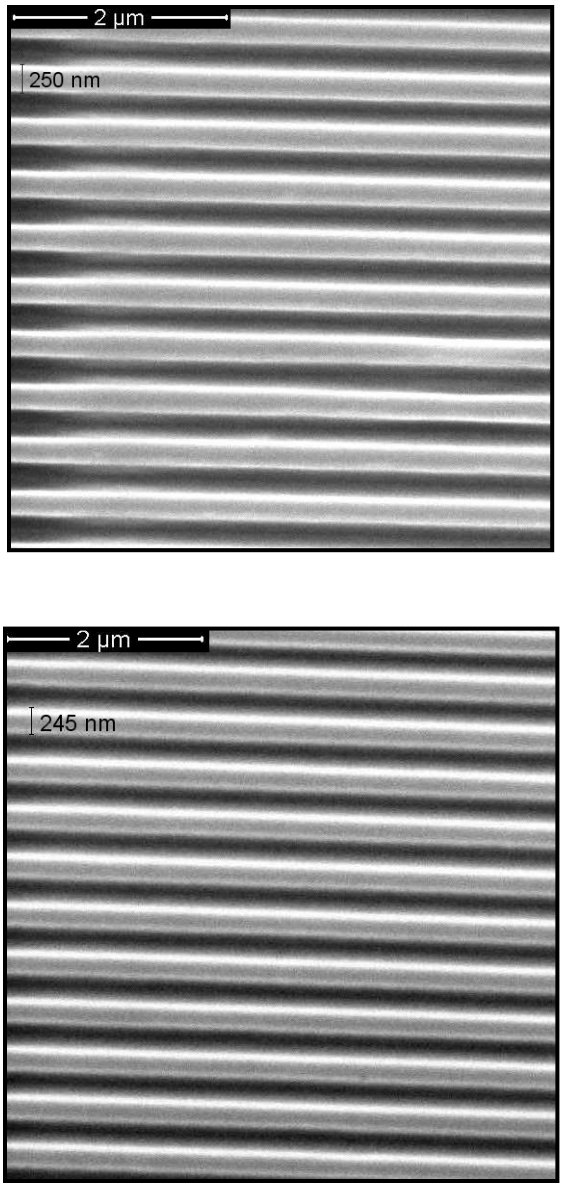

Figure 55. SEM image of nanoribbon made by nanoimprinting Upper: Patterned nanoribbon with higher viscosity. Lower: Patterened naoribbon with lower viscosity.

In addition to nanoimprinting laser interference lithography technique has been investigated. The introduction of this technique can be found in chapter 2. The size and period of the nanomesh can be varied by adjusting the laser wavelength; and angle between the two laser beams. The quality of the patterned graphene is monitored by Raman spectroscopy. Figure 56 shows the Raman spectroscopy data of the graphene film, after photoresist has been spin coated. The absence of *D* peak

demonstrates that the quality of graphene has been well preserved. SEM image of the patterned nanomesh is shown in Figure 57, demonstrating regularly repeating patterns over the entire sample. After deposition of a gold film with a thermal evaporator and the lift-off process, Raman spectroscopy of the sample in Figure 58 shows that graphene is completely removed without any noticeable peak. Thus, instead of the above mentioned two techniques, electron beam lithography is chosen to fabricate nanomesh structures in this thesis.

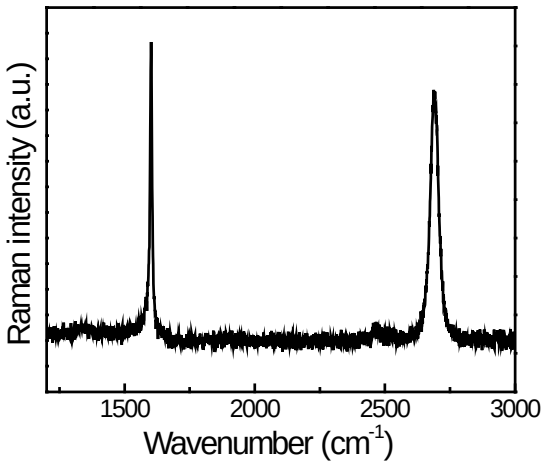

Figure 56. Raman spectrosocopy of CVD graphene after spin coating of intereference lithography photoresist.

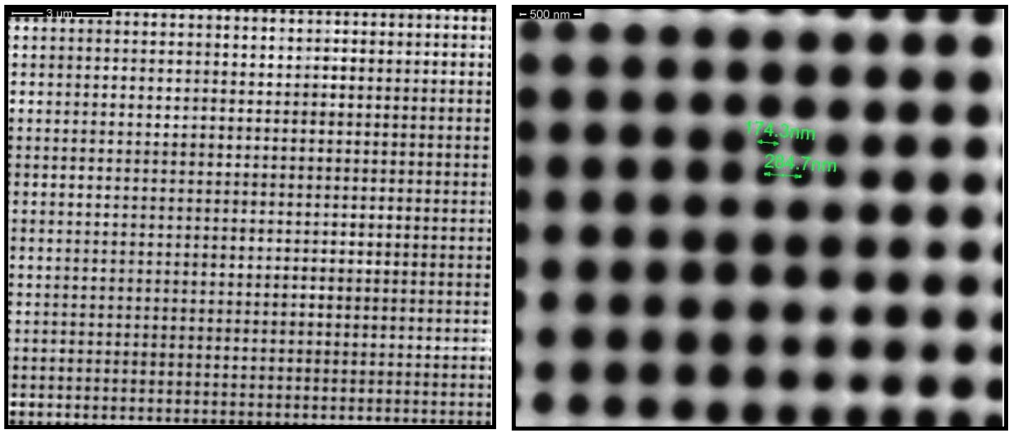

Figure 57. SEM image of intereference lithography patterned nanomesh.

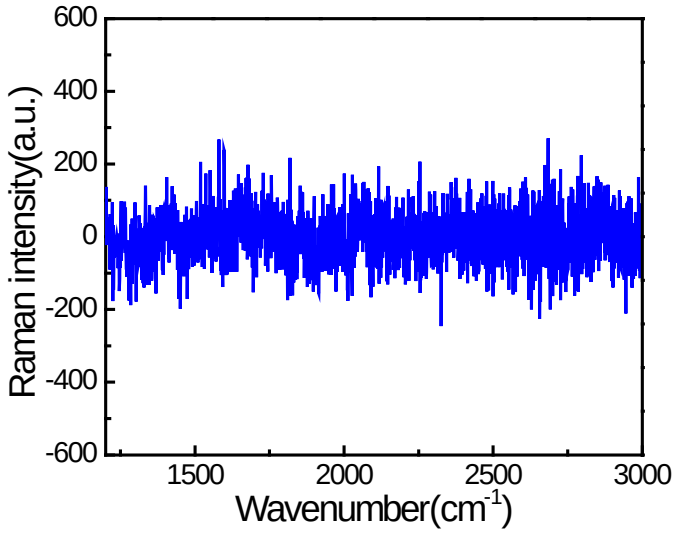

Figure 58. Raman spectroscopy of the sample after lift-off process.

The condition of electron beam lithography is optimized to produce a regularly patterned nanomesh structure. PMMA/MMA double layer electron beam resist is used. To examine the quality of graphene thin film, Raman spectroscopy was taken before carrying out any experimental process. The measurement result is shown in Figure 59, and the absence of *D* peak demonstrates that graphene thin film is of good quality. The size and period of the nanomesh has been varied. To have an unambiguous analysis of the effect of LSPR, the same nanomesh structure without and with nanoparticles are made on the same CVD graphene film. Furthermore, areas without and with graphene film are patterned together during the nanomesh patterning process, therefore the area with metal nanoparticles but without graphene film is also fabricated. After the deposition and lift-off process, the optical characteristics are examined with a UV-Visible-NIR range microspectrophotometer CRAIC system.

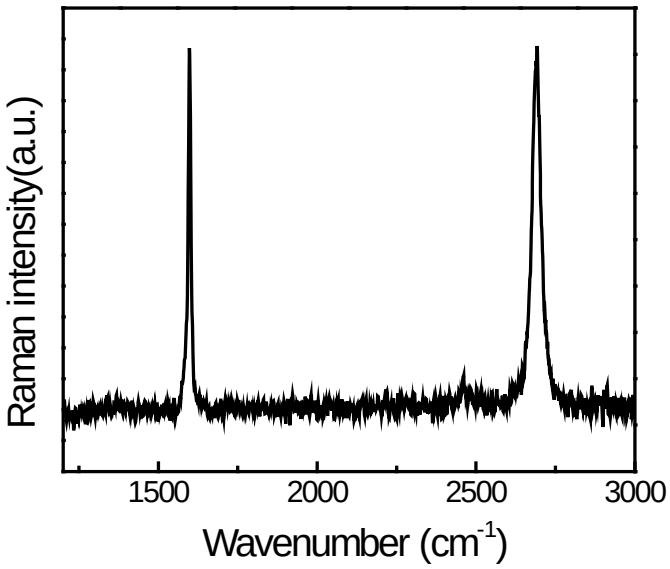

Figure 59. Raman spectroscopy of bare CVD graphene.

6.3 Results and discussion

After sample preparation processes, the Raman spectroscopy data of samples without and with nanoparticles are measured as shown in Figure 60 and 61. The Raman spectroscopy data show that the fabrication processes introduce defects to graphene. However, for both of the cases without and with gold particles, graphene is still in the early phase of amorphization according to the model by Ferrari and Robertson.[133] It is also found that for samples with the same size of holes in the nanomesh but with a larger period, the Raman data show that the defects introduced to graphene film are less. This is reasonable since a larger portion of graphene surface is left over, when the period is longer. AFM is utilized to investigate the patterning result of graphene nanomesh and the results in Figure 62 demonstrate that the graphene nanomesh structure is successfully created after the oxygen plasma etching process. AFM images are also taken after the deposition of gold nanoparticles. Figure 63 shows the AFM image for the sample A in which the diameter of the nanoparticles are ~ 200 nm and the period is 220 nm. Figure 64

shows the sample B, where the diameter of nanoparticles are 200 nm, but the period is 260 nm.

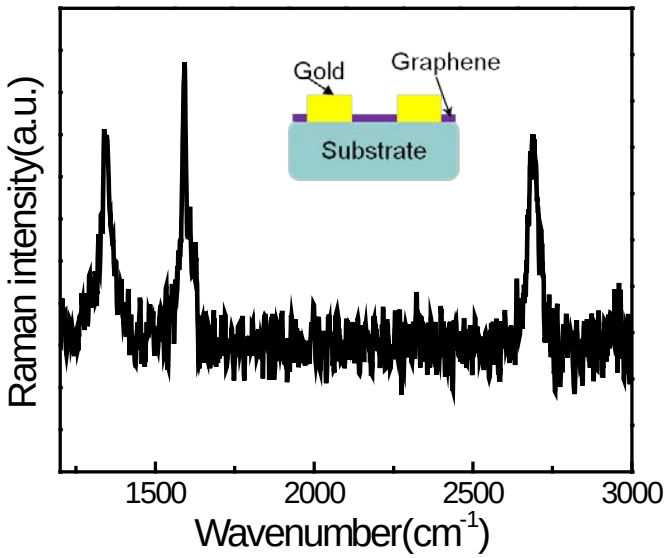

Figure 60. Raman spectroscopy of graphene nanomesh with nanoparticles. Inset: schematic of the cross section view.

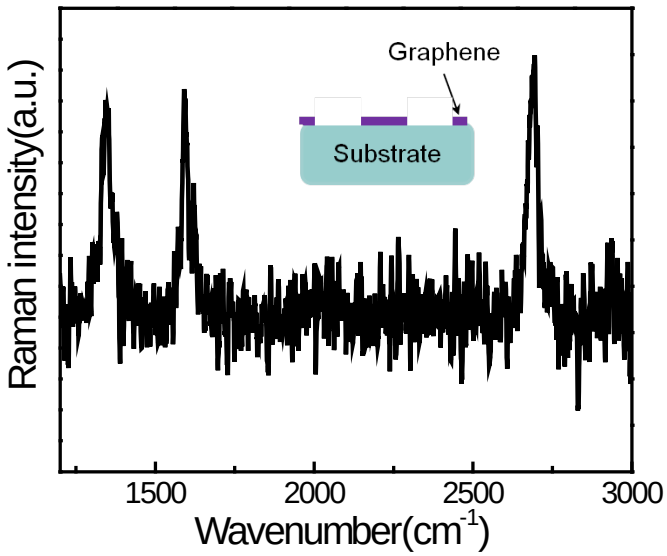

Figure 61. Raman spectroscopy of bare graphene nanomesh. Inset: schematic of the cross section view.

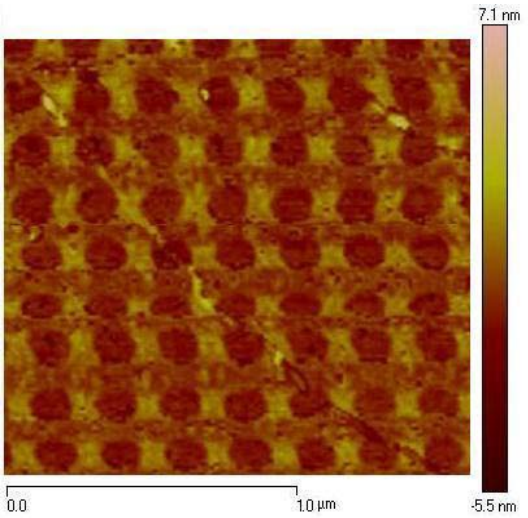

Figure 62. AFM image of graphene nanomesh.

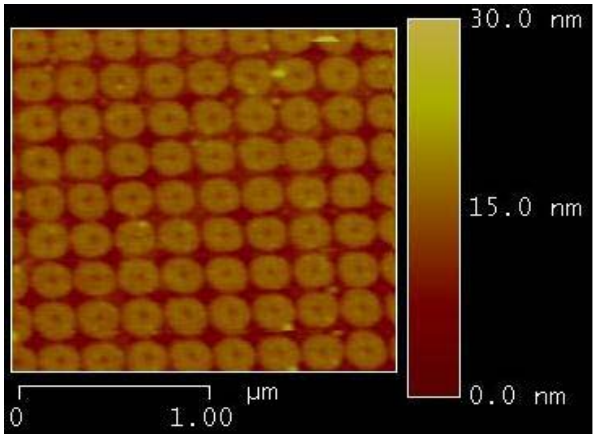

Figure 63. AFM image of graphene nanomesh with gold nanoparticles (sample A).

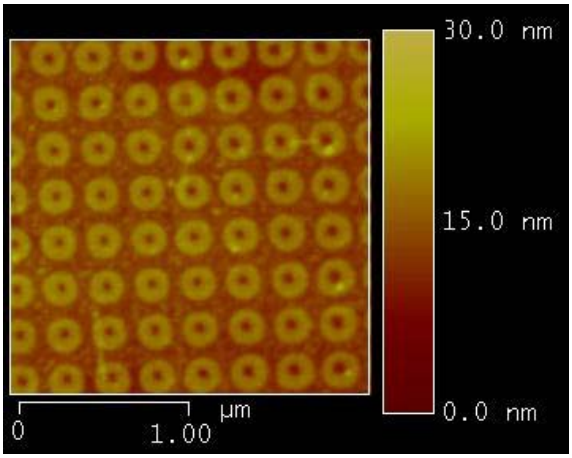

Figure 64. AFM image of graphene nanomesh with gold nanoparticles (sample B).

Finally, the optical characteristics of the samples are investigated by the reflection spectroscopy. Measurements are conducted from four different sample structures; bare graphene thin film, patterned graphene nanomesh, nanoparticle arrays without graphene, and graphene nanomesh with nanoparticles. In order to evaluate the net changes of the optical characteristics between all the patterned samples and bare graphene thin film, the reflectance of every structure is subtracted from the bare graphene reflectance followed by normalization. Figure 65 and 66 shows the relationship between the net reflectance change (ΔR) and wavelength for the sample A and sample B, respectively. In the plots two peaks are observed when gold nanoparticles are included in the structure. It is commonly known that LSPR will increase the absorption of light, and absorption is inversely proportional to the reflectance. Thus the presents of a peak in theΔR spectrum represents an increase of absorption compared to the bare graphene film. One of the peaks is around 610 nm, which agrees well with a resonance wavelength of gold nanoparticles with a diameter ~ 200 nm.[77] The other peak in a shorter wavelength ~ 360 nm might be due to the LSPR quadrupole resonance in the nanoparticles. It is found that as the period increases, both peaks slightly shift to the shorter wavelengths. Another observation is that the intensities of ΔR in the two peaks are higher than that of bare nanoparticle arrays, when graphene is included in the structure. This indicates that the absorption of graphene nanomesh is enhanced due to LSPR with the presents of gold nanoparticles. The enhancement for the sample B is larger compared with the sample A, when graphene nanomesh exists with gold nanoparticles. Further investigation is required to understand this higher enhancement ratio.

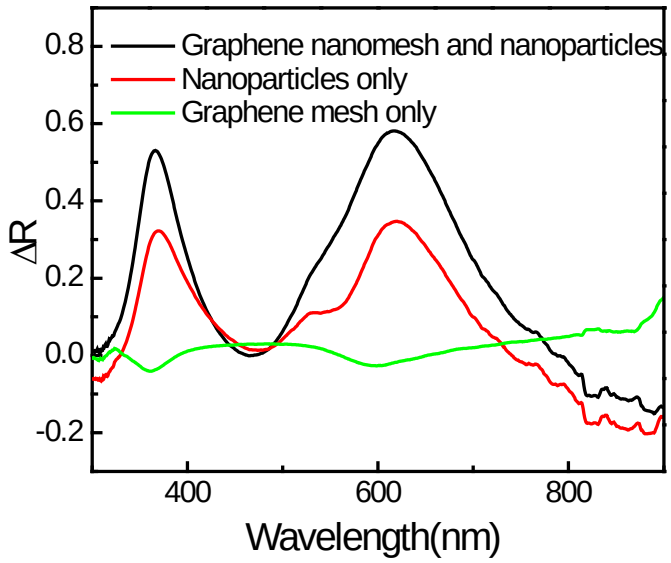

Figure 65. Plot of relationship between ΔR and wavelength for sample A.

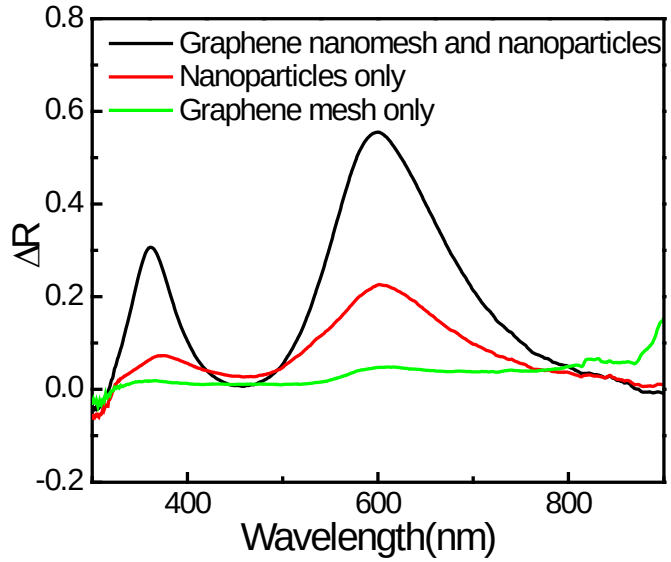

Figure 66. Plot of relationship between ΔR and wavelength for sample B.

6.4 Conclusion

Different nanopatterning techniques are investigated to fabricate graphene nanostructures and electron beam lithography is finally selected to make the graphene nanomesh structure with metal nanoparticles. The quality of graphene is monitored carefully by Raman spectroscopy before and after the experimental processes. Defects are introduced to graphene during the fabrication processes, however, it is still in the early stage of amorphization. The optical characteristics of the samples are investigated through the reflection spectroscopy measurements. It is found that the presence of nanoparticles in the hole of graphene nanomesh largely enhances the absorption of the graphene nanomesh structure around the resonance wavelength of LSPR. This results demonstrate the potential of constructing graphene nanomesh photodetectors with a high on/off ratio, light absorption efficiency, and capability of wavelength selectivity.

Chapter 7: Conclusion and future works

7.1 Conclusion

Graphene is considered as a basic building block for all the other graphitic materials in all other dimensionalities,[43] and it has been intensively studied since its discovery in 2004. The advance in large scale manufacturing of graphene enables mass production of graphene devices. Graphene has been used as the channel material in high frequency transistor device.[29, 33] However, it is believed that the true potential of graphene lies in the optical area. It is demonstrated as a promising candidate to replace ITO as transparent conductive electrodes,[44] and has been also utilized as the active material for optoelectronic devices such as photodetectors.[60] One of the drawbacks of graphene functioning as the active material is the low light absorption over a wide wavelength range. One of the methods to overcome the drawback is to utilize the LSPR enhanced absorption. So far the electromagnetic coupling between graphene and LSPR excited in metal nanoparticles has not been studied systematically.

Therefore, in this thesis the electromagnetic coupling between graphene and metal nanoparticles are studied by varying the spacer layer thickness between the two parties over a very small range first. By varying the spacer layer thickness from 0.3 to 1.8 nm, the resonance wavelength is shifted from 583 to 566 nm. The shift is due to a change in the electromagnetic field coupling strength between the localized surface plasmon excited in the gold nanoparticles and a single layer graphene film. In contrast, when the graphene film is absent from the system, no noticeable shift in the resonance wavelength is observed upon varying the spacer thickness.

After that, the spacer layer thickness is varied over a much wider range, until the saturation of the shifting phenomenon is reached. The system demonstrates a blue-shift of 29 nm, as the thickness of the spacer layer increases from 0 to 15 nm. This is due to the electromagnetic coupling between the localized surface plasmon excited in the nanoparticles and the graphene film. The strength of the coupling

decays exponentially with a decay length of d/R=0.36, where d is the spacer layer thickness and R is the diameter of the Au nanoparticles. The result agrees qualitatively well with the plasmon ruler equation. Interestingly, a further increment of the spacer layer thickness induces a red-shift of 17 nm in the resonance wavelength and the shift saturates when the thickness of the spacer layer increases above 20 nm.

Furthermore, the effect introduced by the electromagnetic coupling between LSPR and metal nanoparticles to SERS of SiC graphene is studied. Different excitation lasers are utilized to study the relationship between the laser wavelength and SERS. The theoretical calculation shows that the extinction spectrum of Au nanoparticles is modulated by the presence of graphene. The experimental results of the relationship between the excitation laser wavelength and the enhancement factor fit well with the calculated results. An exponential relationship is observed between the enhancement factor and the thickness of the spacer layer.

Finally, metal nanoparticles are also utilized together with patterned graphene nanomesh structures. In the proposed structure, electron beam lithography is used to pattern graphene nanomeshes and oxygen plasma is used to etch away graphene in the hole areas. After that, gold nanoparticles are deposited inside the hole areas of the nanomeshes. Reflection spectroscopy is measured to study the optical characteristics of the proposed structure. The result shows that the presence of nanoparticles in the structure largely enhances the absorption of graphene nanomeshes. This shows the potential of utilizing the structure to construct photodetectors with a high on/off ratio, high absorption efficiency, and wavelength selectivity.

7.2 Suggestion of future works

The investigation of the electromagnetic coupling between graphene and LSPR demonstrates that the resonance wavelength of LSPR can be shifted by adjusting the coupling strength between these two parties. It is expected that the shifting range can be enlarged by optimizing the parameters associated with gold nanoparticles. For example, different metal materials can be used to make nanoparticles and the size of nanoparticles can be changed as well. The distance between the nanoparticles is another parameter that can be optimized. After the optimization, a photodetector with a wavelength selection capability can be constructed.

The experiment of graphene nanomesh with nanoparticles demonstrates the potential of building a photodetector with a high on/off ratio, high efficiency, and wavelength selectivity. More investigation of the proposed structure can be carried out. For example, the relationship between the absorption enhancement and the parameters associated with the structure can be investigated. The size and period of the nanomesh can be adjusted. Different metal materials can also be used to make the nanoparticles. The height of the nanoparticles can also be varied. The electrical characteristics of the system can be investigated to analyze the bandgap opening of the structure. The optimization should be done such that the absorption enhancement is high and at the same time the bandgap is also large enough to facilitate a large on/off ratio for the construction of photodetectors. After the optimization process, the photocurrent of the structure can be measured.

References

1 P. R. Wallace, Phys. Rev. 71, 622 (1947).
2 J. C. Slonczewski and P. R. Weiss, Phys. Rev. 109, 272 (1958).
3 E. Fradkin, Phys. Rev. B. 33, 3263 (1986).
4 J. Stangl, Hol, yacute, V., and G. Bauer, Rev. Mod. Phys. 76, 725 (2004).
5 K. S. Novoselov, A. K. Geim, S. V. Morozov, D. Jiang, Y. Zhang, S. V. Dubonos, I. V. Grigorieva, and A. A. Firsov, Science 306, 666 (2004).
6 J. C. Meyer, A. K. Geim, M. I. Katsnelson, K. S. Novoselov, T. J. Booth, and S. Roth, Nature 446, 60 (2007).
7 K. I. Bolotin, K. J. Sikes, Z. Jiang, M. Klima, G. Fudenberg, J. Hone, P. Kim, and H. L. Stormer, Solid State Commun. 146, 351 (2008).
8 C. Lee, X. Wei, J. W. Kysar, and J. Hone, Science 321, 385 (2008).
9 A. A. Balandin, S. Ghosh, W. Bao, I. Calizo, D. Teweldebrhan, F. Miao, and C. N. Lau, Nano Lett. 8, 902 (2008).
10 J. M. Dawlaty, S. Shivaraman, J. Strait, P. George, M. Chandrashekhar, F. Rana, M. G. Spencer, D. Veksler, and Y. Chen, Appl. Phys. Lett. 93, 131905 (2008).
11 X. Li, Y. Zhu, W. Cai, M. Borysiak, B. Han, D. Chen, R. D. Piner, L. Colombo, and R. S. Ruoff, Nano Lett. 9, 4359 (2009).
12 R. R. Nair, P. Blake, A. N. Grigorenko, K. S. Novoselov, T. J. Booth, T. Stauber, N. M. R. Peres, and A. K. Geim, Science 320, 1308 (2008).
13 P. W. Sutter, J.-I. Flege, and E. A. Sutter, Nature Mater. 7, 406 (2008).
14 J. Coraux, A. T. N`Diaye, C. Busse, and T. Michely, Nano Lett. 8, 565 (2008).
15 K. S. Kim, et al., Nature 457, 706 (2009).
16 X. Li, et al., Science 324, 1312 (2009).
17 A. Reina, X. Jia, J. Ho, D. Nezich, H. Son, V. Bulovic, M. S. Dresselhaus, and J. Kong, Nano Lett. 9, 30 (2008).
18 S. Bae, et al., Nature Nanotech. 5, 574 (2010).
19 S. Tanaka, K. Morita, and H. Hibino, Phys. Rev. B. 81, 041406 (2010).
20 Y. Hernandez, et al., Nature Nanotech. 3, 563 (2008).
21 M. Lotya, et al., J. Am. Chem. Soc. 131, 3611 (2009).
22 A. A. Green and M. C. Hersam, Nano Lett. 9, 4031 (2009).
23 S. Stankovich, D. A. Dikin, G. H. B. Dommett, K. M. Kohlhaas, E. J. Zimney, E. A. Stach, R. D. Piner, S. T. Nguyen, and R. S. Ruoff, Nature 442, 282 (2006).
24 S. Stankovich, D. A. Dikin, R. D. Piner, K. A. Kohlhaas, A. Kleinhammes, Y. Jia, Y. Wu, S. T. Nguyen, and R. S. Ruoff, Carbon 45, 1558 (2007).
25 J. Cai, et al., Nature 466, 470 (2010).
26 L. Britnell, et al., Science 335, 947 (2012).

[27] K. S. Novoselov, V. I. Falko, L. Colombo, P. R. Gellert, M. G. Schwab, and K. Kim, Nature 490, 192 (2012).
[28] Y.-M. Lin, C. Dimitrakopoulos, K. A. Jenkins, D. B. Farmer, H.-Y. Chiu, A. Grill, and P. Avouris, Science 327, 662 (2010).
[29] Y. Wu, Y.-M. Lin, A. A. Bol, K. A. Jenkins, F. Xia, D. B. Farmer, Y. Zhu, and P. Avouris, Nature 472, 74 (2011).
[30] Y.-M. Lin, K. A. Jenkins, A. Valdes-Garcia, J. P. Small, D. B. Farmer, and P. Avouris, Nano Lett. 9, 422 (2008).
[31] X. Wang, S. M. Tabakman, and H. Dai, J. Am. Chem. Soc. 130, 8152 (2008).
[32] Z. H. Ni, H. M. Wang, Y. Ma, J. Kasim, Y. H. Wu, and Z. X. Shen, ACS Nano 2, 1033 (2008).
[33] L. Liao, et al., Nature 467, 305 (2010).
[34] K. Seo, S. Lee, H. Yoon, J. In, K. S. K. Varadwaj, Y. Jo, M.-H. Jung, J. Kim, and B. Kim, ACS Nano 3, 1145 (2009).
[35] L. Liao, J. Bai, Y. Qu, Y.-c. Lin, Y. Li, Y. Huang, and X. Duan, Proc. Nati. Acad. Sci. 107, 6711 (2010).
[36] L. Liao, J. Bai, R. Cheng, Y.-C. Lin, S. Jiang, Y. Qu, Y. Huang, and X. Duan, Nano Lett. 10, 3952 (2010).
[37] P. Avouris, Z. Chen, and V. Perebeinos, Nature Nanotech. 2, 605 (2007).
[38] F. Schwierz, Nature Nanotech. 5, 487 (2010).
[39] A. K. Geim, Science 324, 1530 (2009).
[40] D. C. Elias, et al., Science 323, 610 (2009).
[41] T. Ohta, A. Bostwick, T. Seyller, K. Horn, and E. Rotenberg, Science 313, 951 (2006).
[42] K. Kim, J.-Y. Choi, T. Kim, S.-H. Cho, and H.-J. Chung, Nature 479, 338 (2011).
[43] A. K. Geim and K. S. Novoselov, Nature Mater. 6, 183 (2007).
[44] F. Bonaccorso, Z. Sun, T. Hasan, and A. C. Ferrari, Nature Photon. 4, 611 (2010).
[45] D. S. Hecht, L. Hu, and G. Irvin, Adv. Mater. 23, 1482 (2011).
[46] Y. J. Shin, R. Stromberg, R. Nay, H. Huang, A. T. S. Wee, H. Yang, and C. S. Bhatia, Carbon 49, 4070 (2011).
[47] J. Wu, H. A. Becerril, Z. Bao, Z. Liu, Y. Chen, and P. Peumans, Appl. Phys. Lett. 92, 263302 (2008).
[48] X. Wang, L. Zhi, and K. Mullen, Nano Lett. 8, 323 (2007).
[49] X. Li, et al., Adv. Mater. 22, 2743 (2010).
[50] K. F. Mak, M. Y. Sfeir, Y. Wu, C. H. Lui, J. A. Misewich, and T. F. Heinz, Phys. Rev. Lett. 101, 196405 (2008).
[51] Z. Q. Li, E. A. Henriksen, Z. Jiang, Z. Hao, M. C. Martin, P. Kim, H. L. Stormer, and D. N. Basov, Nature Phys. 4, 532 (2008).
[52] T. Mueller, F. Xia, and P. Avouris, Nature Photon. 4, 297 (2010).
[53] F. Wang, Y. Zhang, C. Tian, C. Girit, A. Zettl, M. Crommie, and Y. R. Shen, Science 320, 206 (2008).

[54] Q. Bao, H. Zhang, Y. Wang, Z. Ni, Y. Yan, Z. X. Shen, K. P. Loh, and D. Y. Tang, Adv. Funct. Mater. 19, 3077 (2009).
[55] D. A. B. Miller, Nature Photon. 4, 3 (2010).
[56] G. T. Reed, G. Mashanovich, F. Y. Gardes, and D. J. Thomson, Nature Photon. 4, 518 (2010).
[57] A. Liu, R. Jones, L. Liao, D. Samara-Rubio, D. Rubin, O. Cohen, R. Nicolaescu, and M. Paniccia, Nature 427, 615 (2004).
[58] J. Liu, M. Beals, A. Pomerene, S. Bernardis, R. Sun, J. Cheng, L. C. Kimerling, and J. Michel, Nature Photon. 2, 433 (2008).
[59] Q. Xu, B. Schmidt, S. Pradhan, and M. Lipson, Nature 435, 325 (2005).
[60] M. Liu, X. Yin, E. Ulin-Avila, B. Geng, T. Zentgraf, L. Ju, F. Wang, and X. Zhang, Nature 474, 64 (2011).
[61] F. Xia, T. Mueller, Y.-m. Lin, A. Valdes-Garcia, and P. Avouris, Nature Nanotech. 4, 839 (2009).
[62] J. H. LeeEduardo, K. Balasubramanian, R. T. Weitz, M. Burghard, and K. Kern, Nature Nanotech. 3, 486 (2008).
[63] T. J. Echtermeyer, L. Britnell, P. K. Jasnos, A. Lombardo, R. V. Gorbachev, A. N. Grigorenko, A. K. Geim, A. C. Ferrari, and K. S. Novoselov, Nat. Commun. 2, 458 (2011).
[64] J. Niu, Y. J. Shin, Y. Lee, J.-H. Ahn, and H. Yang, Appl. Phys. Lett. 100, 061116 (2012).
[65] J. Niu, Y. J. Shin, J. Son, Y. Lee, J.-H. Ahn, and H. Yang, Opt. Express 20, 19690 (2012).
[66] Y. Liu, R. Cheng, L. Liao, H. Zhou, J. Bai, G. Liu, L. Liu, Y. Huang, and X. Duan, Nat. Commun. 2, 579 (2011).
[67] F. Schedin, E. Lidorikis, A. Lombardo, V. G. Kravets, A. K. Geim, A. N. Grigorenko, K. S. Novoselov, and A. C. Ferrari, ACS Nano 4, 5617 (2010).
[68] J. niu, V. G. Truong, H. Huang, S. Tripathy, C. Qiu, A. T. S. Wee, T. Yu, and H. Yang, Appl. Phys. Lett. 100, 191601 (2012).
[69] U. Kreibig and M. Vollmer, *Optical properties of metal clusters* (Springer-Verlag, Berlin, Germany, 1995).
[70] K. L. Kelly, E. Coronado, L. L. Zhao, and G. C. Schatz, J. Phys. Chem. B 107, 668 (2002).
[71] M. Faraday, Phil. Trans. R. Soc. 147, 145 (1857).
[72] G. Mie, Annalen der Physik 330, 377 (1908).
[73] S. Underwood and P. Mulvaney, Langmuir 10, 3427 (1994).
[74] M. M. Alvarez, J. T. Khoury, T. G. Schaaff, M. N. Shafigullin, I. Vezmar, and R. L. Whetten, J. Phys. Chem. B 101, 3706 (1997).
[75] S. Link and M. A. El-Sayed, J. Phys. Chem. B 103, 4212 (1999).
[76] C. L. Haynes and R. P. Van Duyne, J. Phys. Chem. B 105, 5599 (2001).
[77] P. K. Jain, K. S. Lee, I. H. El-Sayed, and M. A. El-Sayed, J. Phys. Chem. B 110, 7238 (2006).
[78] S. Peng, J. M. McMahon, G. C. Schatz, S. K. Gray, and Y. Sun, Proc. Nati. Acad. Sci. 107, 14530 (2010).
[79] S. Lal, S. Link, and N. J. Halas, Nature Photon. 1, 641 (2007).

[80] P. Nagpal, N. C. Lindquist, S.-H. Oh, and D. J. Norris, Science 325, 594 (2009).
[81] M. J. Banholzer, J. E. Millstone, L. Qin, and C. A. Mirkin, Chem. Soc. Rev. 37, 885 (2008).
[82] N. Fang, H. Lee, C. Sun, and X. Zhang, Science 308, 534 (2005).
[83] M. F. Craciun, S. Russo, M. Yamamoto, and S. Tarucha, Nano Today 6, 42 (2011).
[84] K. S. Novoselov, D. Jiang, F. Schedin, T. J. Booth, V. V. Khotkevich, S. V. Morozov, and A. K. Geim, Proc. Nati. Acad. Sci. USA 102, 10451 (2005).
[85] Y. Zhang, T.-T. Tang, C. Girit, Z. Hao, M. C. Martin, A. Zettl, M. F. Crommie, Y. R. Shen, and F. Wang, Nature 459, 820 (2009).
[86] M. F. Craciun, RussoS, YamamotoM, J. B. Oostinga, A. F. Morpurgo, and TaruchaS, Nature Nanotech. 4, 383 (2009).
[87] Z. H. Ni, H. M. Wang, J. Kasim, H. M. Fan, T. Yu, Y. H. Wu, Y. P. Feng, and Z. X. Shen, Nano Lett. 7, 2758 (2007).
[88] P. Nemes-Incze, Z. Osváth, K. Kamarás, and L. P. Biró, Carbon 46, 1435 (2008).
[89] A. Gupta, G. Chen, P. Joshi, S. Tadigadapa, and Eklund, Nano Lett. 6, 2667 (2006).
[90] Z. Chen, Y.-M. Lin, M. J. Rooks, and P. Avouris, Phys. E. 40, 228 (2007).
[91] P. N. Nirmalraj, T. Lutz, S. Kumar, G. S. Duesberg, and J. J. Boland, Nano Lett. 11, 16 (2010).
[92] Y. Zhang, V. W. Brar, F. Wang, C. Girit, Y. Yayon, M. Panlasigui, A. Zettl, and M. F. Crommie, Nature Phys. 4, 627 (2008).
[93] V. W. Brar, Y. Zhang, Y. Yayon, T. Ohta, J. L. McChesney, A. Bostwick, E. Rotenberg, K. Horn, and M. F. Crommie, Appl. Phys. Lett. 91, 122102 (2007).
[94] S. L. Wong, H. Huang, W. Chen, and A. T. S. Wee, MRS. Bull. 37, 1195 (2012).
[95] P. Mallet, F. Varchon, C. Naud, L. Magaud, C. Berger, and J. Y. Veuillen, Phys. Rev. B. 76, 041403 (2007).
[96] P. Lauffer, K. V. Emtsev, R. Graupner, T. Seyller, L. Ley, S. A. Reshanov, and H. B. Weber, Phys. Rev. B. 77, 155426 (2008).
[97] S. Shivaraman, M. V. S. Chandrashekhar, J. Boeckl, and M. Spencer, J. Electron. Mater. 38, 725 (2009).
[98] D. J. Gardiner, *Practical Raman spectroscopy* (Springer-Verlag, New York, 1989).
[99] K. Kneipp, H. Kneipp, I. Itzkan, R. R. Dasari, and M. S. Feld, Chemical Reviews 99, 2957 (1999).
[100] A. C. Ferrari, et al., Phys. Rev. Lett. 97, 187401 (2006).
[101] DasA, et al., Nat Nano 3, 210 (2008).
[102] M. A. Pimenta, G. Dresselhaus, M. S. Dresselhaus, L. G. Cancado, A. Jorio, and R. Saito, Physical Chemistry Chemical Physics 9, 1276 (2007).

[103] I. Calizo, A. A. Balandin, W. Bao, F. Miao, and C. N. Lau, Nano Letters 7, 2645 (2007).
[104] Z. H. Ni, T. Yu, Y. H. Lu, Y. Y. Wang, Y. P. Feng, and Z. X. Shen, ACS Nano 2, 2301 (2008).
[105] Z. H. Ni, W. Chen, X. F. Fan, J. L. Kuo, T. Yu, A. T. S. Wee, and Z. X. Shen, Physical Review B 77, 115416 (2008).
[106] X. Shen, H. Wang, and T. Yu, Nanoscale 5, 3352 (2013).
[107] S. G. Kumar and J. V. R. Rao, International journal of nanotechnolgoy and application 3, 1 (2013).
[108] Z. Luo, L. A. Somers, Y. Dan, T. Ly, N. J. Kybert, E. J. Mele, and A. T. C. Johnson, Nano Lett. 10, 777 (2010).
[109] H. Zhou, C. Qiu, Z. Liu, H. Yang, L. Hu, J. Liu, H. Yang, C. Gu, and L. Sun, J. Am. Chem. Soc. 132, 944 (2009).
[110] L. A. Somers, N. A. Zimbovskaya, A. T. Johnson, and E. J. Mele, Phys. Rev. B 82, 115430 (2010).
[111] C. N. R. Rao, G. U. Kulkarni, P. J. Thomas, and P. P. Edwards, Chem. Soc. Rev. 29, 27 (2000).
[112] Y. Lu, B. Goldsmith, D. R. Strachan, J. H. Lim, Z. Luo, and A. T. C. Johnson, Small 6, 2748 (2010).
[113] M. Y. Han, B. Özyilmaz, Y. Zhang, and P. Kim, Phys. Rev. Lett. 98, 206805 (2007).
[114] X. Li, X. Wang, L. Zhang, S. Lee, and H. Dai, Science 319, 1229 (2008).
[115] X. Wang, Y. Ouyang, X. Li, H. Wang, J. Guo, and H. Dai, Phys. Rev. Lett. 100, 206803 (2008).
[116] L. A. Ponomarenko, F. Schedin, M. I. Katsnelson, R. Yang, E. W. Hill, K. S. Novoselov, and A. K. Geim, Science 320, 356 (2008).
[117] J. Bai, X. Zhong, S. Jiang, Y. Huang, and X. Duan, Nature Nanotech. 5, 190 (2010).
[118] S. S. Datta, D. R. Strachan, S. M. Khamis, and A. T. C. Johnson, Nano Lett. 8, 1912 (2008).
[119] H. Yan, T. Low, W. Zhu, Y. Wu, M. Freitag, X. Li, F. Guinea, P. Avouris, and F. Xia, Nature Photon. 7, 394 (2013).
[120] C. Wang, J. K. Morton, Z. Fu, W.-D. Li, and S. Y. Chou, Nanotechnology 22 (2011).
[121] X. Liang, Y.-S. Jung, S. Wu, A. Ismach, D. L. Olynick, S. Cabrini, and J. Bokor, Nano Lett. 10, 2454 (2010).
[122] C. J. M. V. Rijn, J. Micro-Nanolith. MEM. 5 (2006).
[123] S. Bae, et al., Nat. Nanotech. 5, 574 (2010).
[124] Y. Lee, S. Bae, H. Jang, S. Jang, S.-E. Zhu, S. H. Sim, Y. I. Song, B. H. Hong, and J.-H. Ahn, Nano Lett. 10, 490 (2010).
[125] T. Klar, M. Perner, S. Grosse, G. von Plessen, W. Spirkl, and J. Feldmann, Phys. Rev. B 80, 4249 (1998).
[126] A. Campion and P. Kambhampati, Chem. Soc. Rev. 27, 241 (1998).
[127] R. M. Bakker, H.-K. Yuan, Z. Liu, V. P. Drachev, A. V. Kildishev, V. M. Shalaev, R. H. Pedersen, S. Gresillon, and A. Boltasseva, Appl. Phys. Lett. 92, 043101 (2008).

[128] S. Pillai, K. R. Catchpole, T. Trupke, and M. A. Green, journal article 101, 093105 (2007).
[129] S. W. Hwang, et al., Phys. Rev. Lett. 105, 127403 (2010).
[130] S. Kawata, M. Ohtsu, and M. Irie, *Near-field optics and surface plasmon polaritons* (Springer, Berlin, 2001).
[131] M. Hu, A. Ghoshal, M. Marquez, and P. G. Kik, J. Phys. Chem. C 114, 7509 (2010).
[132] T. Okamoto and I. Yamaguchi, J. Phys. Chem. C 107, 10321 (2003).
[133] A. C. Ferrari and J. Robertson, Phys. Rev. B. 61, 14095 (2000).
[134] B. Dlubak, et al., Appl. Phys. Lett. 97, 092502 (2010).
[135] D. C. Kim, D.-Y. Jeon, H.-J. Chung, Y. Woo, J. K. Shin, and S. Seo, Nanotechnology 20, 375703 (2009).
[136] G. Isic, et al., J. Nanophotonics 5 (2011).
[137] E. D. Palik and G. Ghosh, *Handbook of optical constants of solids* (Academic Press, Orlando, Florida, 1998).
[138] T. Søndergaard and S. I. Bozhevolnyi, Phys. Rev. B 67, 165405 (2003).
[139] M. Xiao, S. Bozhevolnyi, and O. Keller, App. Phys. A 62, 115 (1996).
[140] O. Keller, M. Xiao, and S. Bozhevolnyi, Surf. Sci. 280, 217 (1993).
[141] A. B. Evlyukhin and E. V. Evlyukhina, J. Opt. Technol. 71, 384 (2004).
[142] Z. Li, B. Gu, and G. Yang, Phys. Rev. B 55, 10883 (1997).
[143] P. K. Jain, W. Huang, and M. A. El-Sayed, Nano Lett. 7, 2080 (2007).
[144] T. Klar, M. Perner, S. Grosse, G. von Plessen, W. Spirkl, and J. Feldmann, Phys. Rev. Lett. 80, 4249 (1998).
[145] T. Okamoto and I. Yamaguchi, J. Phys. Chem. B 107, 10321 (2003).
[146] G. Isic, et al., J. Nanophotonics 5, 051809 (2011).
[147] S. K. Ghosh and T. Pal, Chem. Rev. 107, 4797 (2007).
[148] L. Genzel and T. P. Martin, Surf. Sci. 34, 33 (1973).
[149] T. J. Norman, C. D. Grant, D. Magana, J. Z. Zhang, J. Liu, D. Cao, F. Bridges, and A. Van Buuren, J. Phys. Chem. B 106, 7005 (2002).
[150] A. N. Shipway, M. Lahav, R. Gabai, and I. Willner, Langmuir 16, 8789 (2000).
[151] T. R. Jensen, M. L. Duval, K. L. Kelly, A. A. Lazarides, G. C. Schatz, and R. P. Van Duyne, J. Phys. Chem. B 103, 9846 (1999).
[152] C. L. Du, Y. M. You, K. Johnson, H. L. Hu, X. J. Zhang, and Z. X. Shen, Plasmonics 5, 105 (2010).
[153] M. Hu, A. Ghoshal, M. Marquez, and P. G. Kik, J. Phys. Chem. C 114, 7509 (2010).
[154] F. Tuinstra and J. L. Koenig, J. Chem. Phys 53, 1126 (1970).
[155] A. C. Ferrari and J. Robertson, Phys. Rev. B 61, 14095 (2000).
[156] A. Das, et al., Nature Nanotech. 3, 210 (2008).
[157] M. A. Pimenta, G. Dresselhaus, M. S. Dresselhaus, L. G. Cancado, A. Jorio, and R. Saito, Phys. Chem. Chem. Phys. 9, 1276 (2007).
[158] I. Calizo, A. A. Balandin, W. Bao, F. Miao, and C. N. Lau, Nano Lett. 7, 2645 (2007).
[159] L. Gao, W. Ren, B. Liu, R. Saito, Z.-S. Wu, S. Li, C. Jiang, F. Li, and H.-M. Cheng, ACS Nano 3, 933 (2009).

[160] K. Kneipp, H. Kneipp, I. Itzkan, R. R. Dasari, and M. S. Feld, Chem. Rev. 99, 2957 (1999).
[161] S. Lecomte, H. Wackerbarth, T. Soulimane, G. Buse, and P. Hildebrandt, J. Am. Chem. Soc. 120, 7381 (1998).
[162] P. Kambhampati, C. M. Child, M. C. Foster, and A. Campion, J. Chem. Phys. 108, 5013 (1998).
[163] N. A. Abu Hatab, J. M. Oran, and M. J. Sepaniak, ACS Nano 2, 377 (2008).
[164] N.-J. Kim, J. Phys. Chem. C 114, 13979 (2010).
[165] K. H. Hsu, J. H. Back, K.-H. Fung, P. M. Ferreira, M. Shim, and N. X. Fang, J. Raman Spectrosc. 41, 1124 (2010).
[166] H. Huang, W. Chen, S. Chen, and A. T. S. Wee, ACS Nano 2, 2513 (2008).
[167] Y. J. Shin, Y. Wang, H. Huang, G. Kalon, A. T. Wee, Z. Shen, C. S. Bhatia, and H. Yang, Langmuir 26, 3798 (2010).
[168] S. K. Ghosh and T. Pal, Chem. Rev. 107, 4797 (2007).
[169] A. D. McFarland, M. A. Young, J. A. Dieringer, and R. P. Van Duyne, J. Phys. Chem. B 109, 11279 (2005).
[170] X. Zhang, M. A. Young, O. Lyandres, and R. P. Van Duyne, J. Am. Chem. Soc. 127, 4484 (2005).
[171] C. L. Haynes and R. P. Van Duyne, J. Phys. Chem. B 107, 7426 (2003).
[172] J. A. Dieringer, A. D. McFarland, N. C. Shah, D. A. Stuart, A. V. Whitney, C. R. Yonzon, M. A. Young, X. Zhang, and R. P. Van Duyne, Faraday Discuss. 132, 9 (2006).
[173] H. Raether, *Surface plasmons on smooth and rough surfaces and on gratings* (Springer-Verlag, Berlin, 1988).
[174] L. Xie, X. Ling, Y. Fang, J. Zhang, and Z. Liu, J. Am. Chem. Soc. 131, 9890 (2009).
[175] X. Ling, L. Xie, Y. Fang, H. Xu, H. Zhang, J. Kong, M. S. Dresselhaus, J. Zhang, and Z. Liu, Nano Lett. 10, 553 (2009).
[176] Y. Wang, Z. Ni, H. Hu, Y. Hao, C. P. Wong, T. Yu, J. T. L. Thong, and Z. X. Shen, Appl. Phys. Lett. 97, 163111 (2010).
[177] E. Hao and G. C. Schatz, J. Chem. Phys. 120, 357 (2004).

Appendices

Journal publication

[1] **Jing Niu**, Young Jun Shin, Jaesung Son, Youngbin Lee, Jong Hyun Ahn, and Hyunsoo Yang, *"Electromagnetic coupling between graphene and Au nanoparticles induced shifting of surface plasmon resonance"* **Optics Express** 20, 19690 (2012)

[2] **Jing Niu**, Viet Giang Truong, Han Huang, Sudhiranjan Tripathy, Caiyu Qiu, Andrew T.S. Wee, Ting Yu, and Hyunsoo Yang, *"Study of electromagnetic enhancement for surface enhanced Raman spectroscopy of SiC graphene"* **Applied Physics Letters** 100, 191601 (2012)

[3] **Jing Niu**, Young Jun Shin, Youngbin Lee, Jong-Hyun Ahn, and Hyunsoo Yang, *"Graphene induced tunability of the surface plasmon resonance"* **Applied Physics Letters** 100, 061116 (2012)

[4] Kalon Gopinadhan, Young Jun Shin, Indra Yudhistira, **Jing Niu**, and Hyunsoo Yang, *"Giant magnetoresistance in single-layer graphene flakes with a gate-voltage-tunable weak antilocalization"* **Phys. Rev. B** 88, 195429 (2013)

[5] Yang Wu, Xuezhong Ruan, Chih-Hsin Chen, Young Jun Shin, Youngbin Lee, **Jing Niu**, Jingbo Liu, Yuanfu Chen, Kun-Lin Yang, Xinhai Zhang, Jong-Hyun Ahn, and Hyunsoo Yang, *"Graphene/liquid crystal based terahertz phase shifters"* **Optics Express** 21, 21395 (2013)

[6] Xue Peng Qiu, Young Jun Shin, **Jing Niu**, Narayanapillai Kulothungasagaran, Gopinadhan Kalon, Caiyu Qiu, Ting Yu, and Hyunsoo Yang, "*Disorder-free sputtering method on graphene"* **AIP Advances** 2, 032121 (2012)

[7] Young Jun Shin, Gopinadhan Kalon, Jaesung Son, Jae Hyun Kwon, **Jing Niu**, Charanjit S. Bhatia, Gengchiau Liang, and Hyunsoo Yang, *"Tunneling characteristics of graphene"* **Applied Physics Letters**, 97, 252102 (2010)

Conference Publications

[1] **Jing Niu,** Young Jun Shin, Youngbin Lee, Jong-Hyun Ahn, and Hyunsoo Yang, *"Graphene induced tunability of the surface plasmon resonance"* International Conference of Young Researchers on Advanced Materials, 1th to 6th Jul 2012, Singapore

[2] **Jing Niu**, Viet Giang Truong, Han Huang, Sudhiranjan Tripathy, Caiyu Qiu, Andrew T.S. Wee, Ting Yu, and Hyunsoo Yang, *"Surface-enhanced Raman spectroscopy of graphene on SiC substrates"* International Conference on Materials for Advanced Technologies, 26th Jun to 1th Jul 2011, Singapore

[3] **Jing Niu**, Young Jun Shin, Ajeesh Mavolil Sahadevan, Charanjit Singh Bhatia, Hyunsoo Yang, *"Quantum size effect of metal nanoparticles on graphene"* International Conference on Materials for Advanced Technologies, 26th Jun to 1th Jul 2011, Singapore